

Nonequilibrium materials: using ultrashort laser pulses to change band structures



2016 SPIE Defense + Commercial Sensing Meeting
Ultrafast Bandgap Photonics Conference
Baltimore, MD, 18 April 2016



Introduction

SCIENCE

4 May 1979, Volume 204, Number 4392

Laser Annealing of Ion-Implanted Semiconductors

C. W. White, J. Narayan, R. T. Young

Impurities can be implanted in the near-surface region of solids by a process in which the impurity ions are accelerated in an electrostatic field to a desired energy and then made to impinge on the solid targets. This process, known as ion implantation, has made a significant impact on the electronics industry, where it is used to dope semiconductors. It is often accompanied by undesirable consequences such as precipitation of dopants in the implanted region, degradation of certain electrical properties, decomposition of the substrate in the case of compound semiconductors, and usually only partial removal of lattice damage in the implanted layer. Recently, interest (1) has been generated in the possibility of using laser annealing to repair the damage. This process is based on the fact that the energy of a laser beam can be focused to a small area, and the energy density can be made high enough to raise the temperature of the substrate to a level where the lattice damage is annealed. This process is particularly attractive for highly automated device fabrication. A third and potentially very important, advantage of laser annealing is that it enables highly localized annealing to be performed simply by focusing the incident laser light to the desired dimensions (21). This may permit the "writing" of regions of localized electrical activity on an ion-implanted wafer and could have profound implications for device processing.

Another advantage for some applications is that laser annealing can be carried out in air because the surface region subjected to high temperatures cools so rapidly that introduction of significant amounts of impurities from the atmosphere is minimized. This should be a particularly attractive feature for highly automated device fabrication. A third and potentially very important, advantage of laser annealing is that it enables highly localized annealing to be performed simply by focusing the incident laser light to the desired dimensions (21). This may permit the "writing" of regions of localized electrical activity on an ion-implanted wafer and could have profound implications for device processing.

C.W.White, J.Narayan, R.T.Young, *Science* 204, 461-468 (1979)

Summary. The physical and electrical properties of ion-implanted silicon annealed by laser radiation are described. Particular emphasis is placed on the annealing of ion-implanted silicon annealed by radiation from pulsed ruby laser. Particular emphasis is placed on the annealing of ion-implanted silicon annealed by radiation from pulsed ruby laser. Particular emphasis is placed on the annealing of ion-implanted silicon annealed by radiation from pulsed ruby laser.

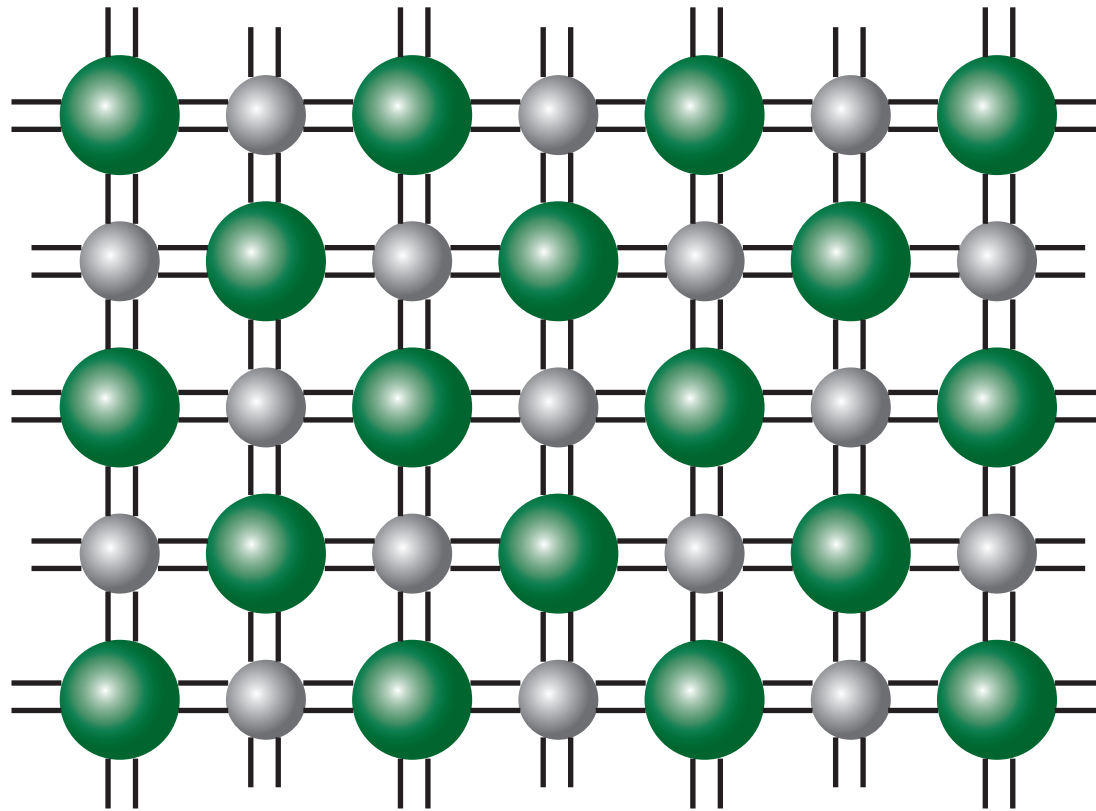
work performed at the ORNL on the characterization of ion-implanted silicon annealed by radiation from pulsed ruby laser. Particular emphasis is placed on the annealing of ion-implanted silicon annealed by radiation from pulsed ruby laser.

Introduction

can we optically control the state of a solid?

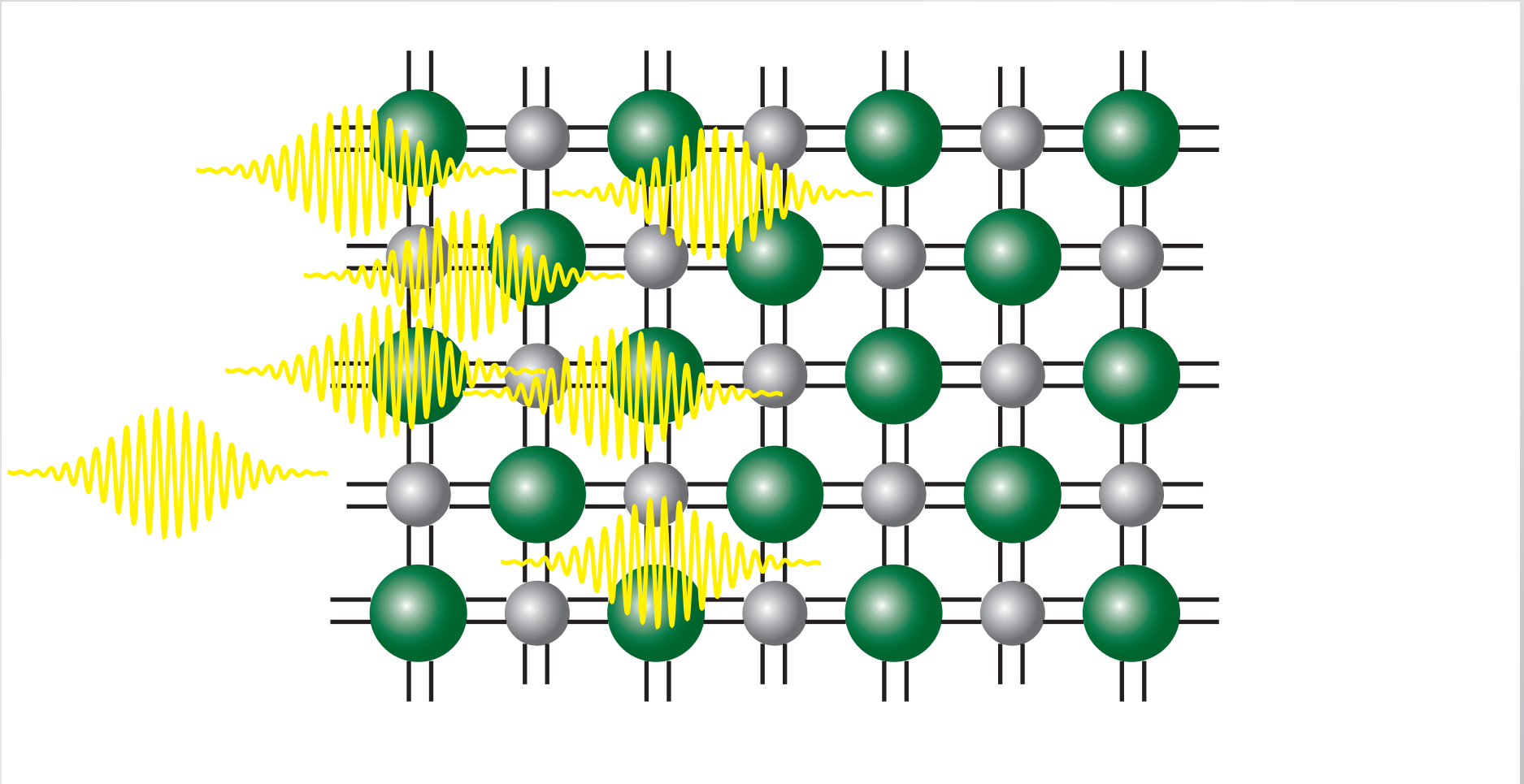
Introduction

can we optically control the state of a solid?



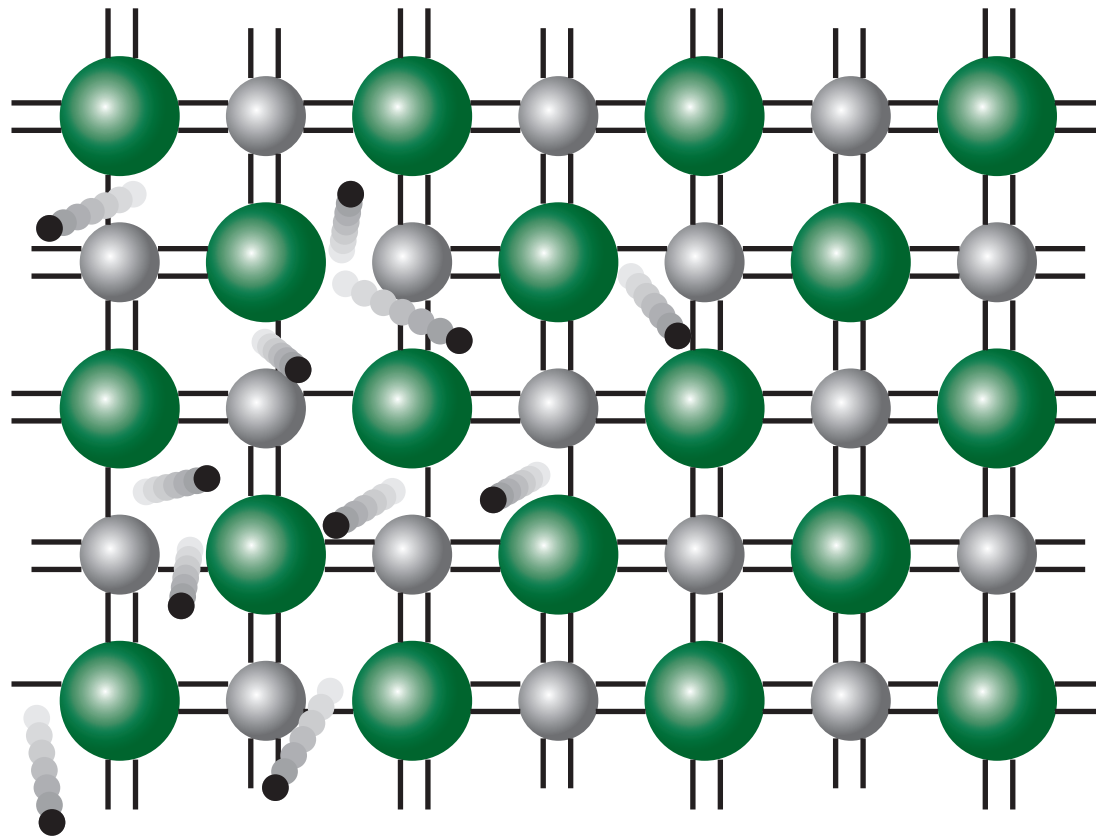
Introduction

photons excite valence electrons...



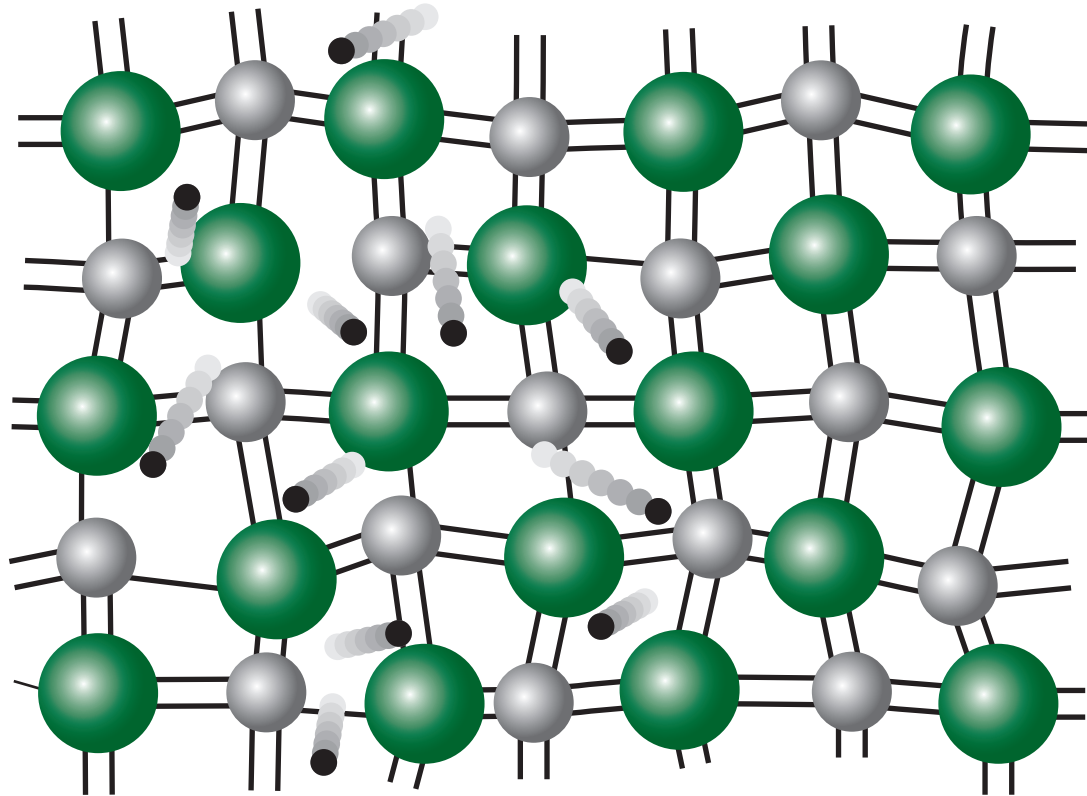
Introduction

...and create free carriers...



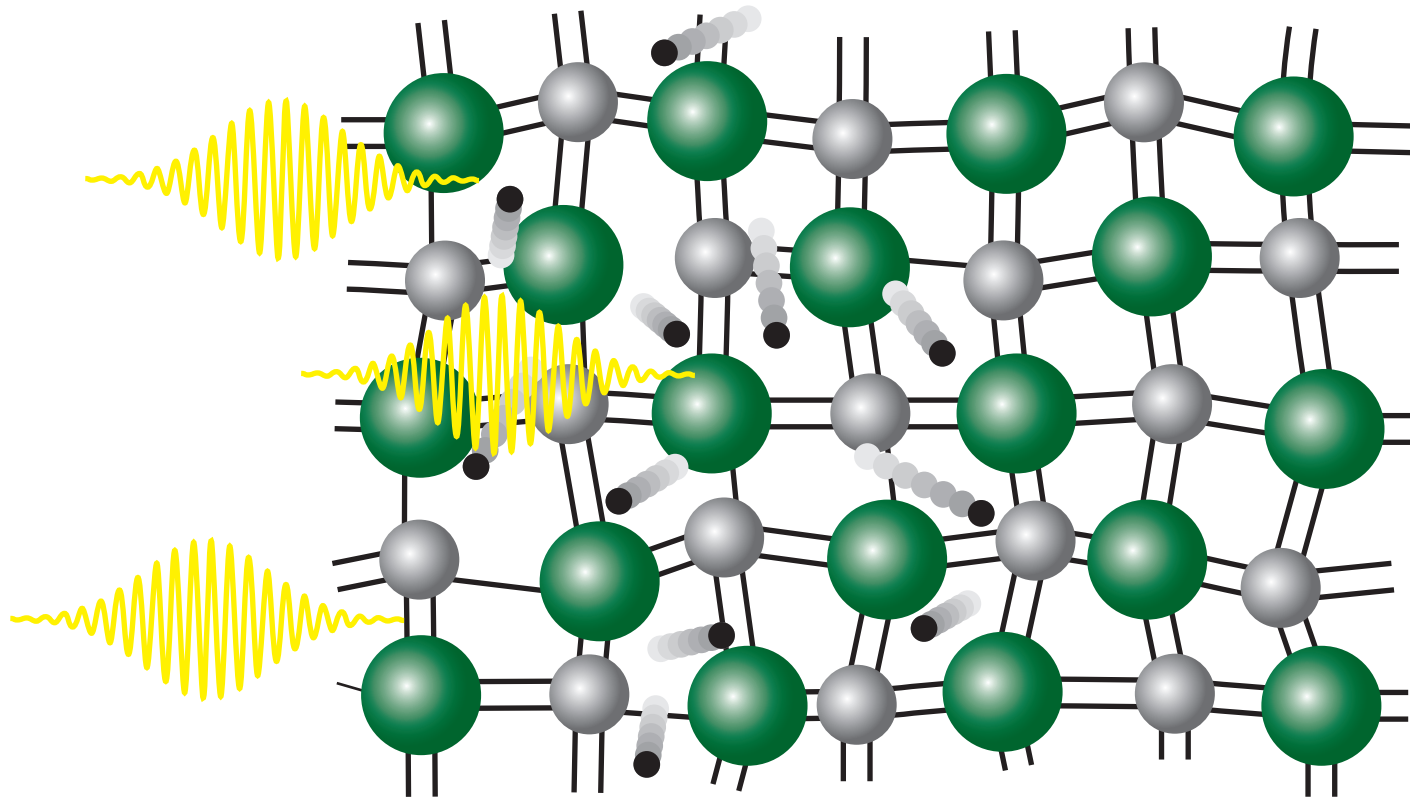
Introduction

...causing electronic and structural changes...



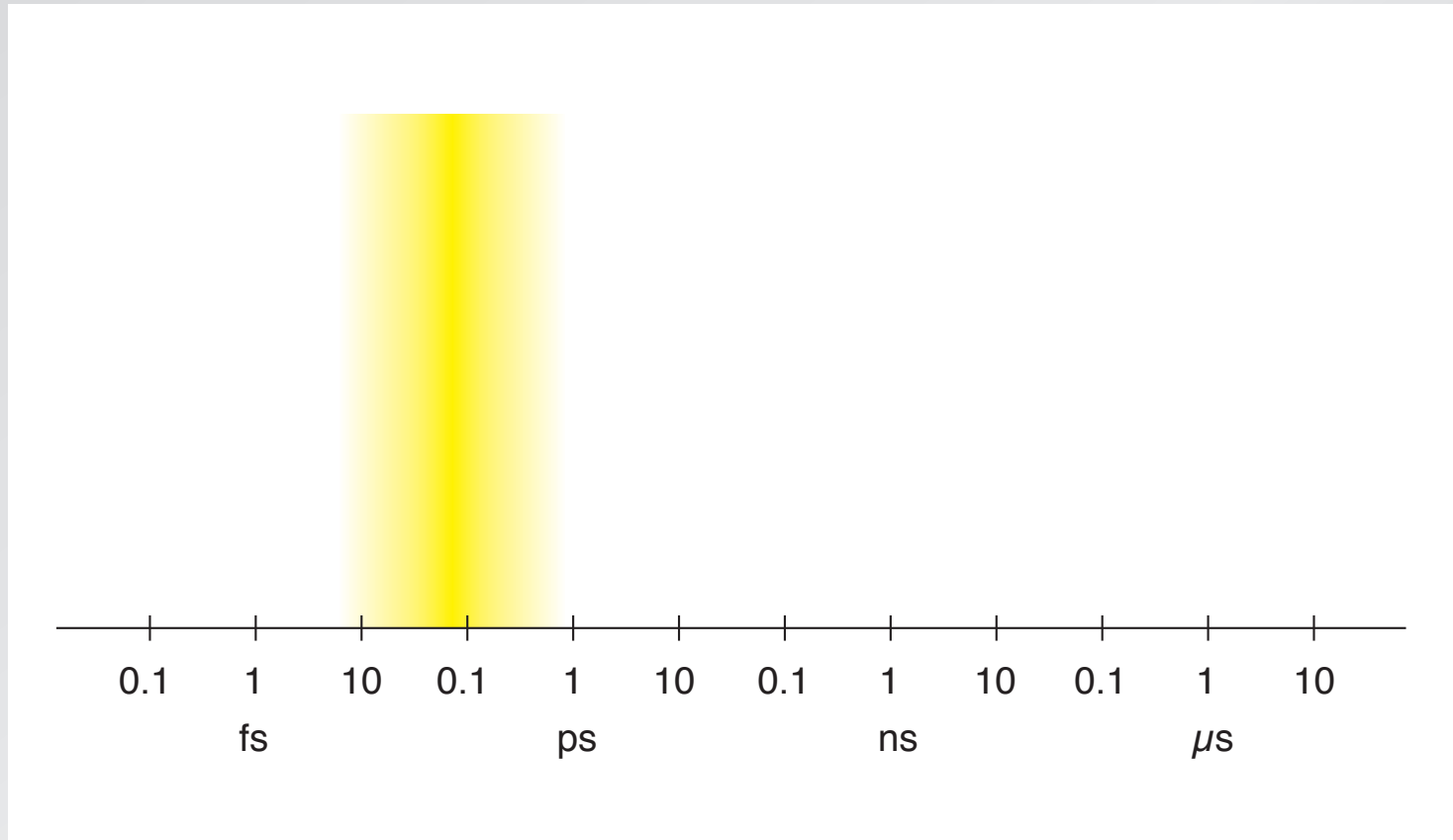
Introduction

...which we can detect with a second laser pulse.



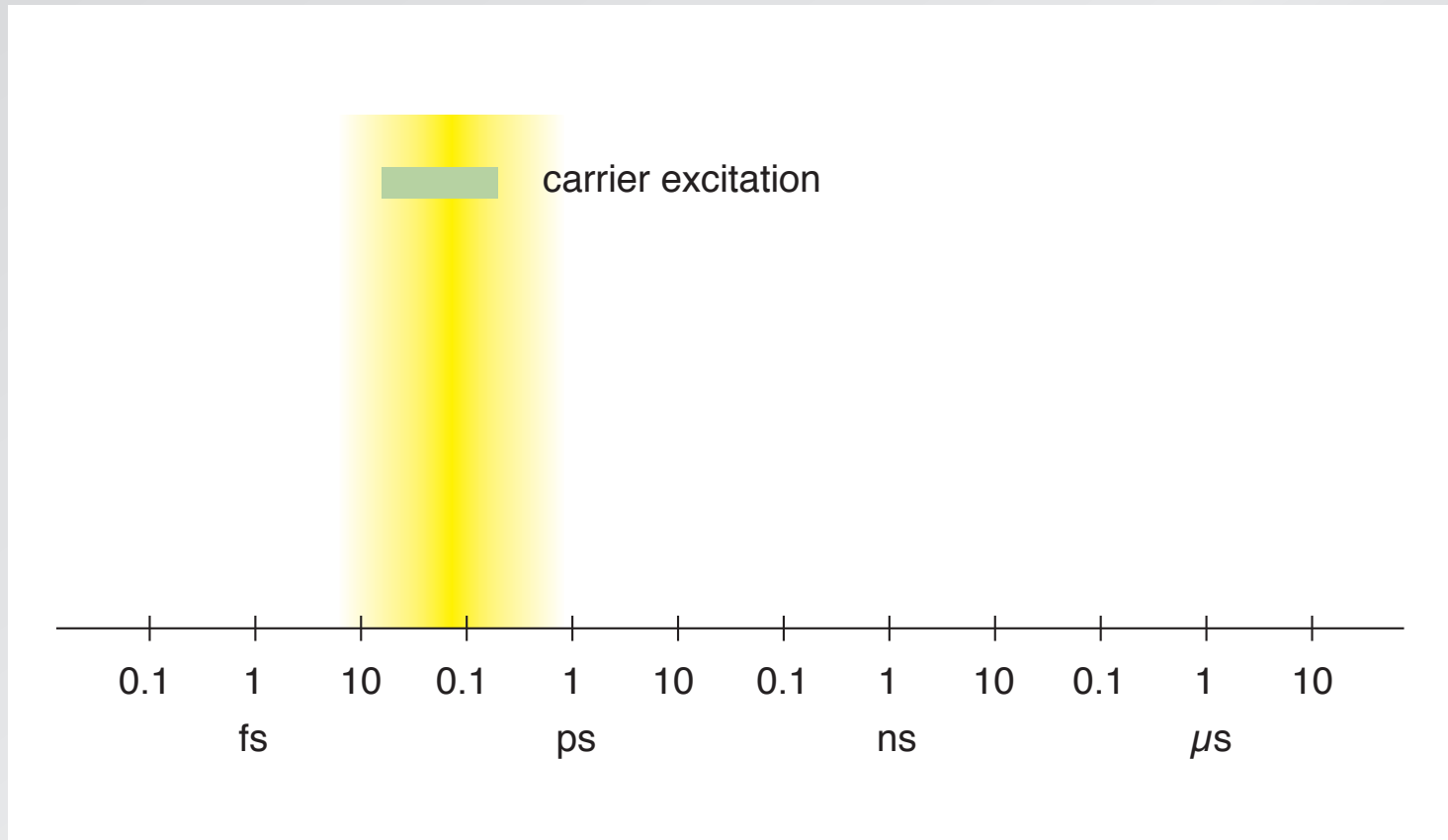
Introduction

relevant time scales



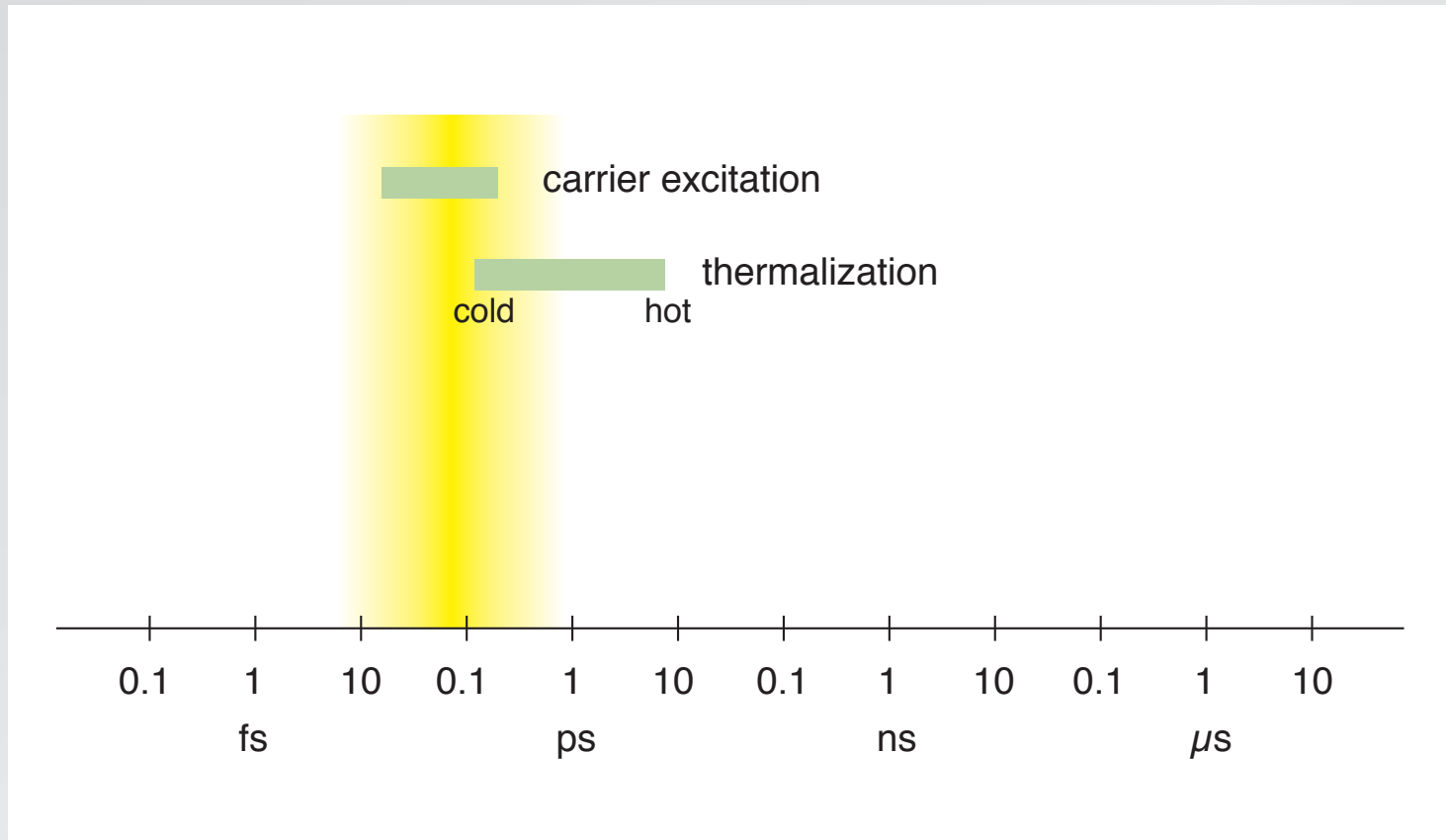
Introduction

relevant time scales



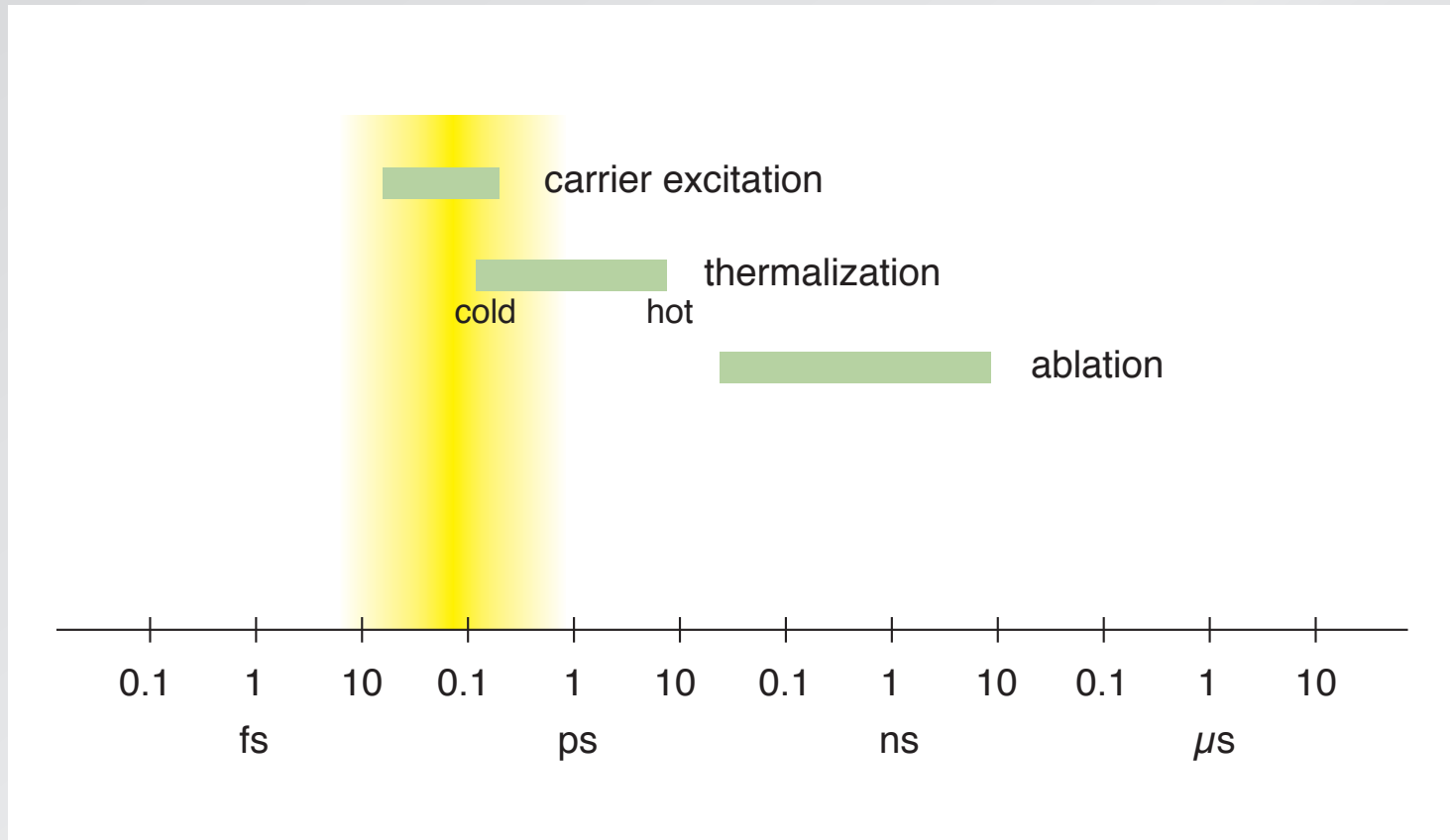
Introduction

relevant time scales



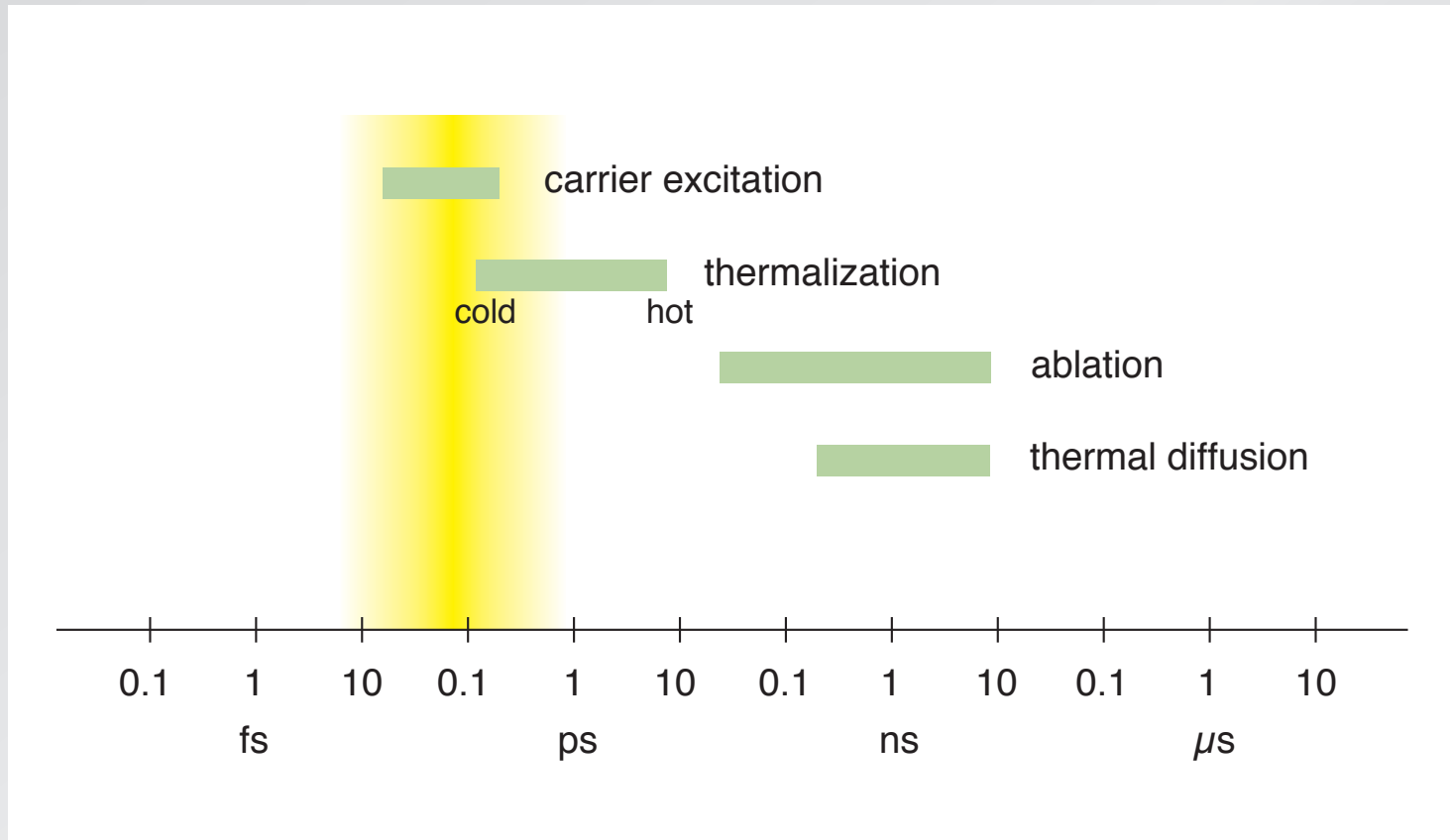
Introduction

relevant time scales



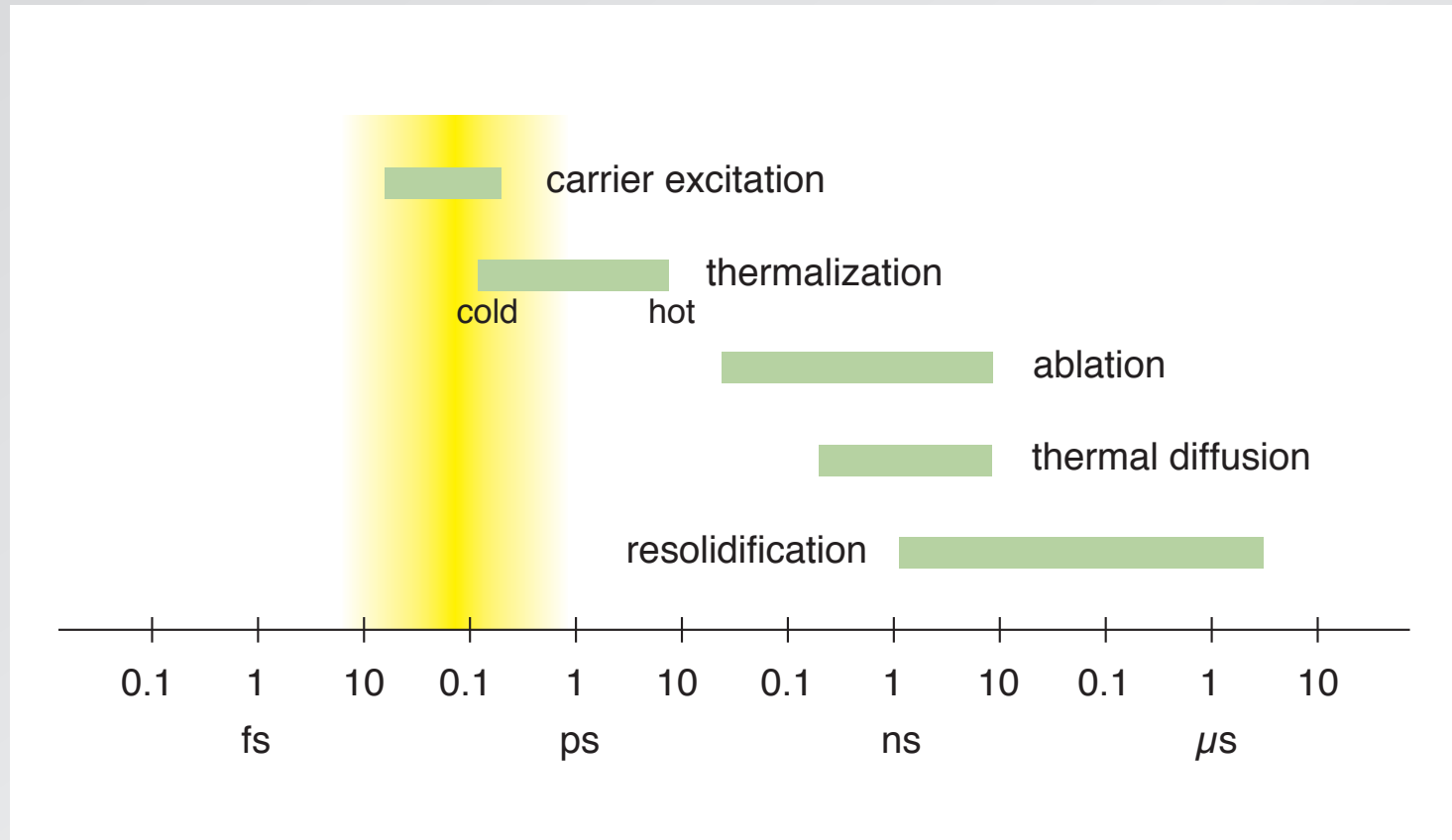
Introduction

relevant time scales



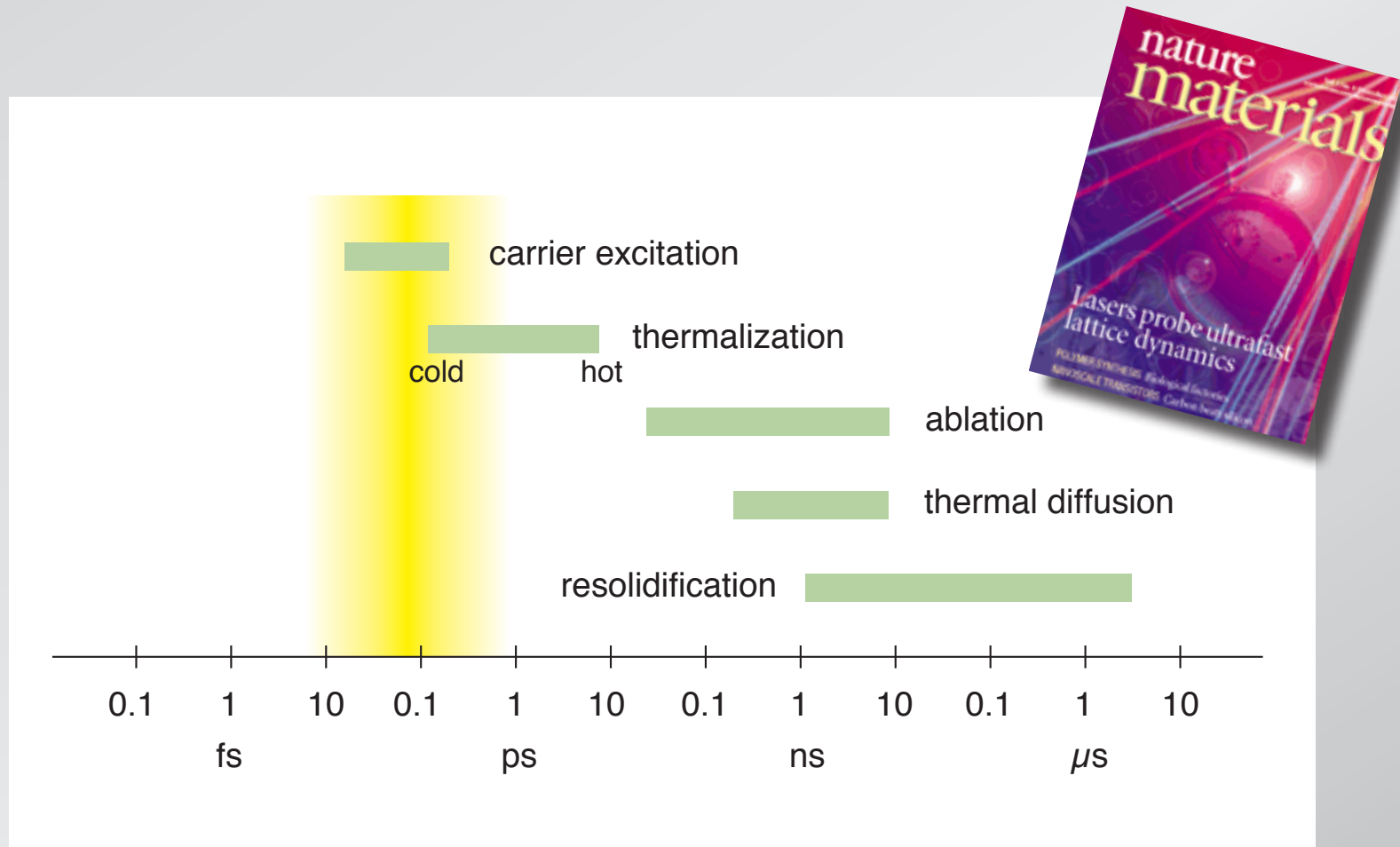
Introduction

relevant time scales



Introduction

relevant time scales

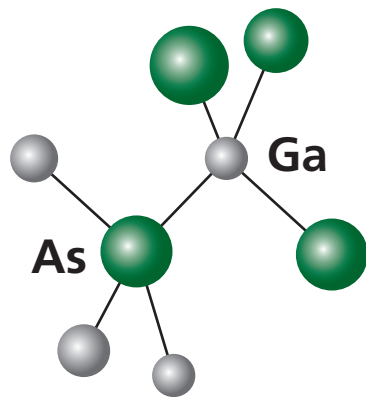


Outline

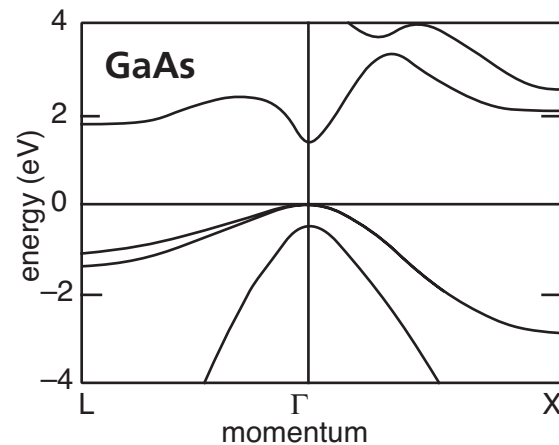
- **transient band structure changes**
- **creating an intermediate band**
- **semiconductor to metal transition**

Transient band structure changes

structure

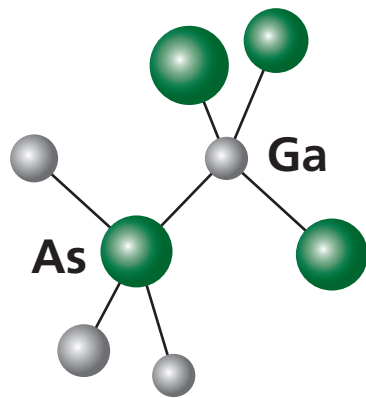


band structure

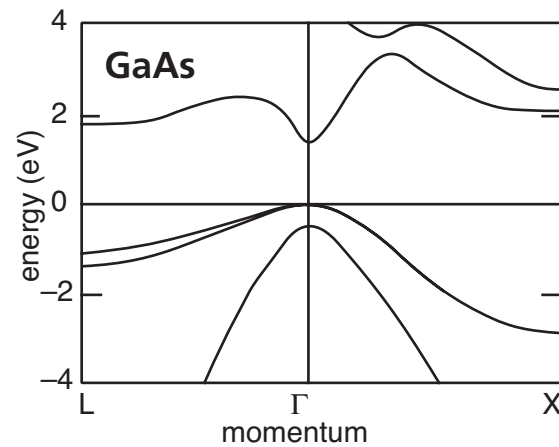


Transient band structure changes

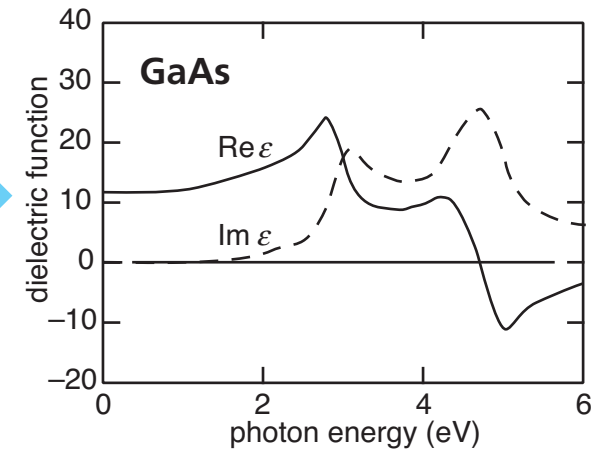
structure



band structure

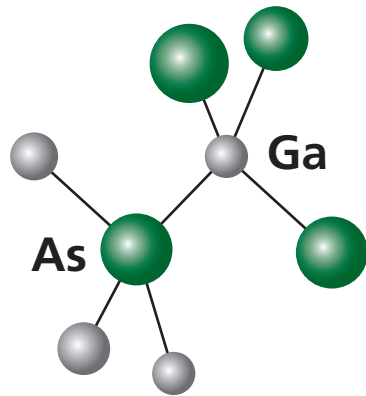


dielectric function

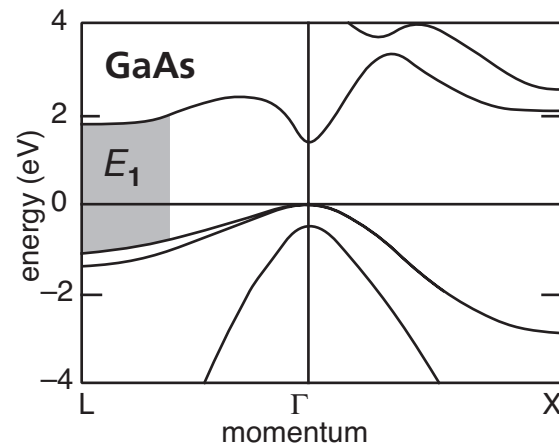


Transient band structure changes

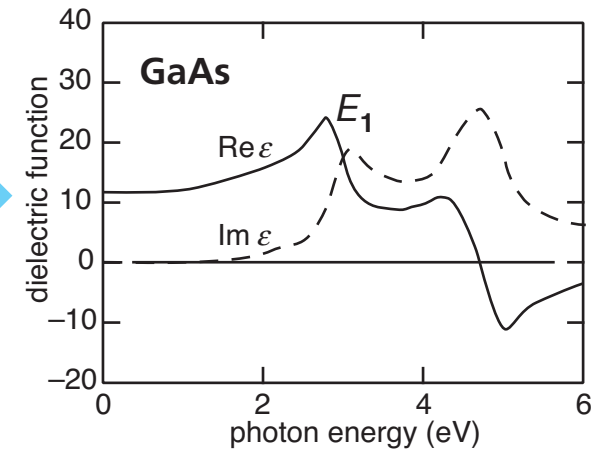
structure



band structure

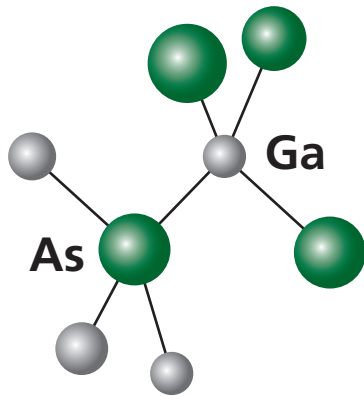


dielectric function

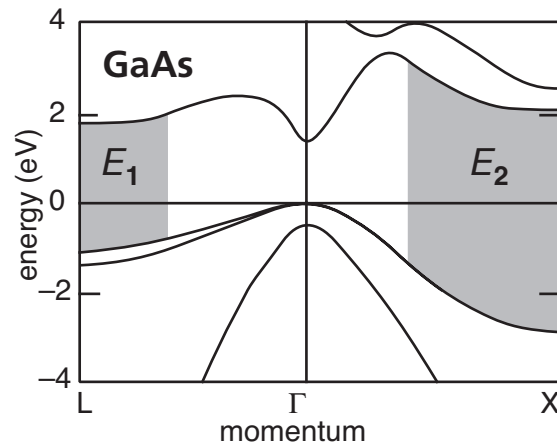


Transient band structure changes

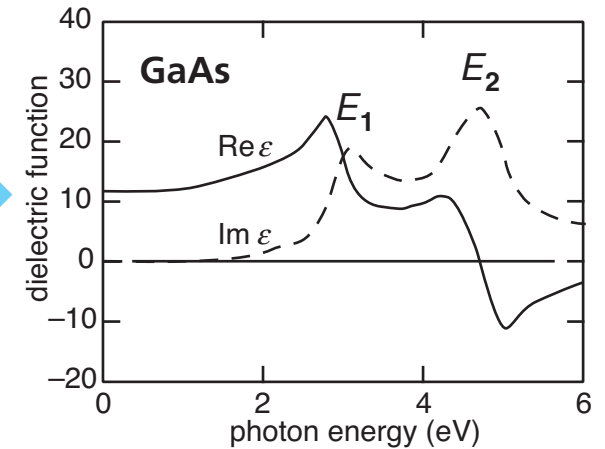
structure



band structure

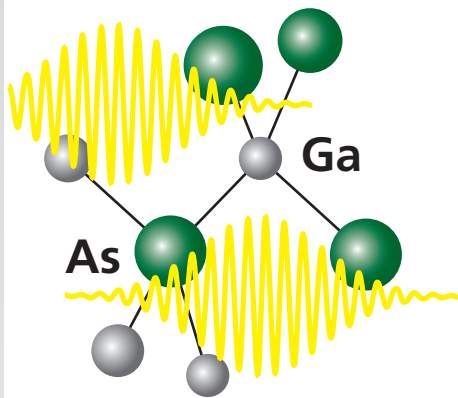


dielectric function

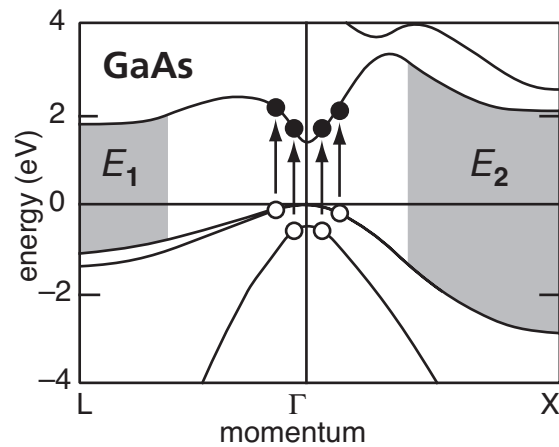


Transient band structure changes

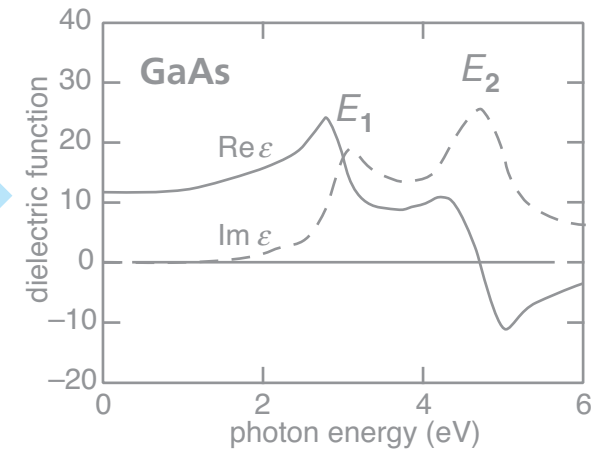
structure



band structure

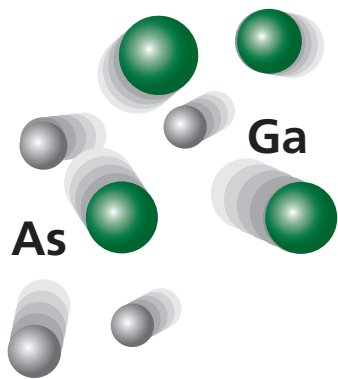


dielectric function

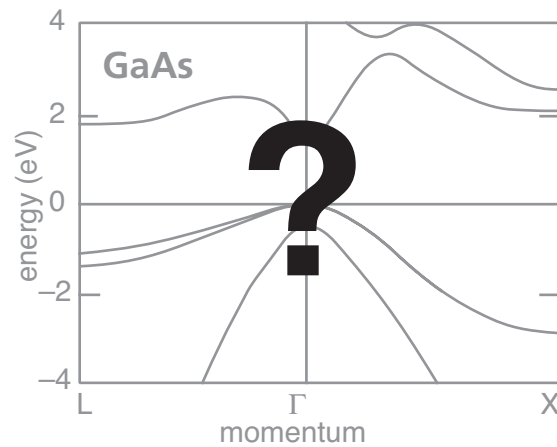


Transient band structure changes

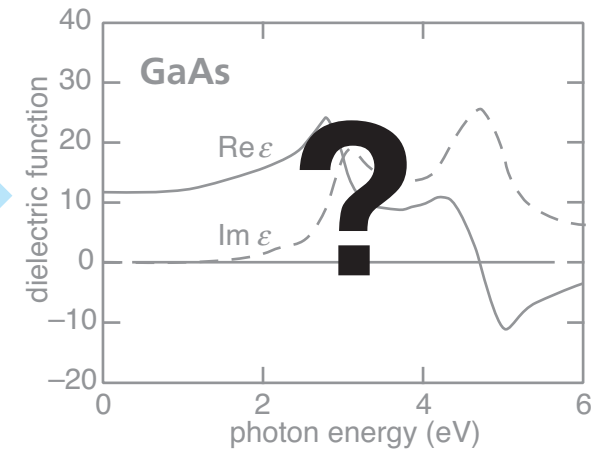
structure



band structure

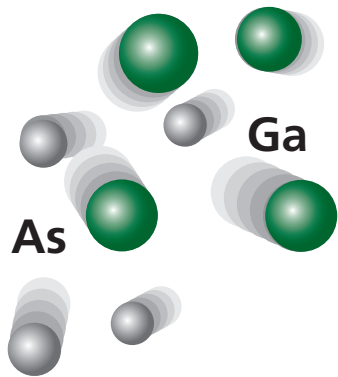


dielectric function

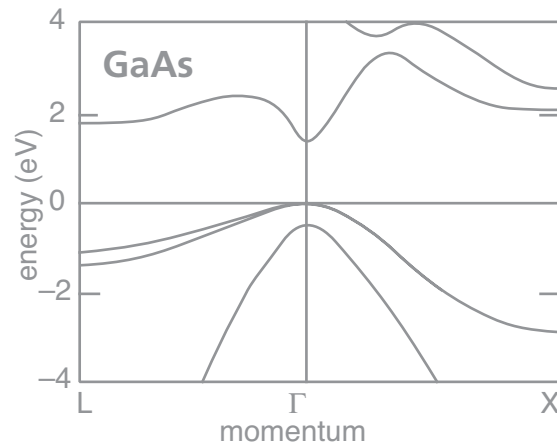


Transient band structure changes

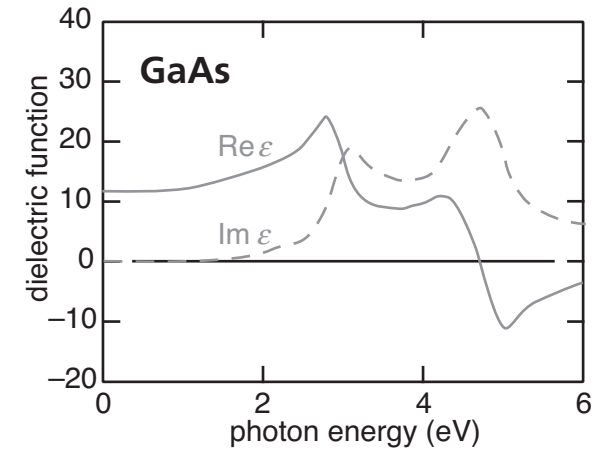
structure



band structure

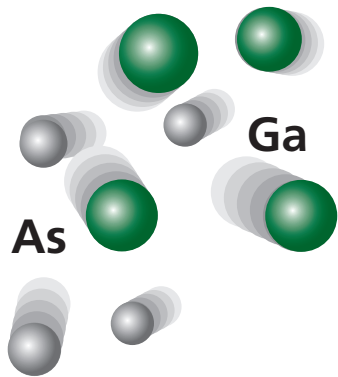


dielectric function

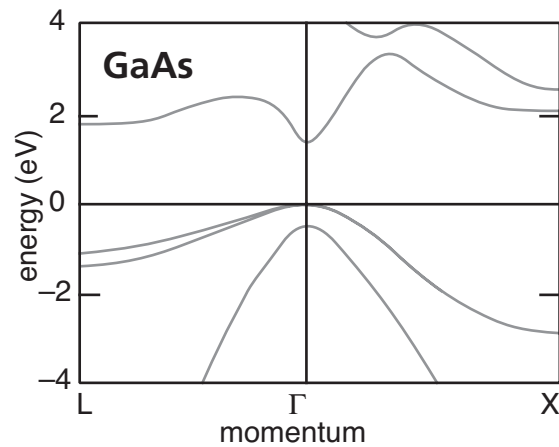


Transient band structure changes

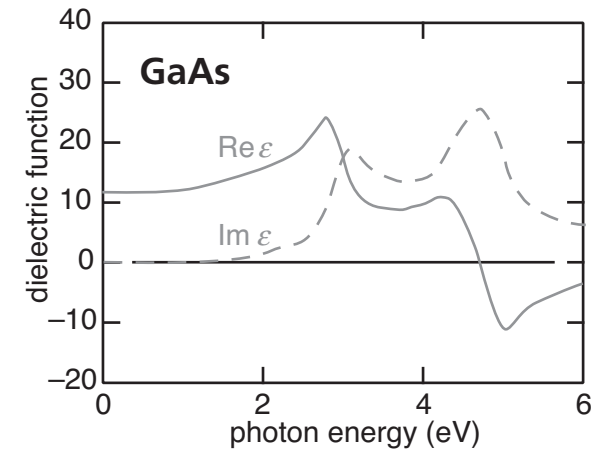
structure



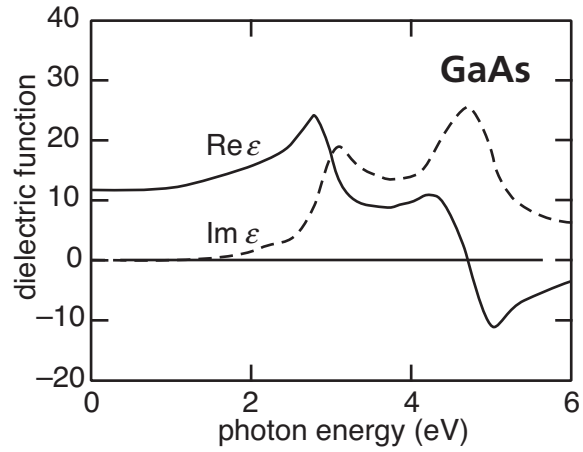
band structure



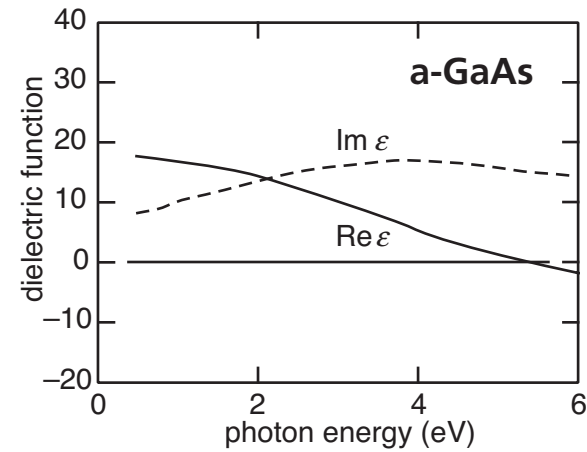
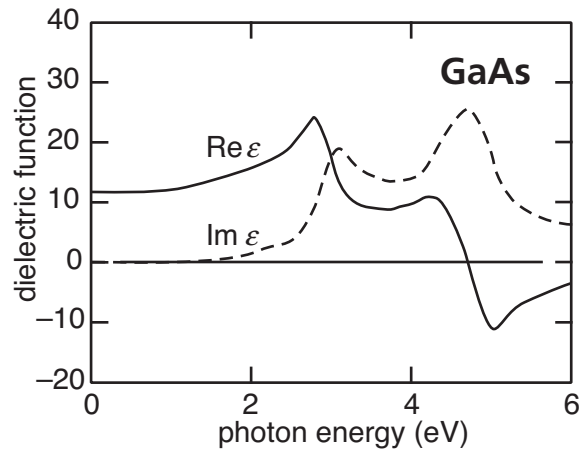
dielectric function



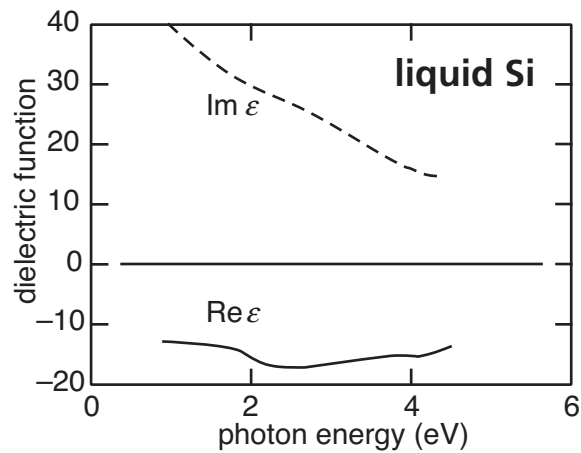
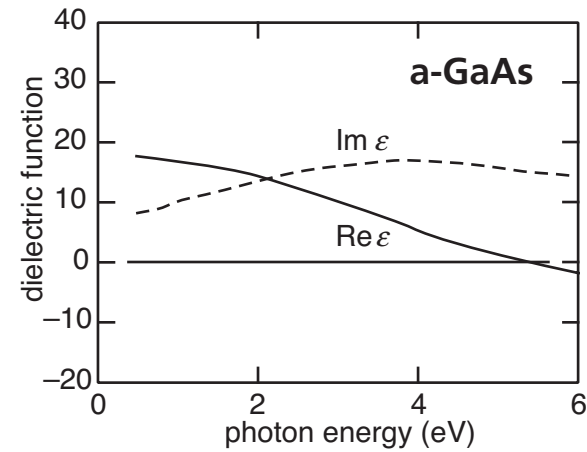
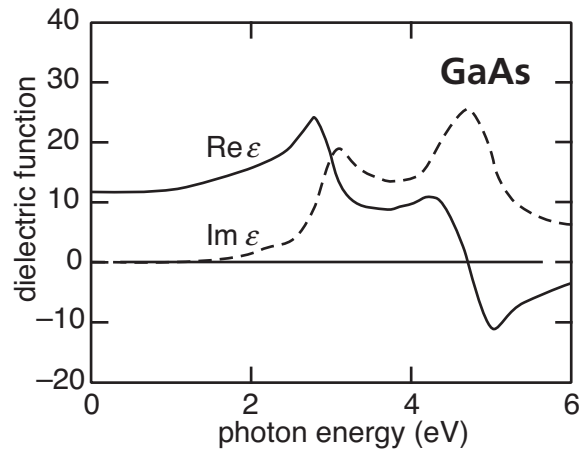
Transient band structure changes



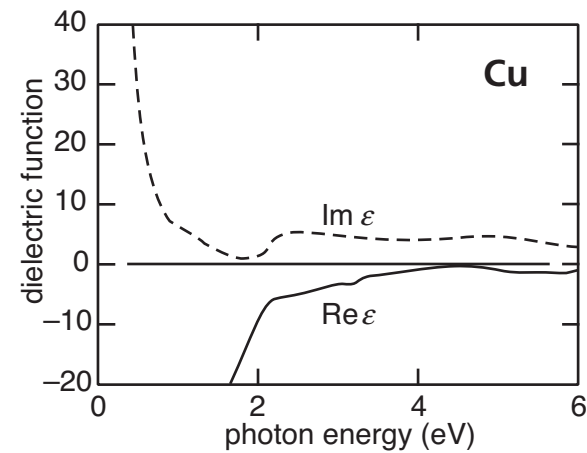
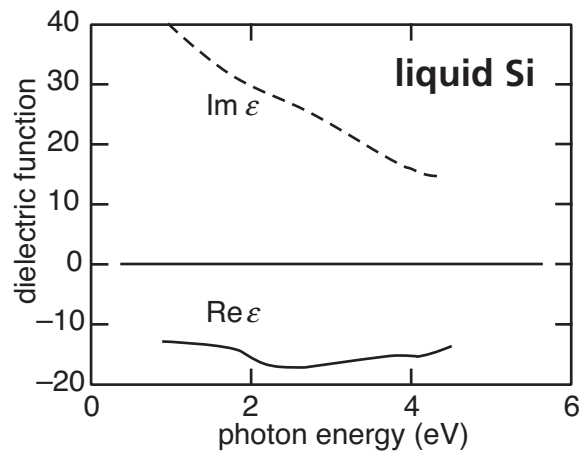
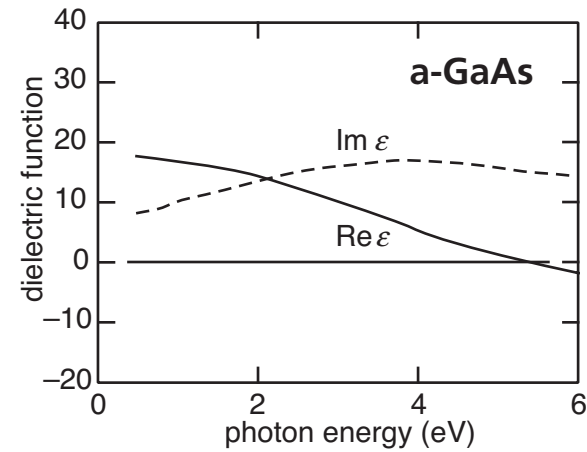
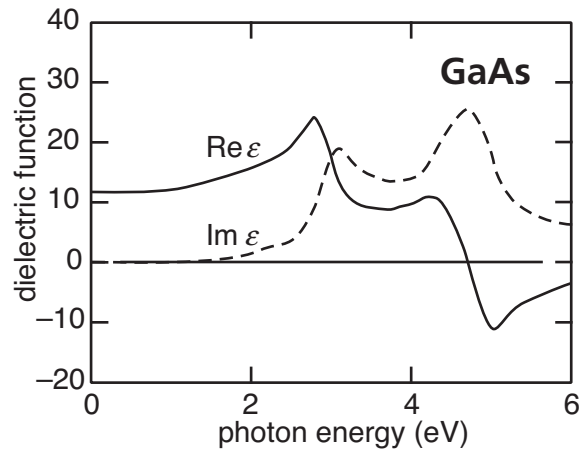
Transient band structure changes



Transient band structure changes

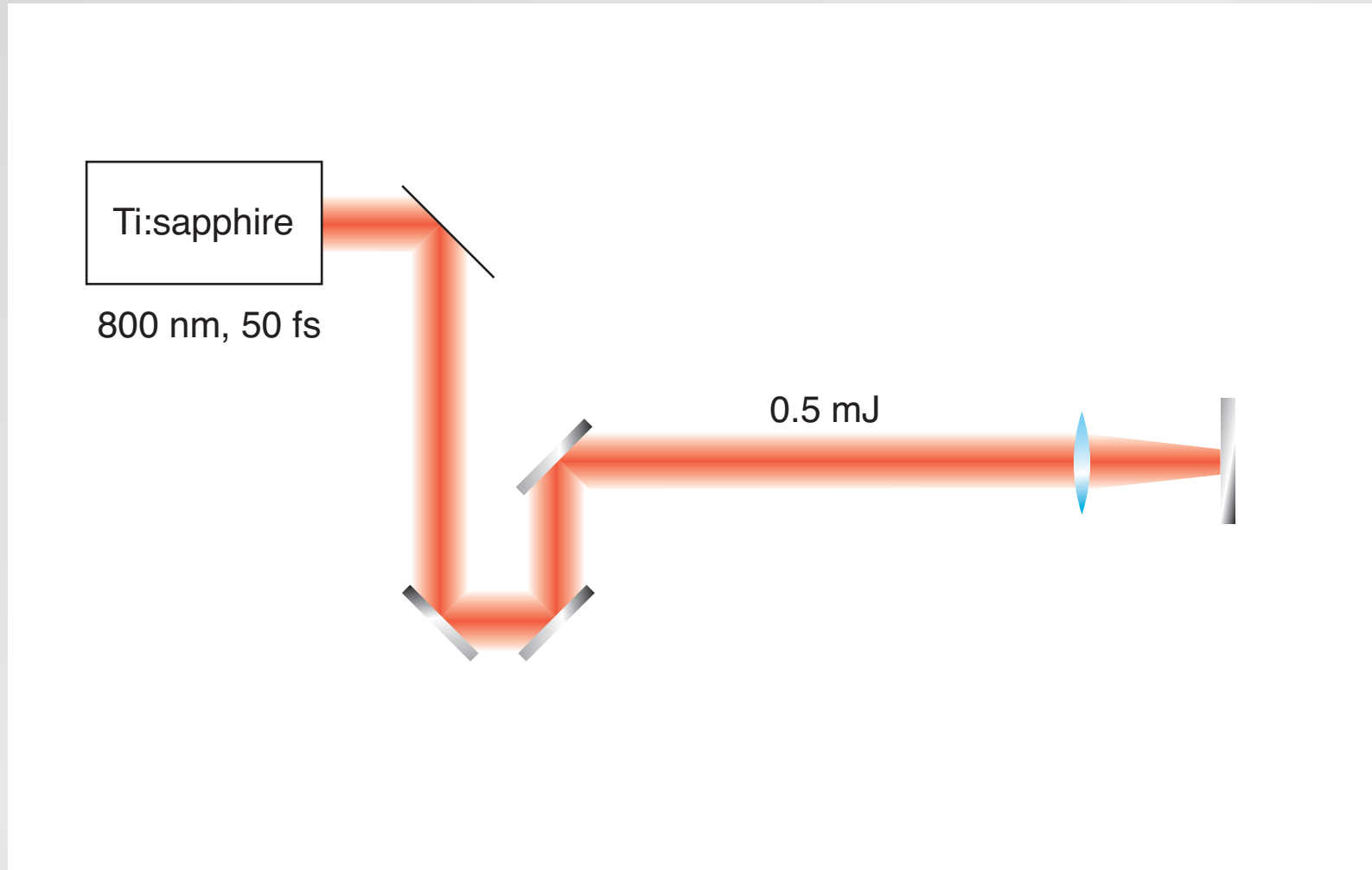


Transient band structure changes



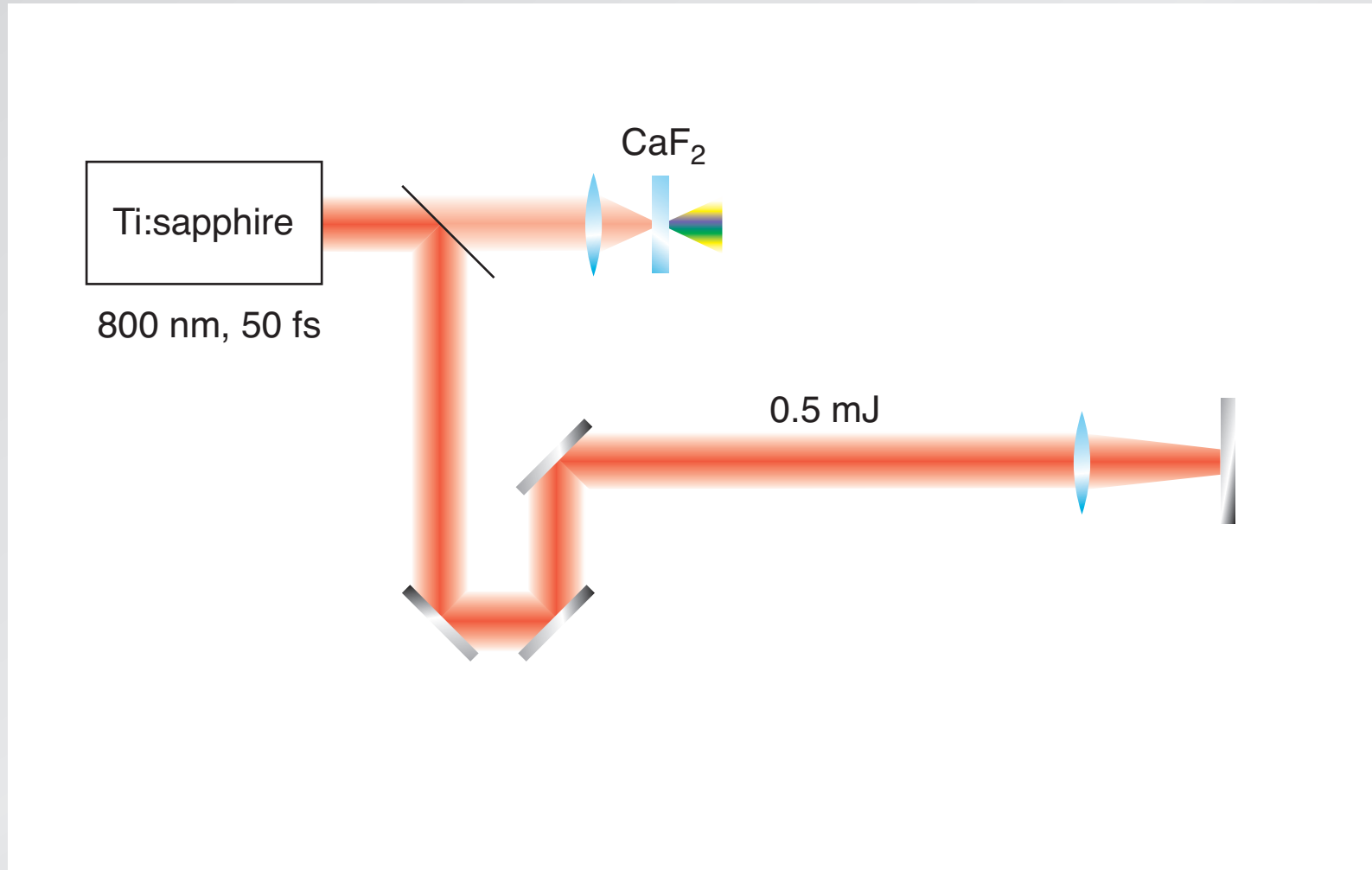
Transient band structure changes

time-resolved dual-angle reflectometry



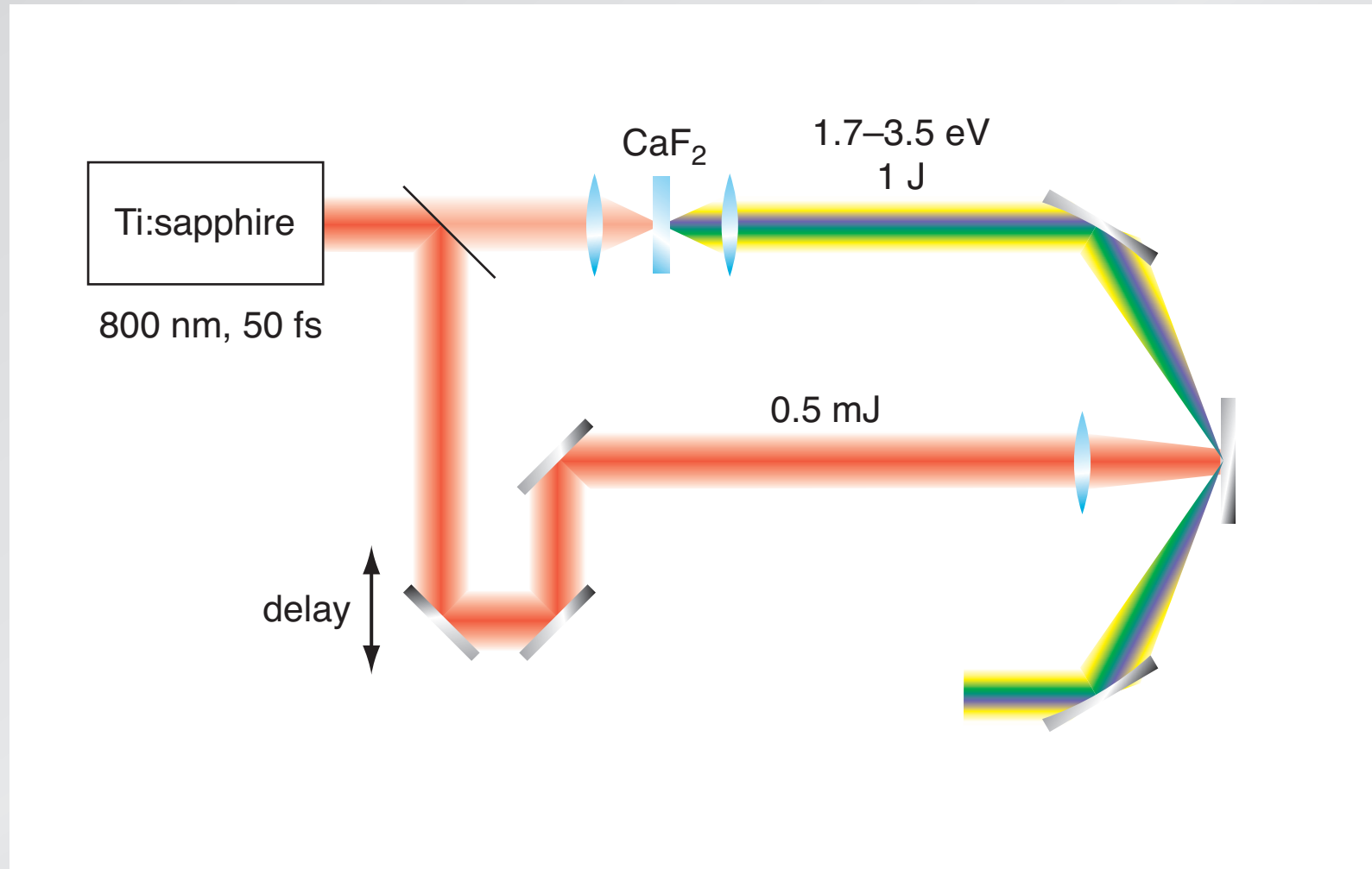
Transient band structure changes

time-resolved dual-angle reflectometry



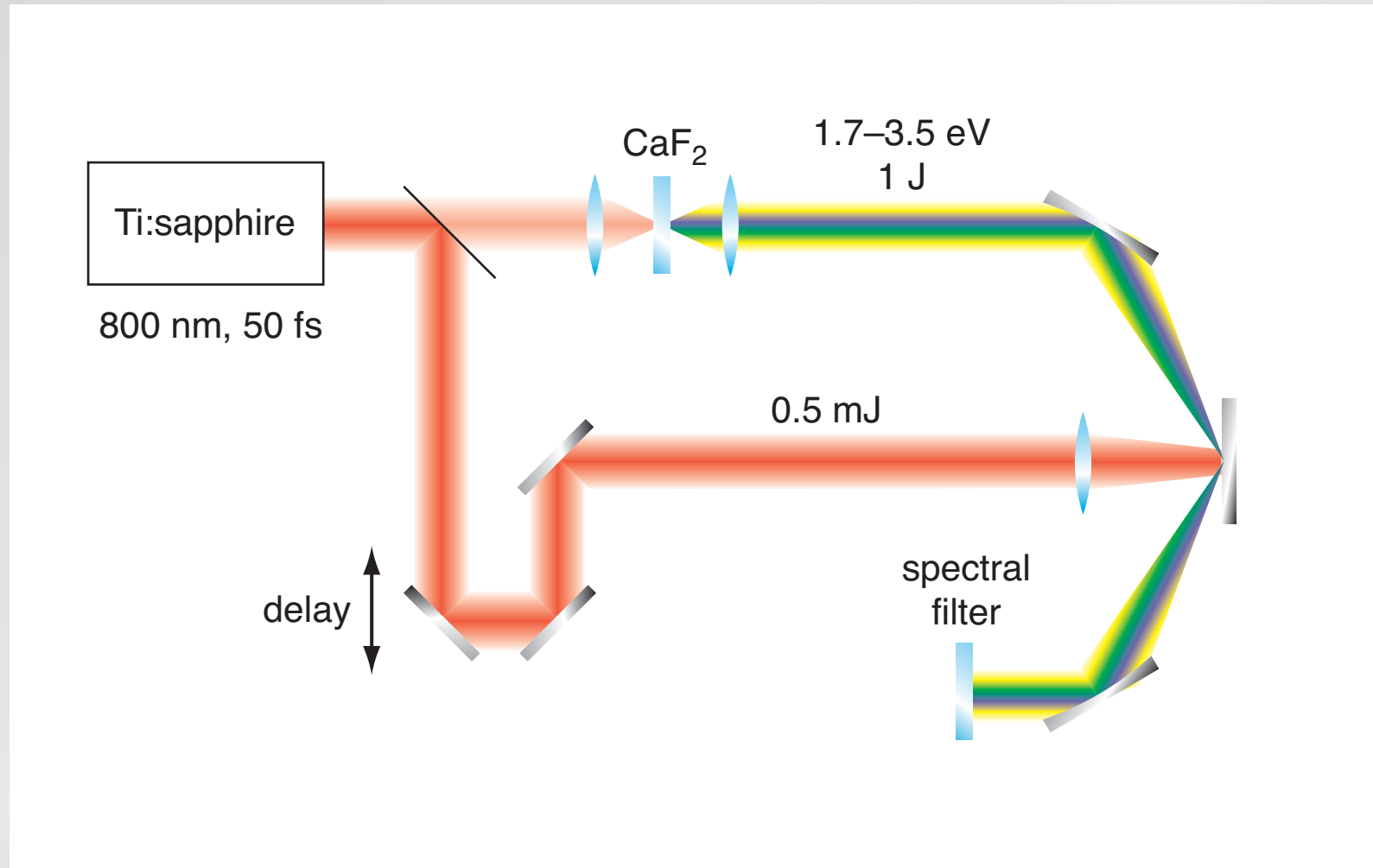
Transient band structure changes

time-resolved dual-angle reflectometry



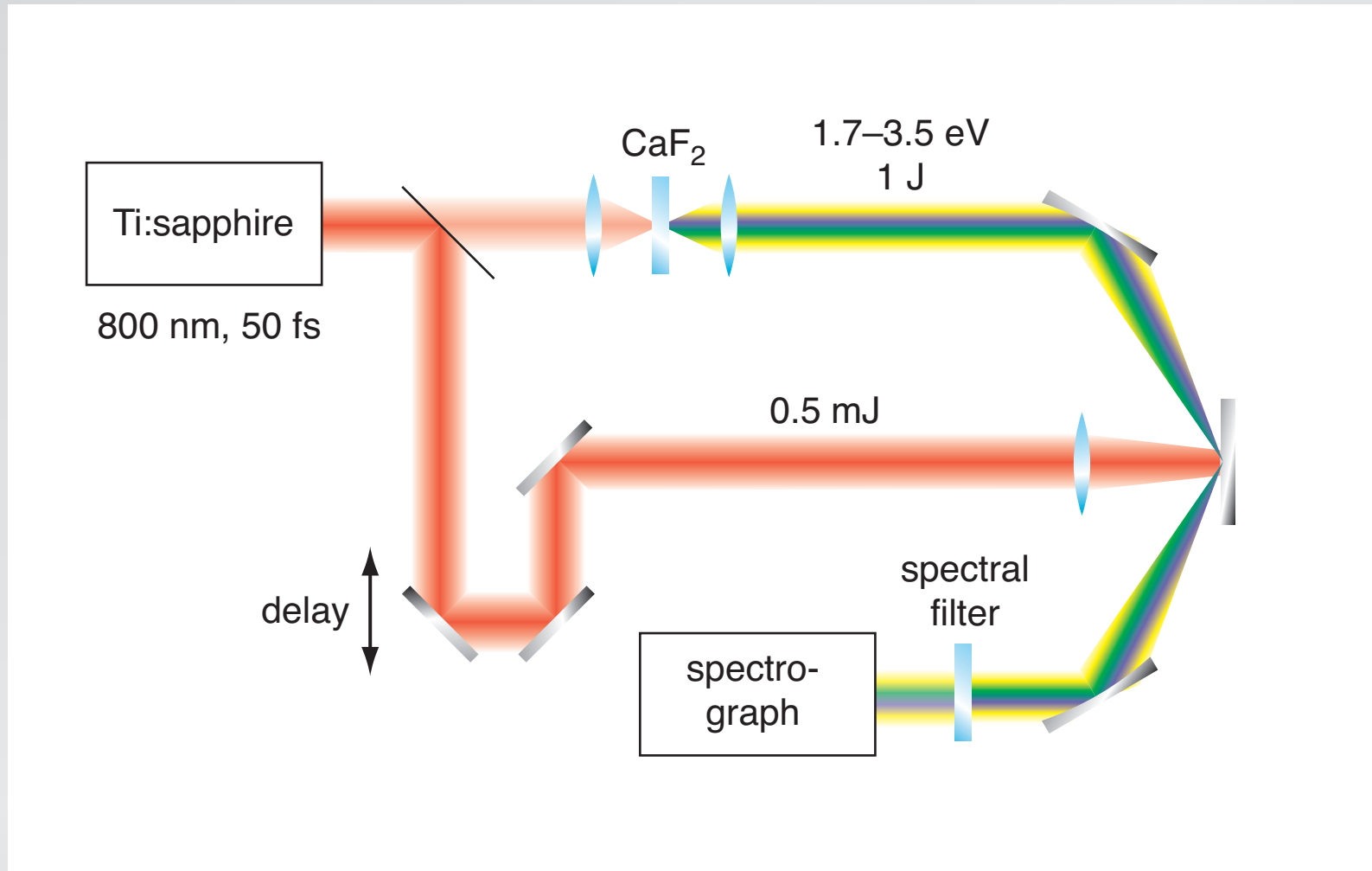
Transient band structure changes

time-resolved dual-angle reflectometry



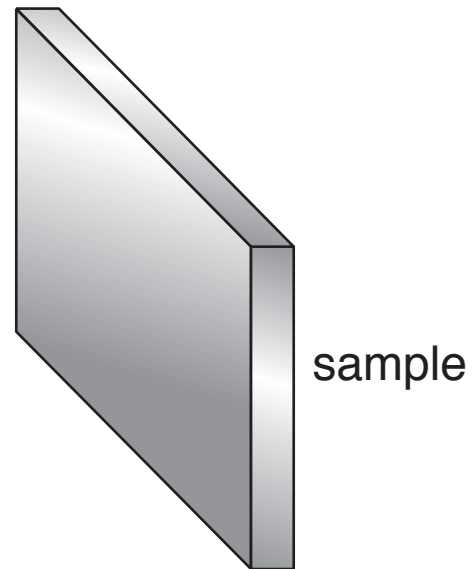
Transient band structure changes

time-resolved dual-angle reflectometry



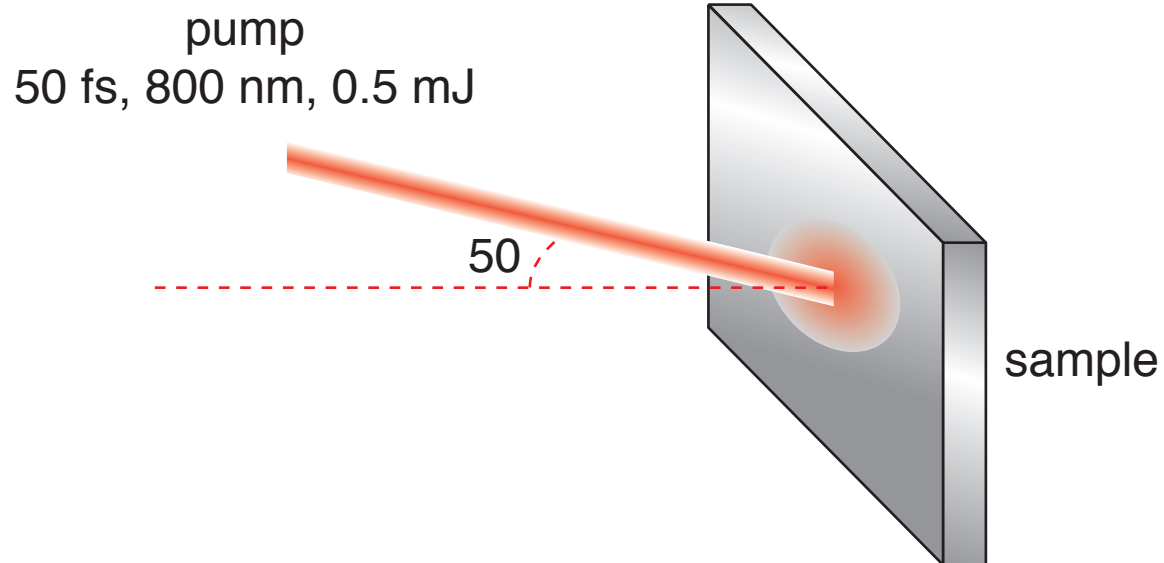
Transient band structure changes

time-resolved dual-angle reflectometry



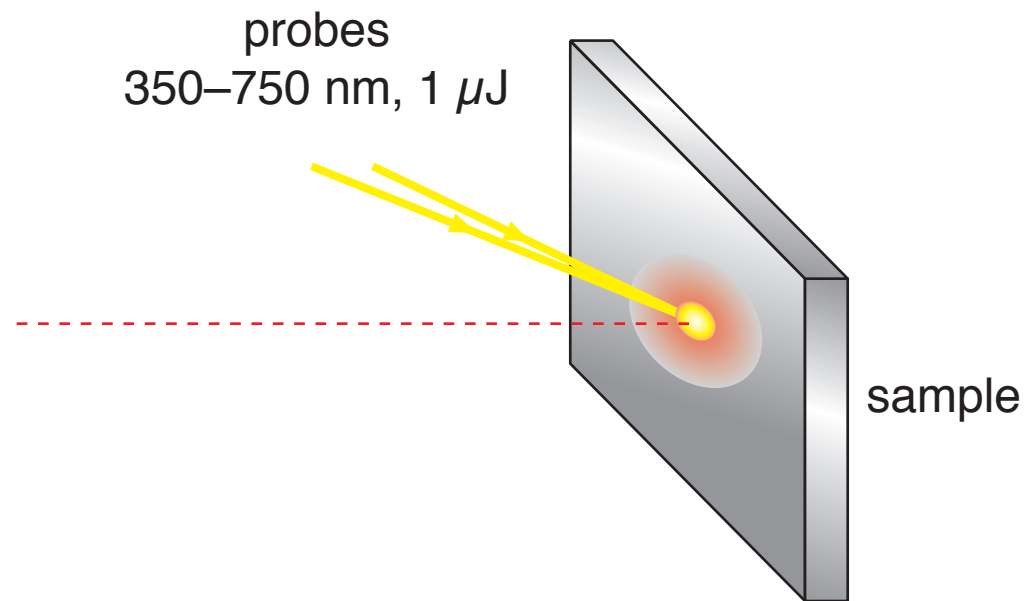
Transient band structure changes

time-resolved dual-angle reflectometry



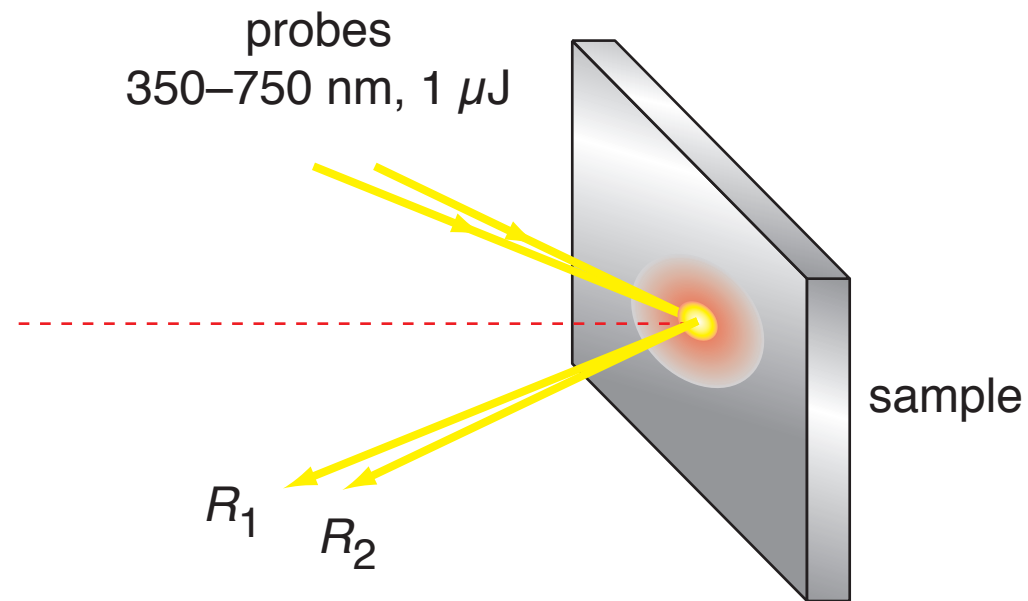
Transient band structure changes

time-resolved dual-angle reflectometry



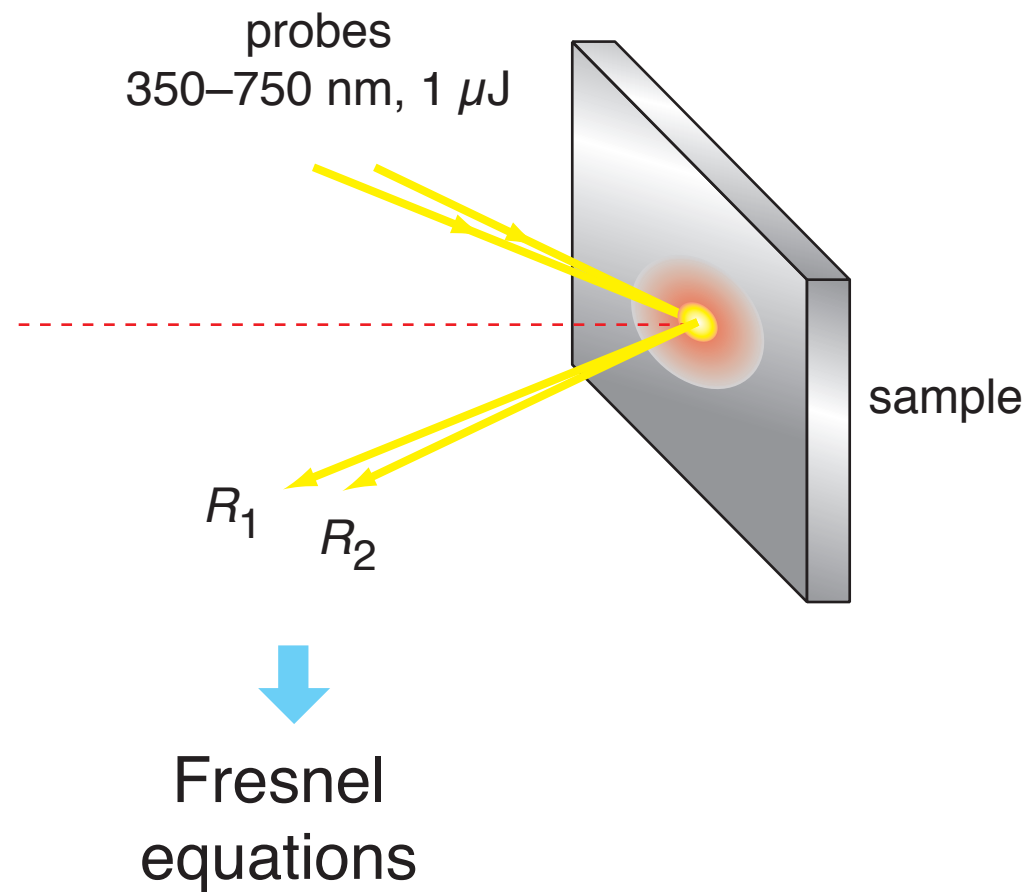
Transient band structure changes

time-resolved dual-angle reflectometry



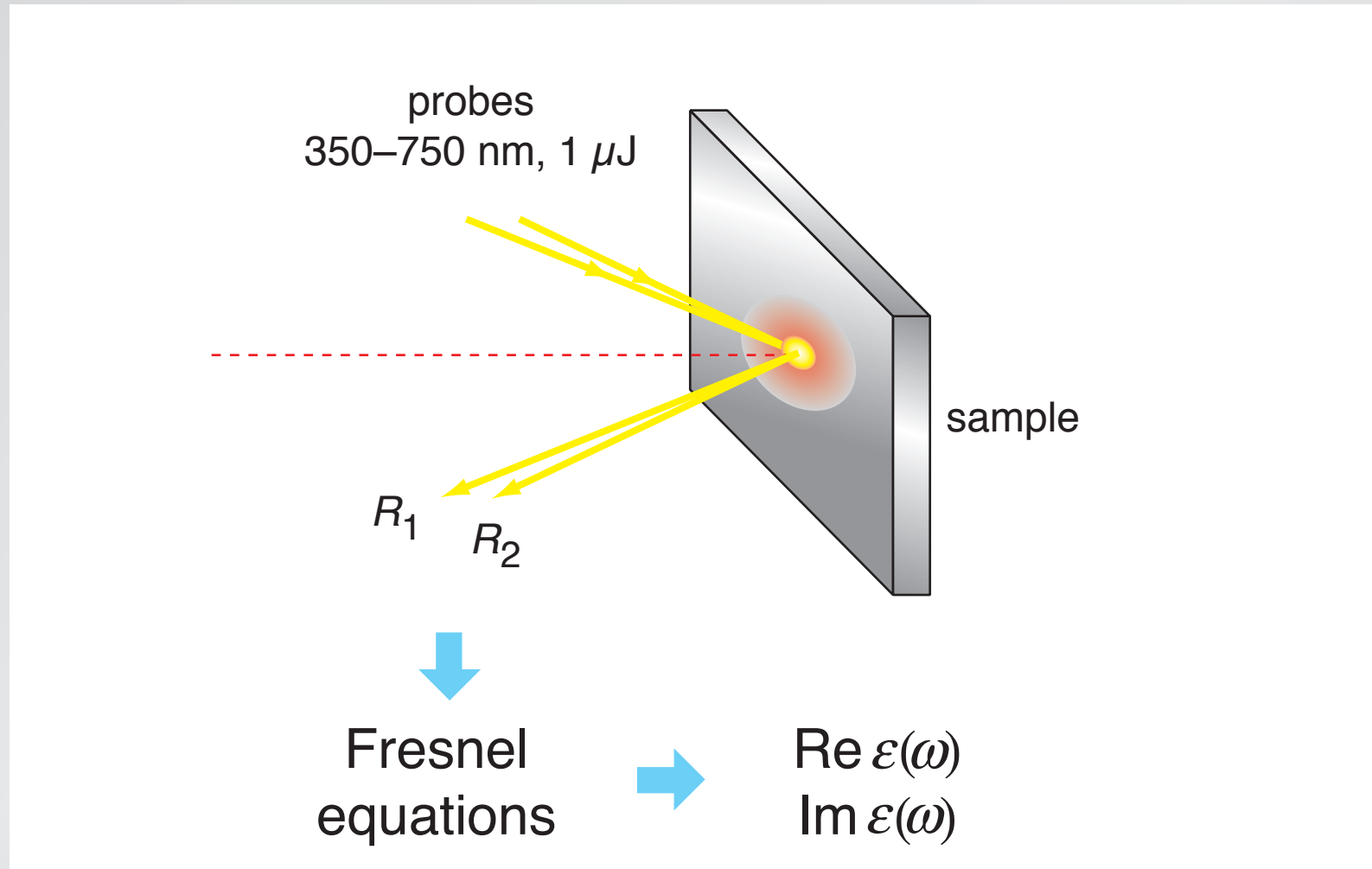
Transient band structure changes

time-resolved dual-angle reflectometry

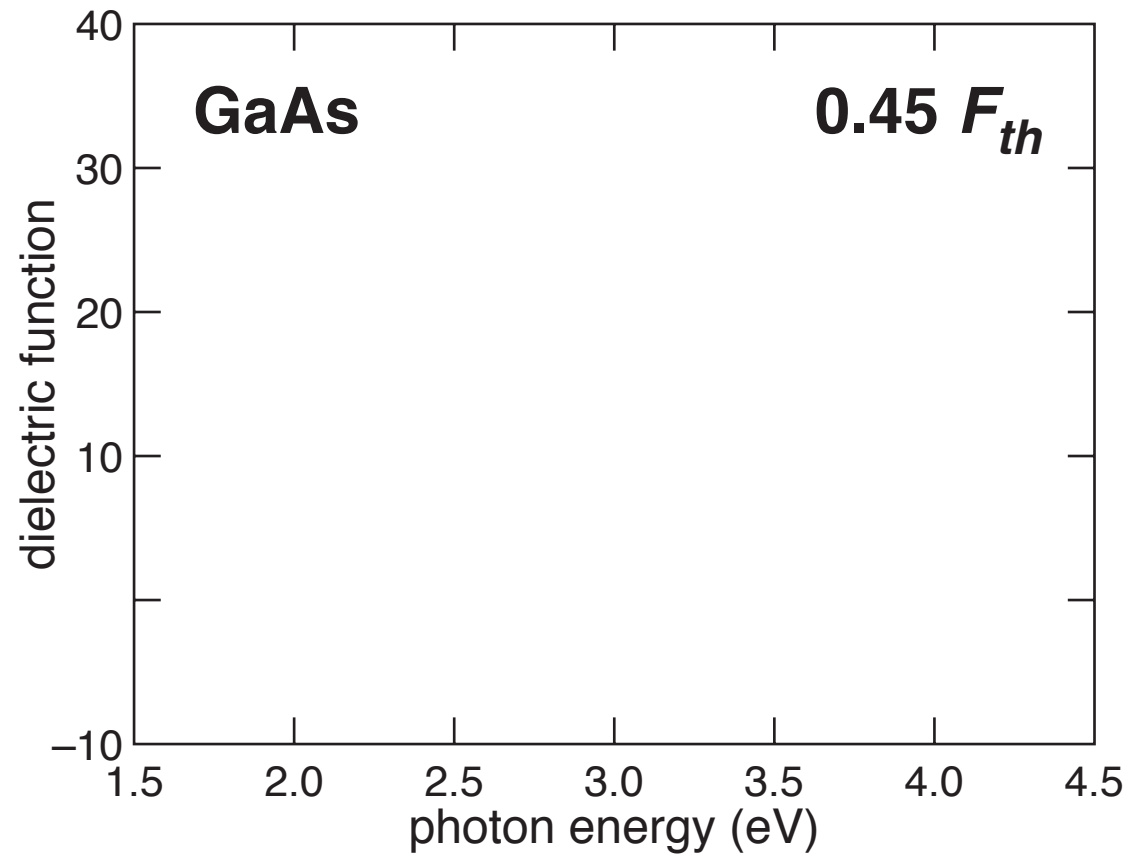


Transient band structure changes

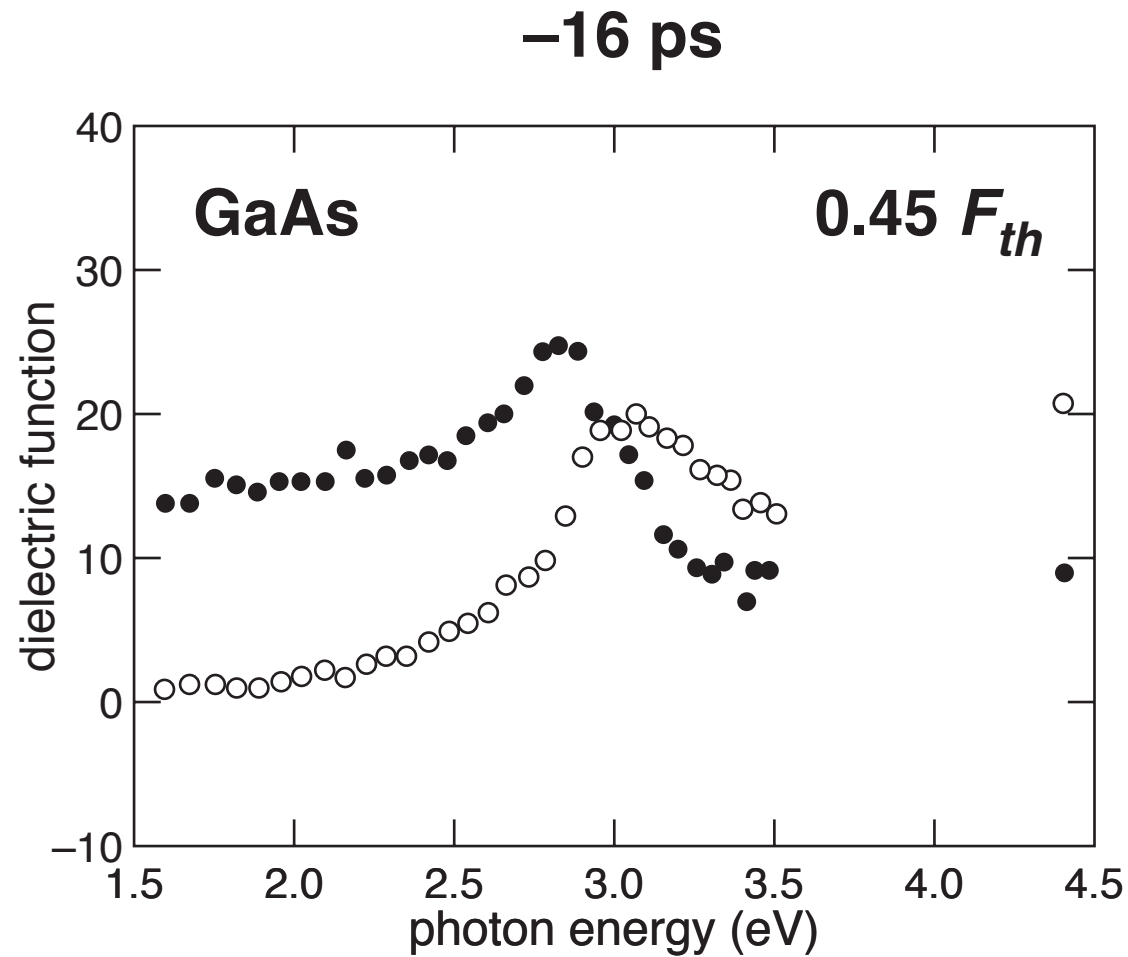
time-resolved dual-angle reflectometry



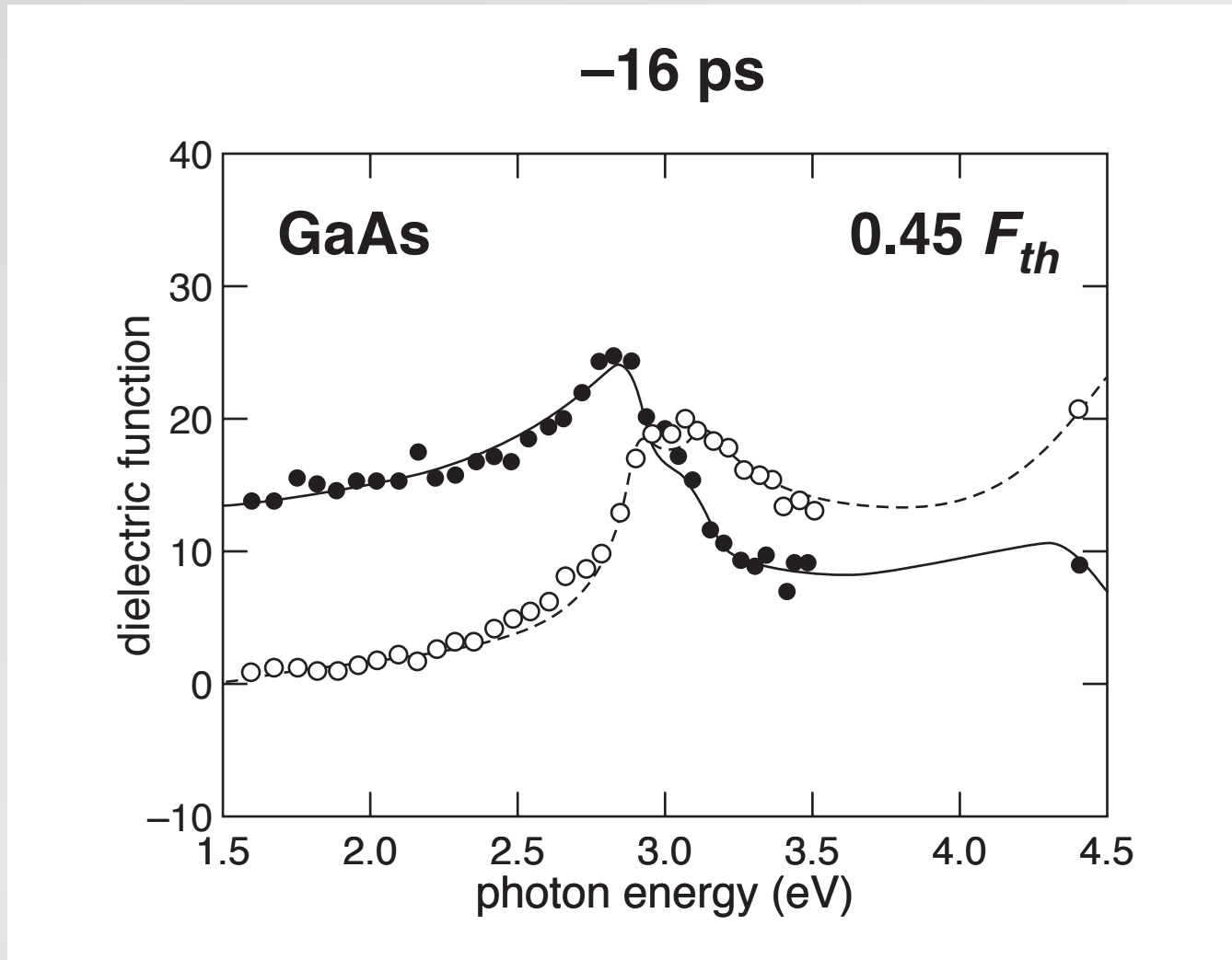
Transient band structure changes



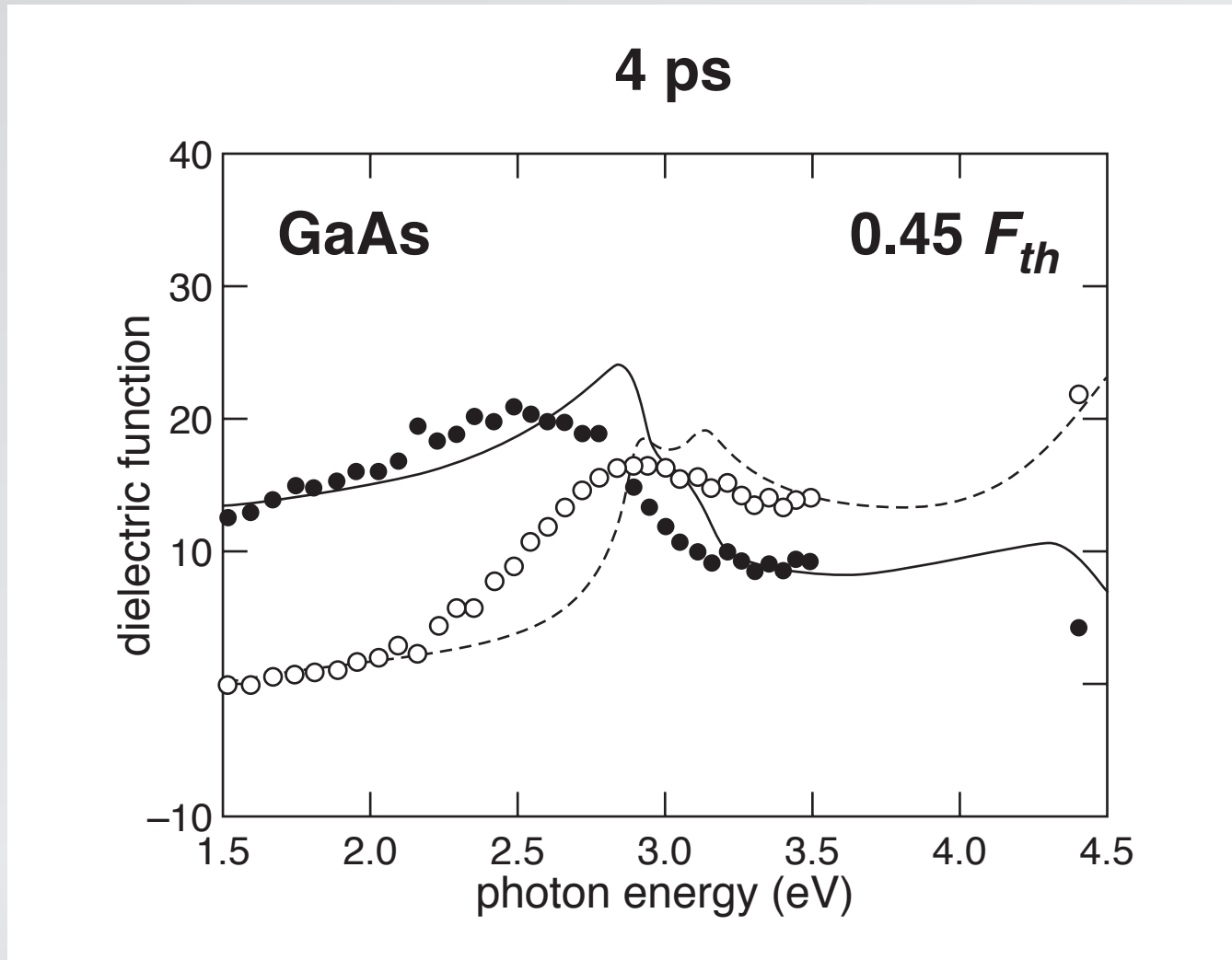
Transient band structure changes



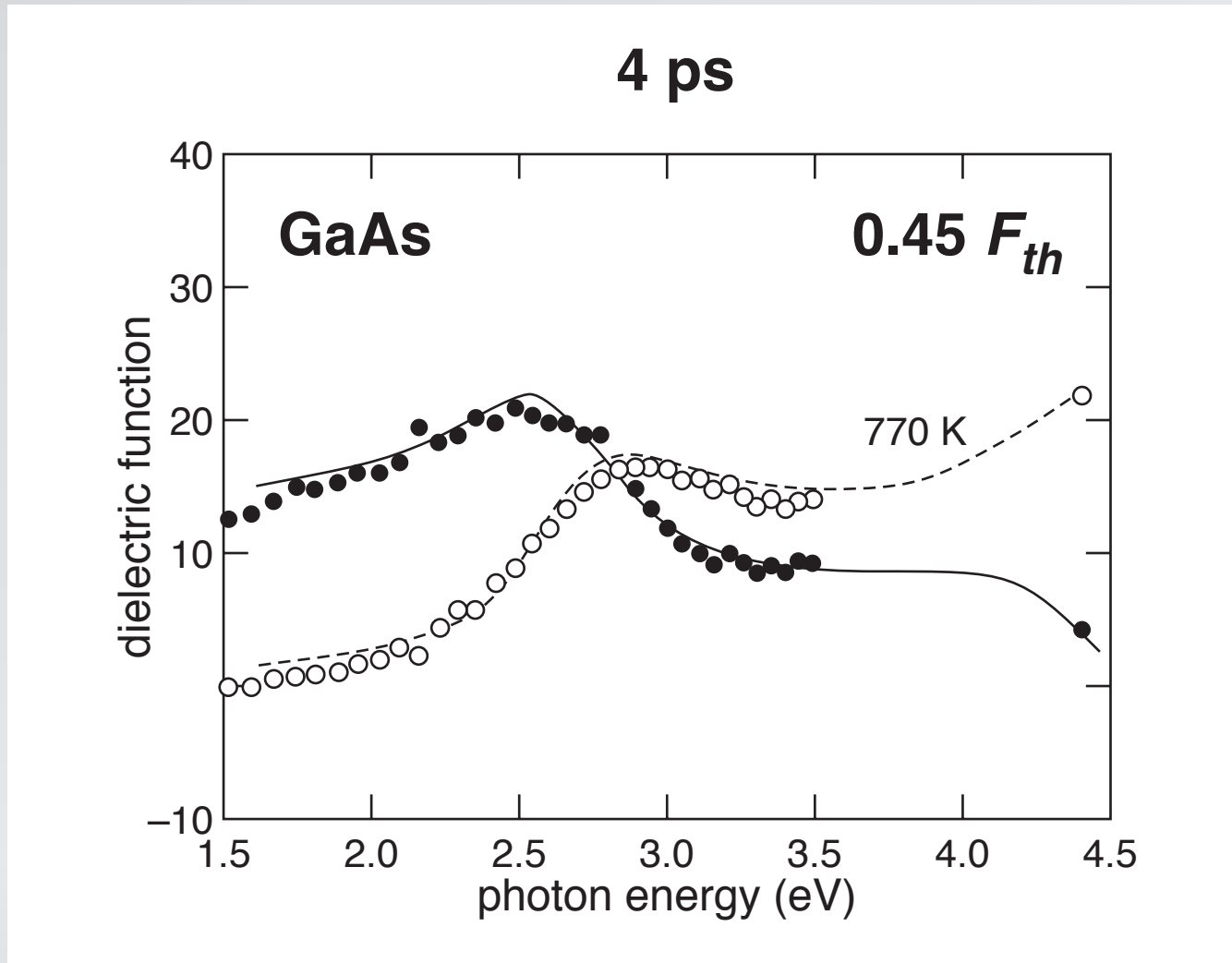
Transient band structure changes



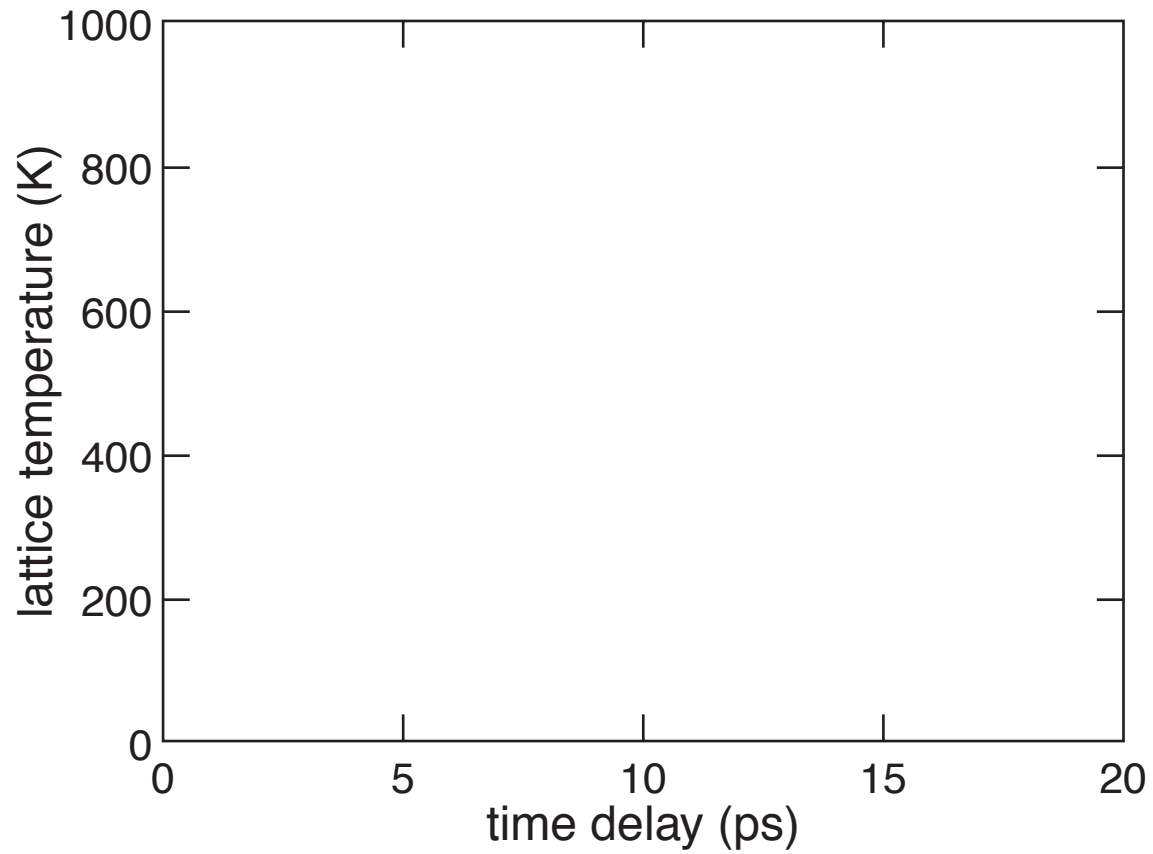
Transient band structure changes



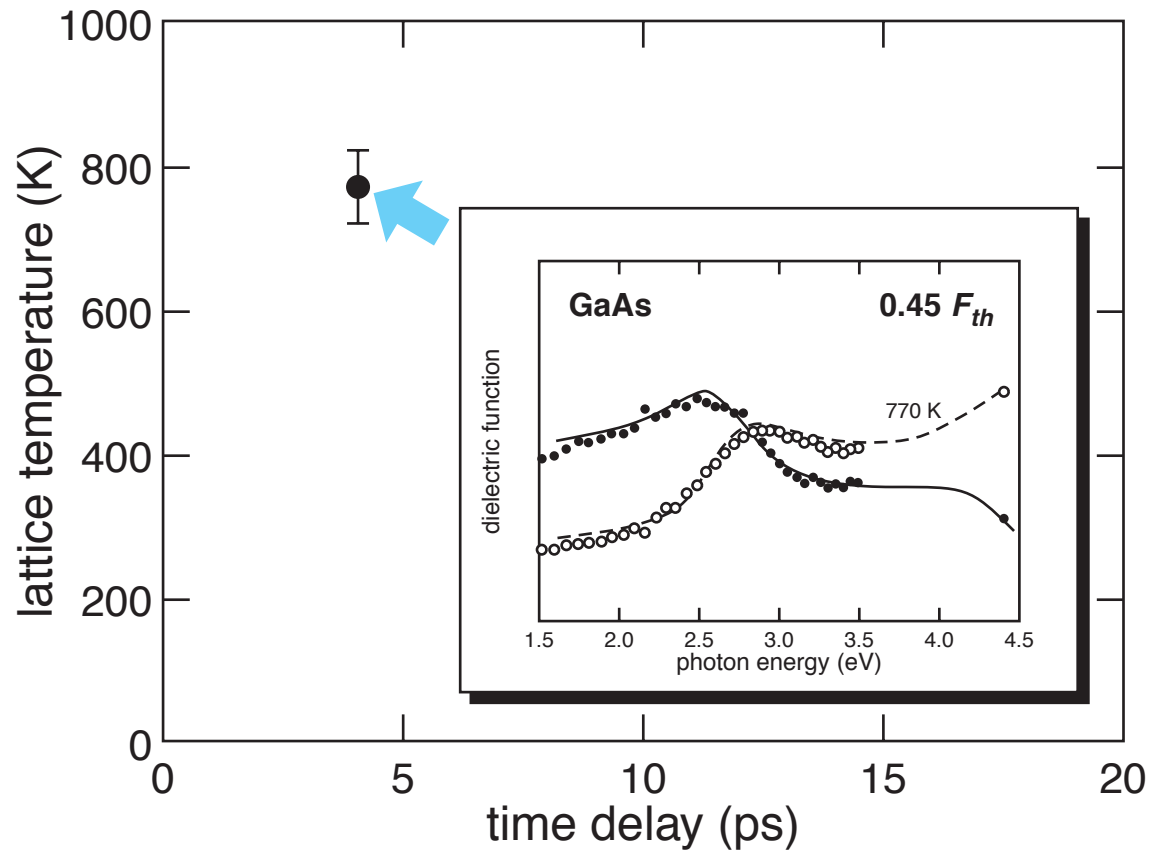
Transient band structure changes



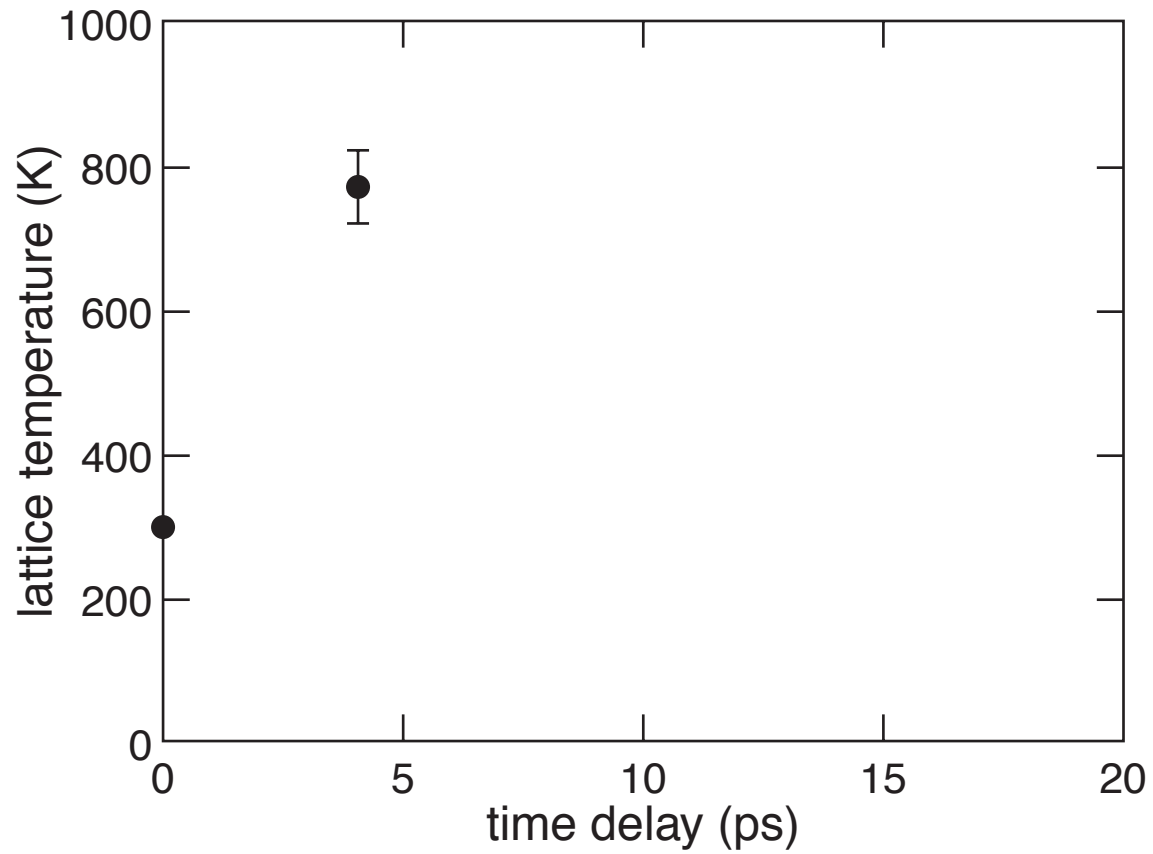
Transient band structure changes



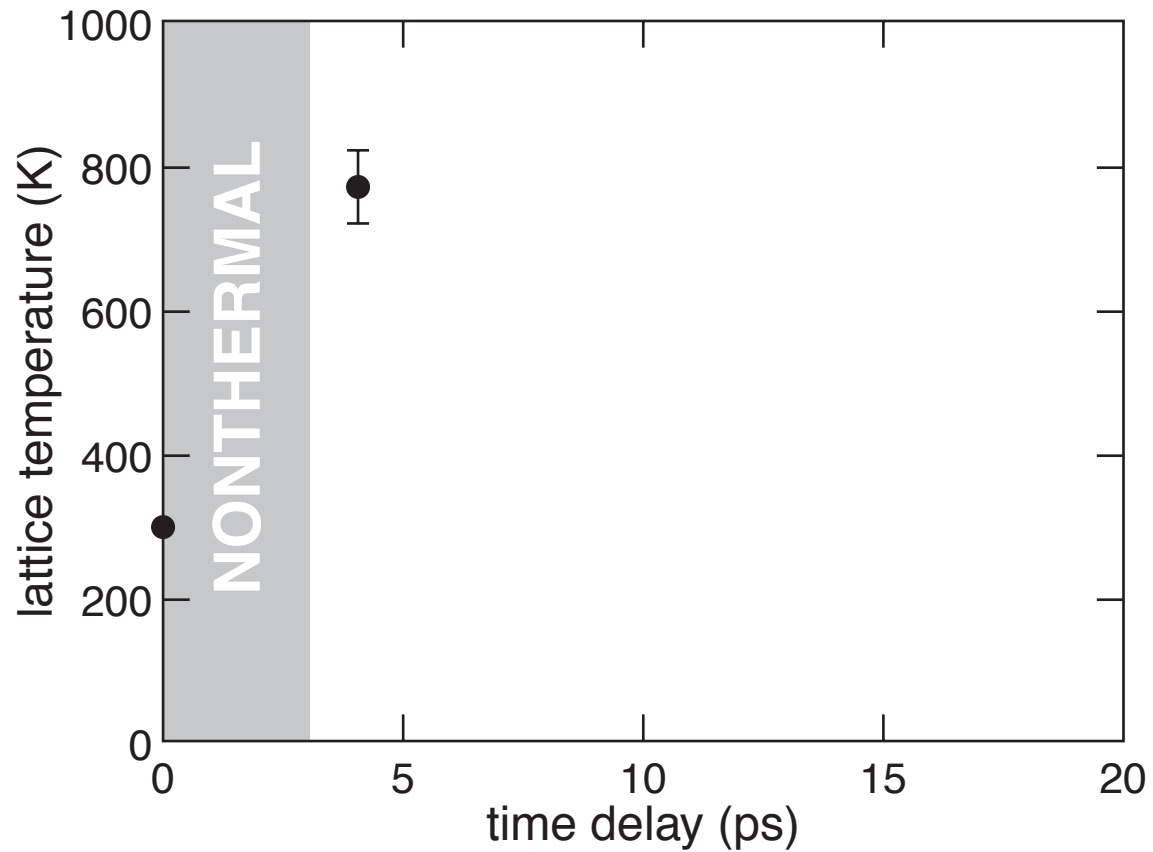
Transient band structure changes



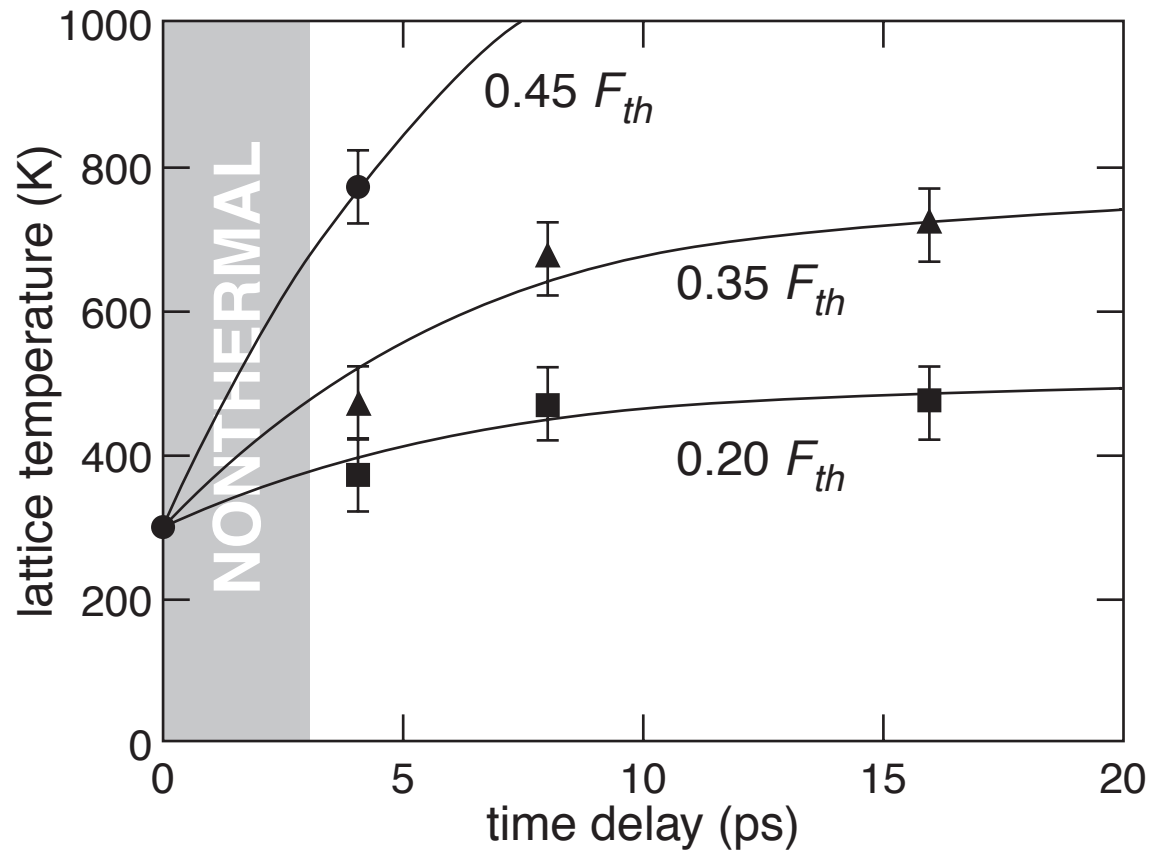
Transient band structure changes



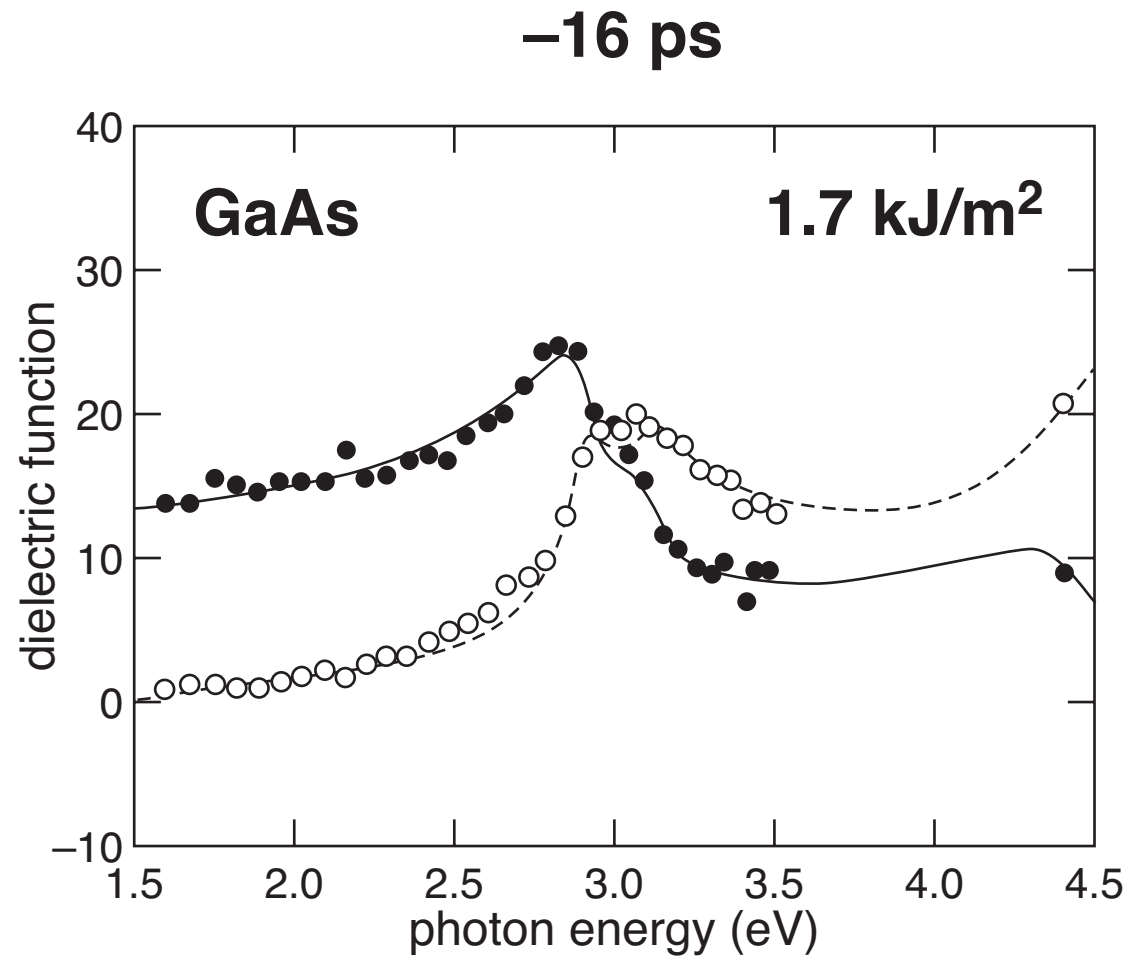
Transient band structure changes



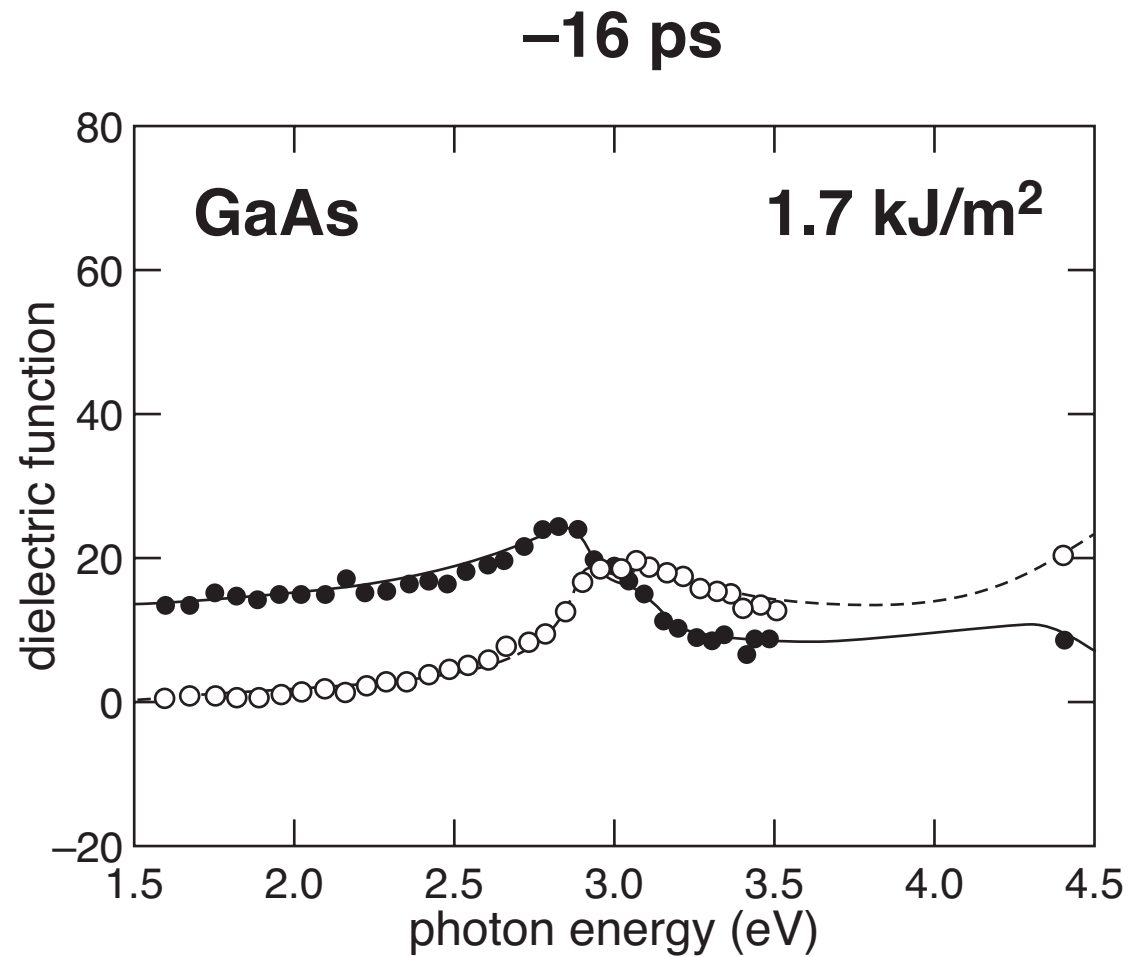
Transient band structure changes



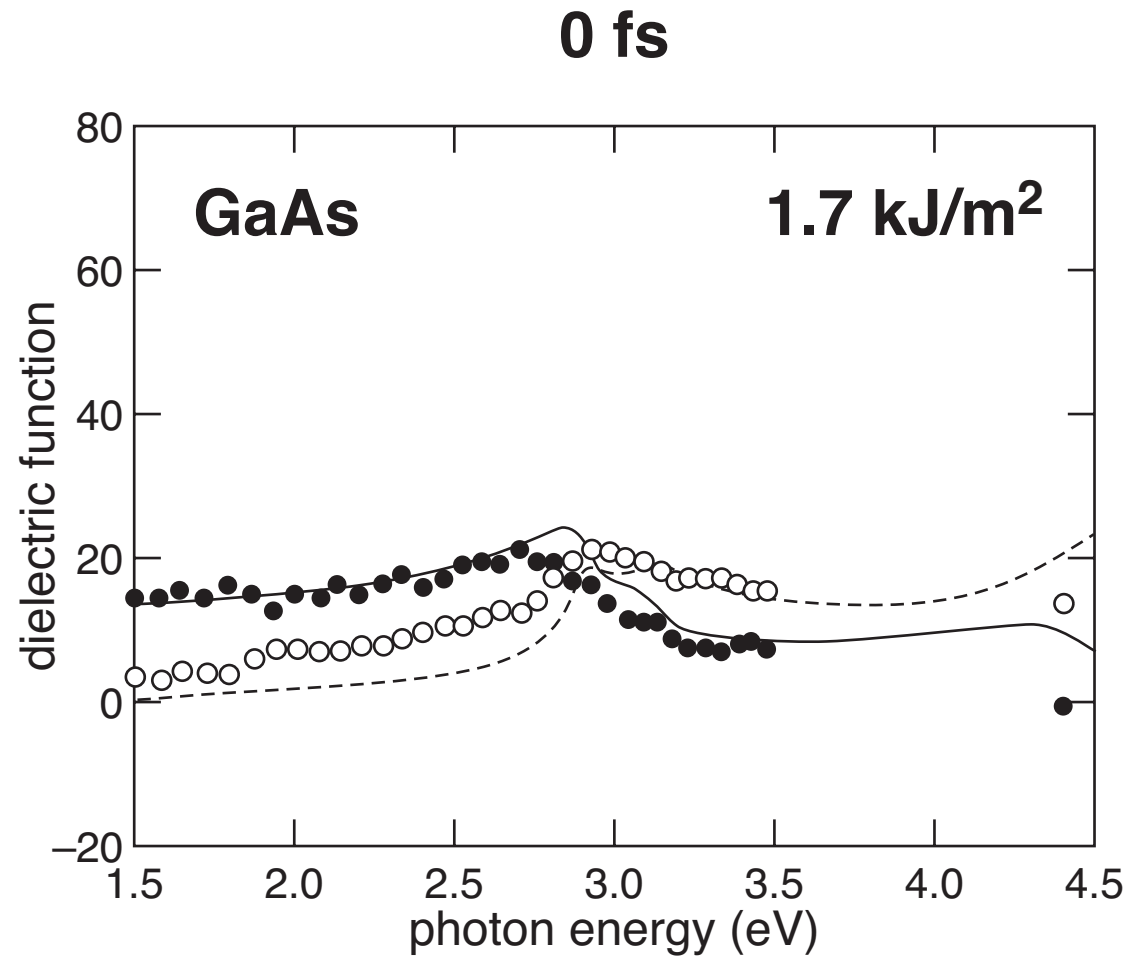
Transient band structure changes



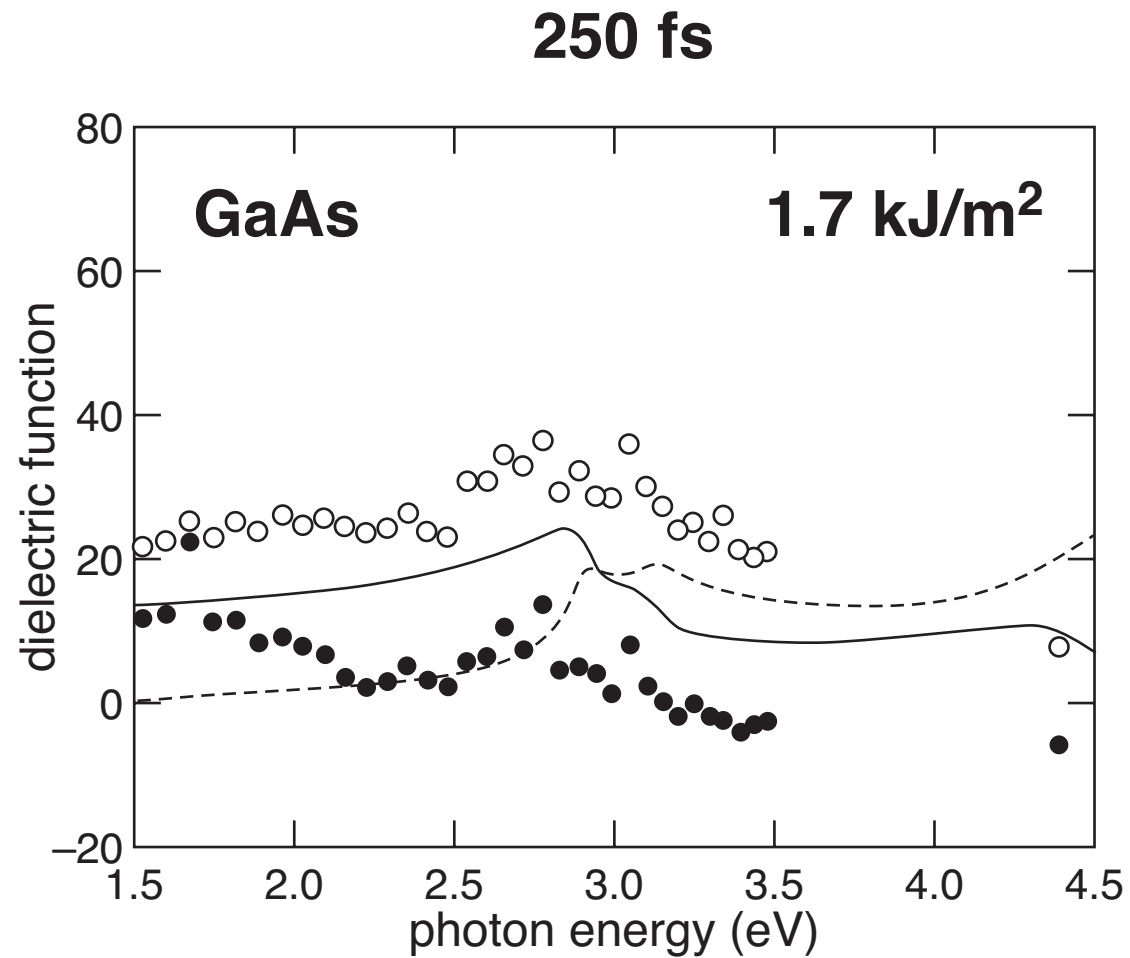
Transient band structure changes



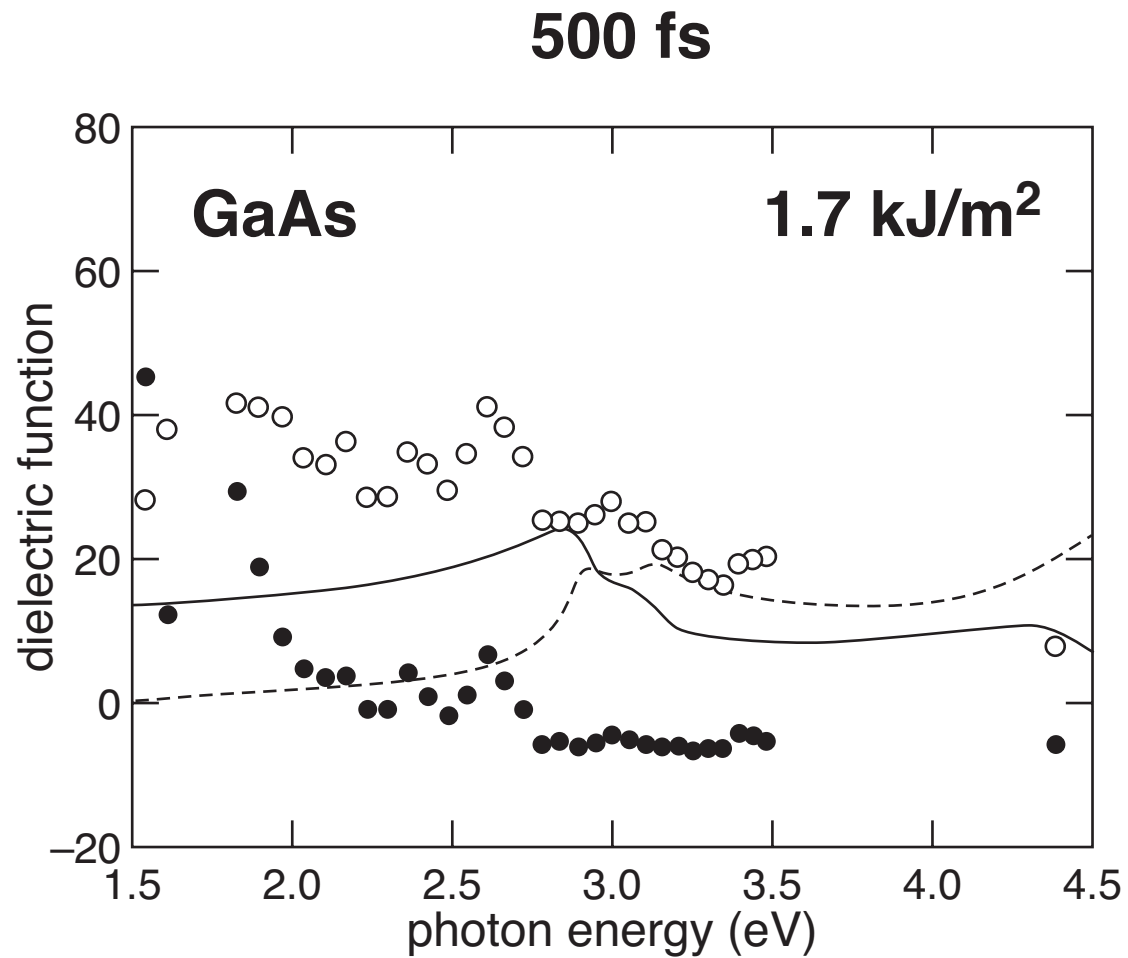
Transient band structure changes



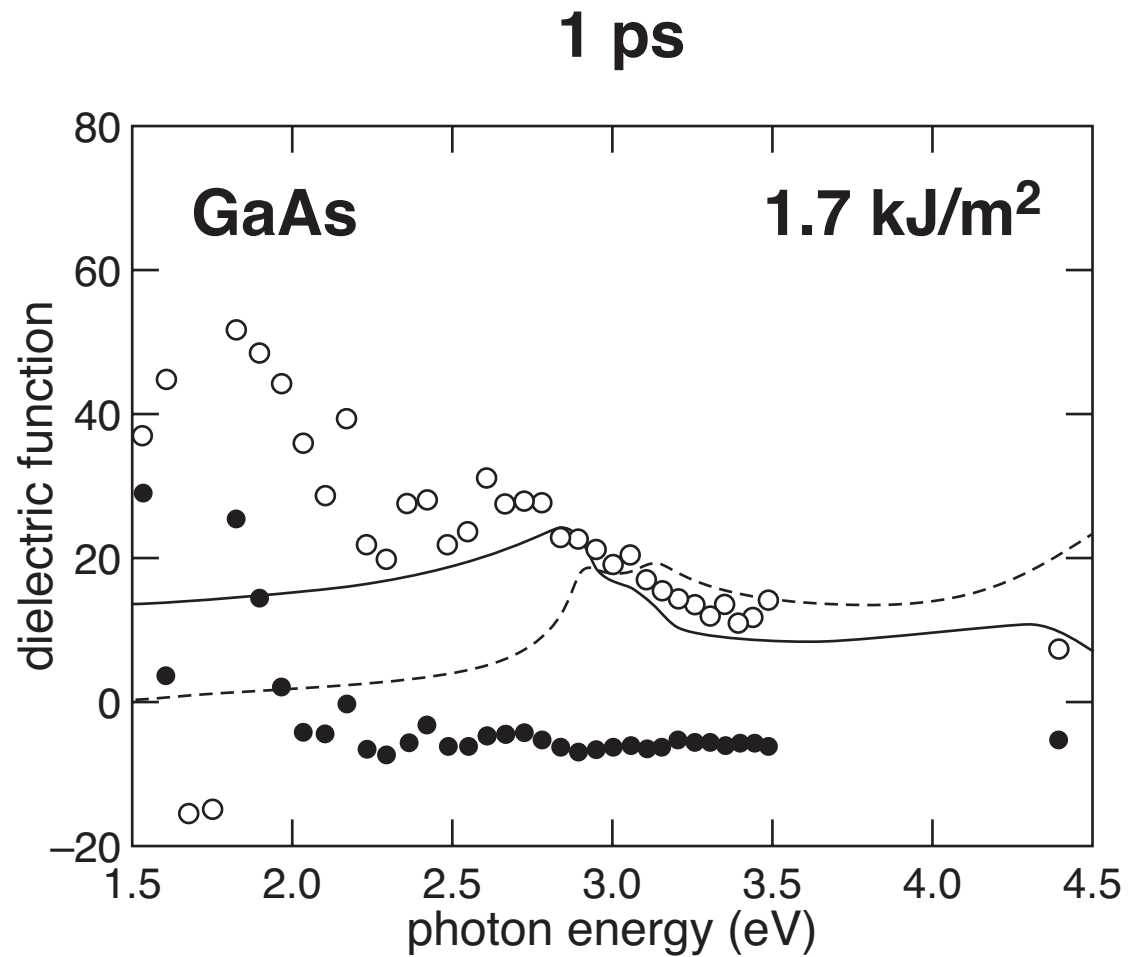
Transient band structure changes



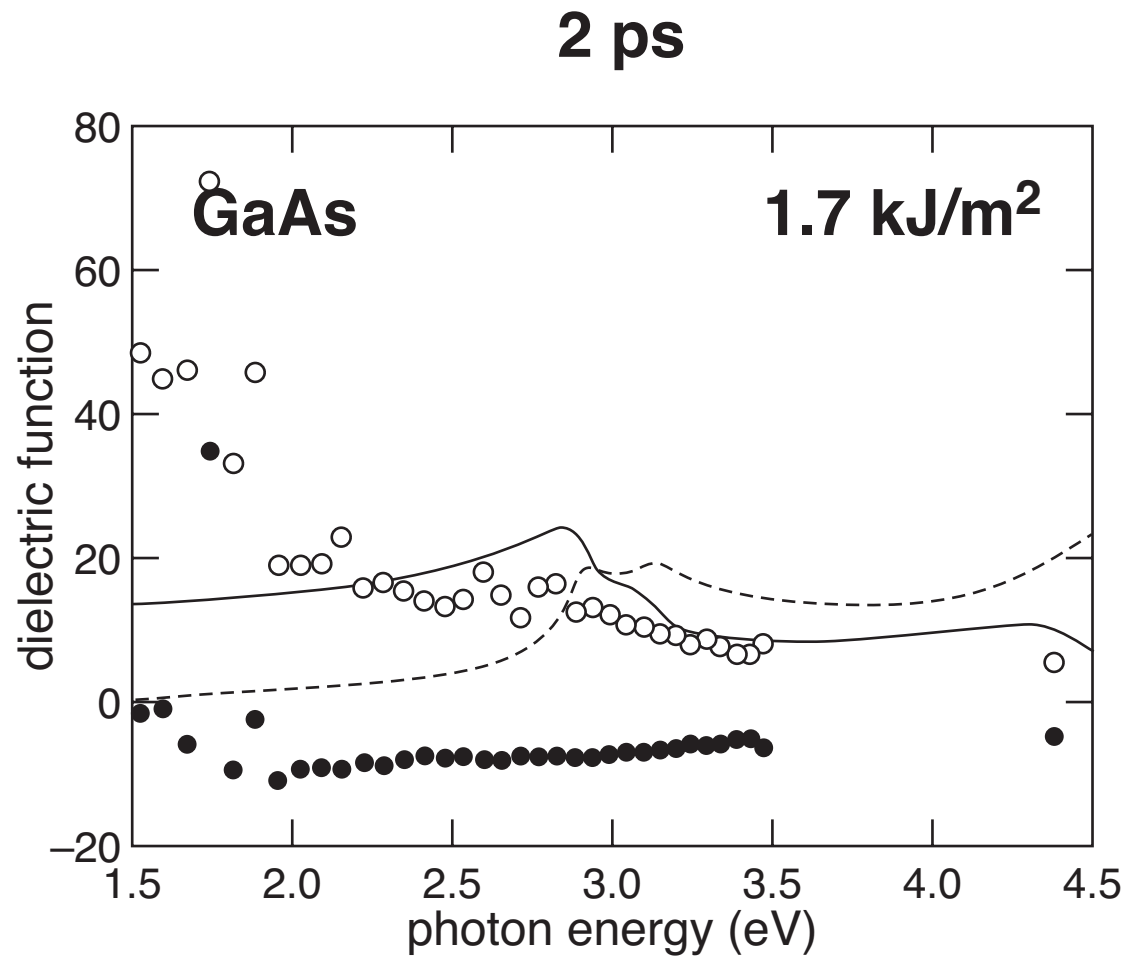
Transient band structure changes



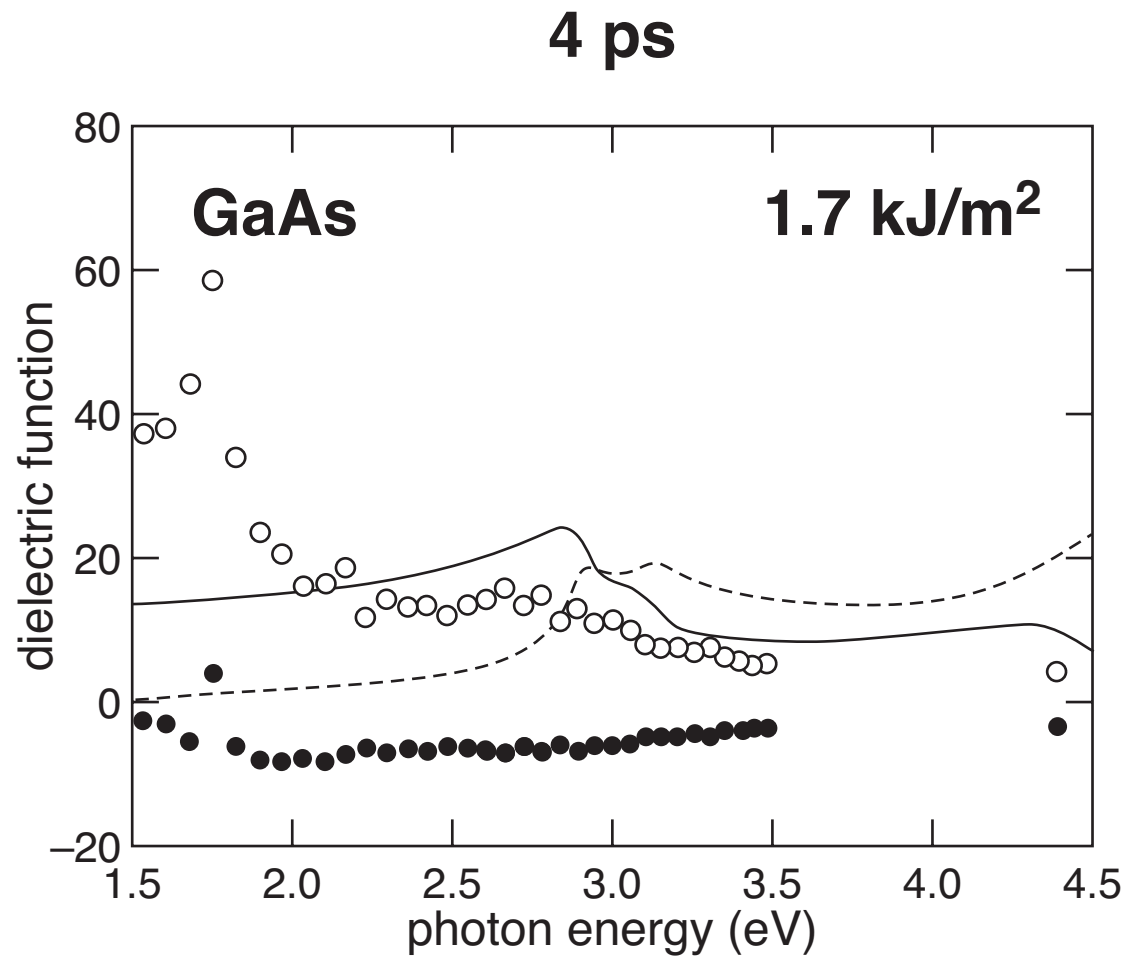
Transient band structure changes



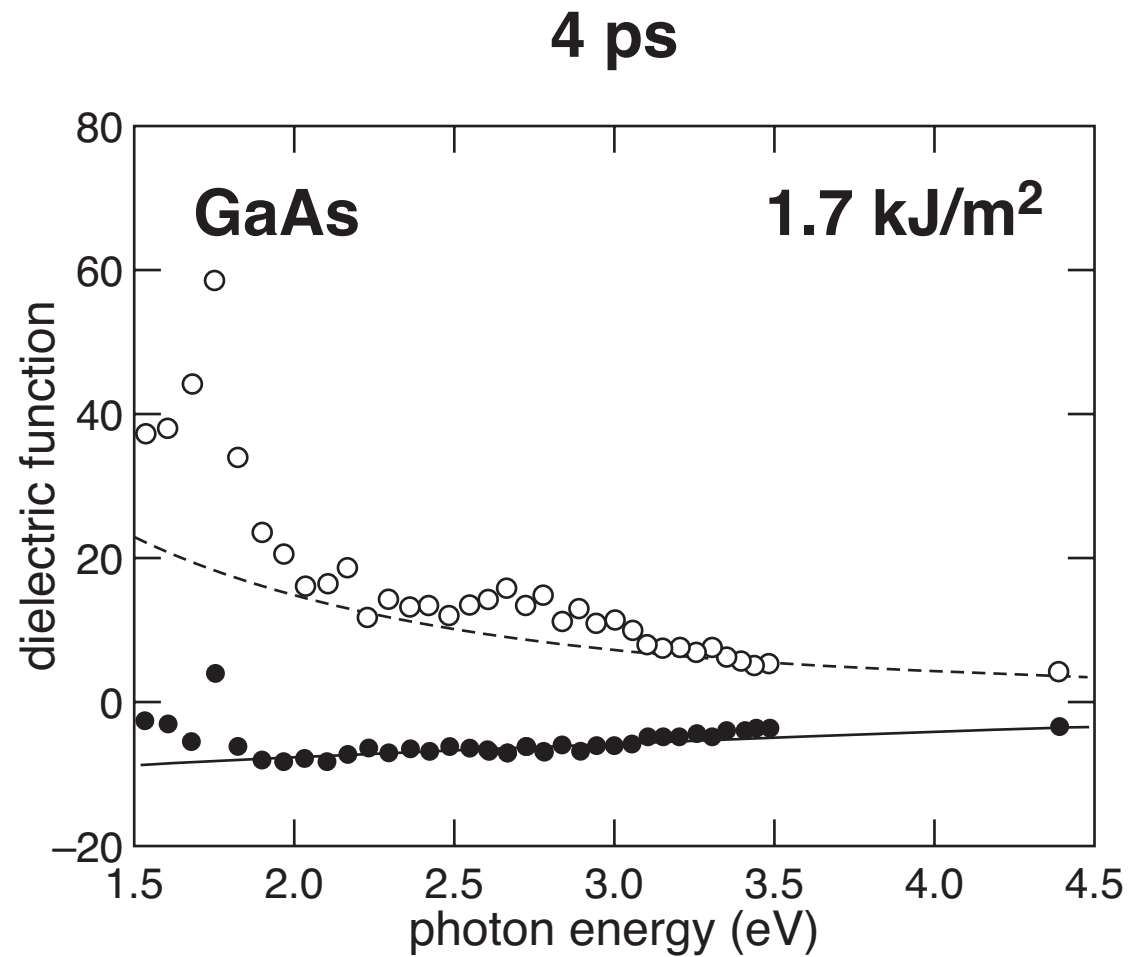
Transient band structure changes



Transient band structure changes



Transient band structure changes



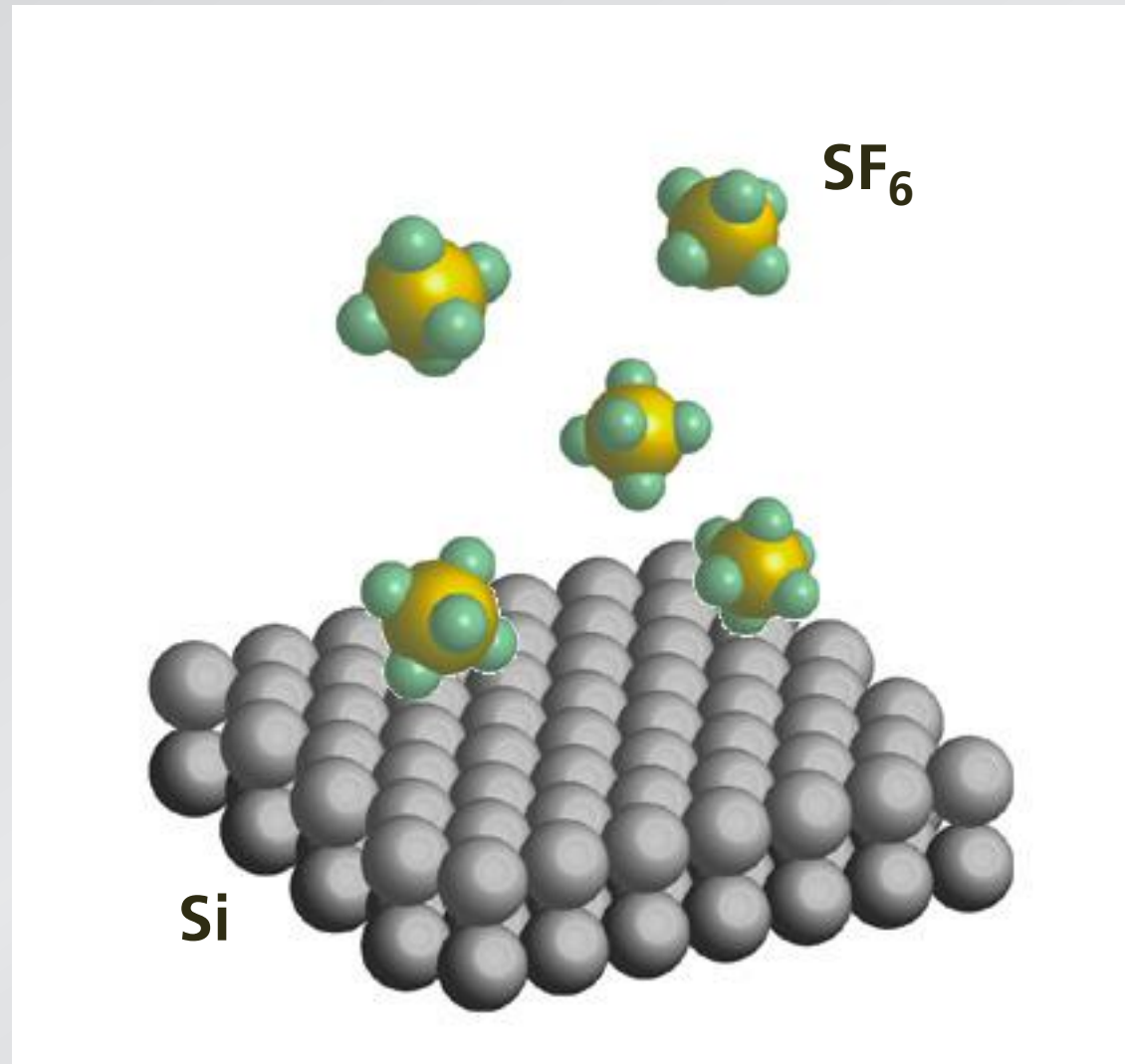
Transient band structure changes

can observe dielectric to metallic transition

Outline

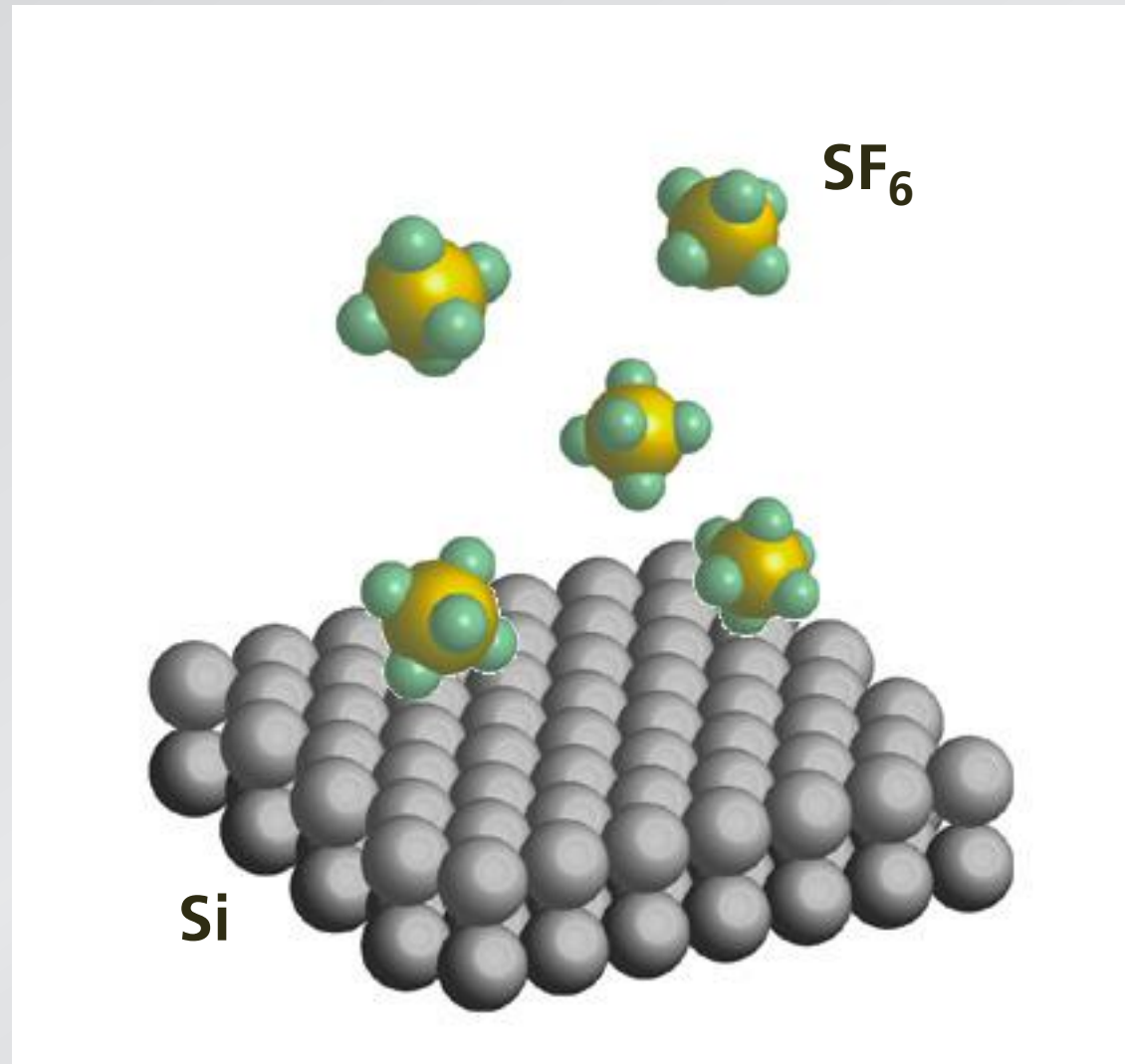
- **transient band structure changes**
- **creating an intermediate band**
- **semiconductor to metal transition**

Creating intermediate band



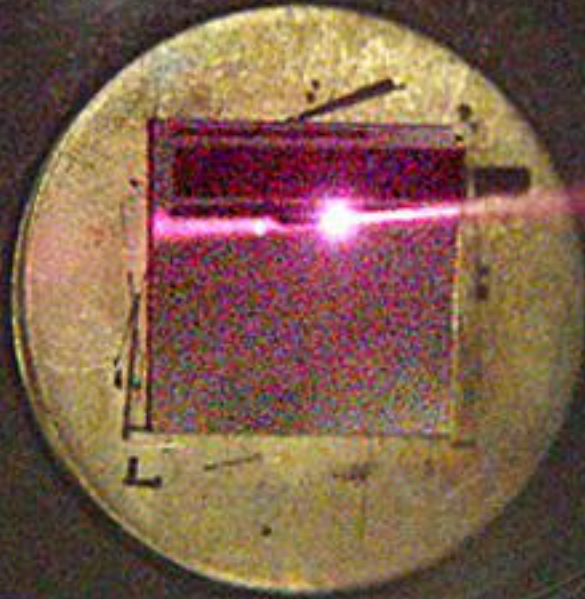
capturing dopants with fs pulses

Creating intermediate band



irradiate with 100-fs 10 kJ/m² pulses

Creating intermediate band

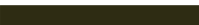


Creating intermediate band



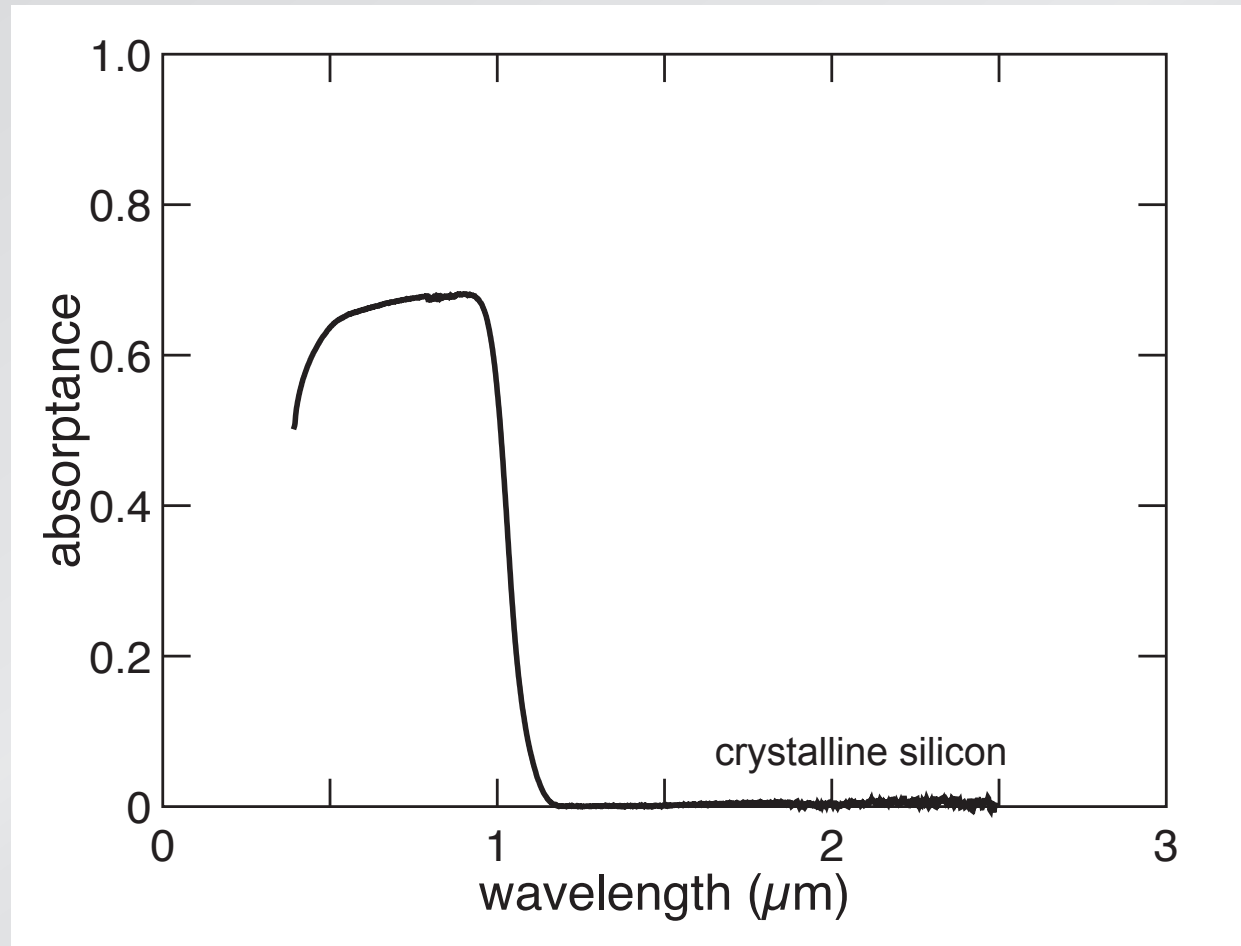
Creating intermediate band

3 μm



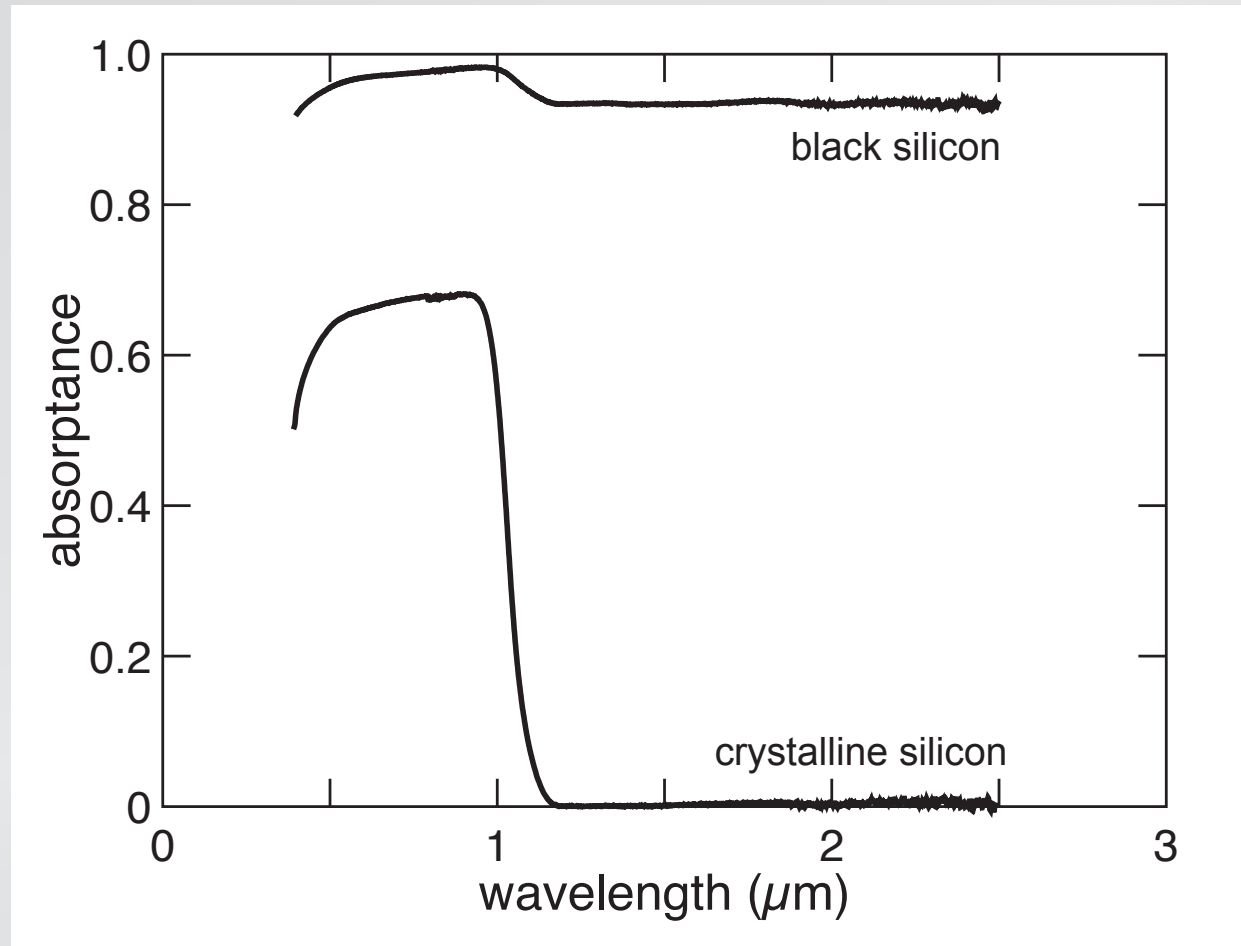
Creating intermediate band

absorptance ($1 - R_{int} - T_{int}$)

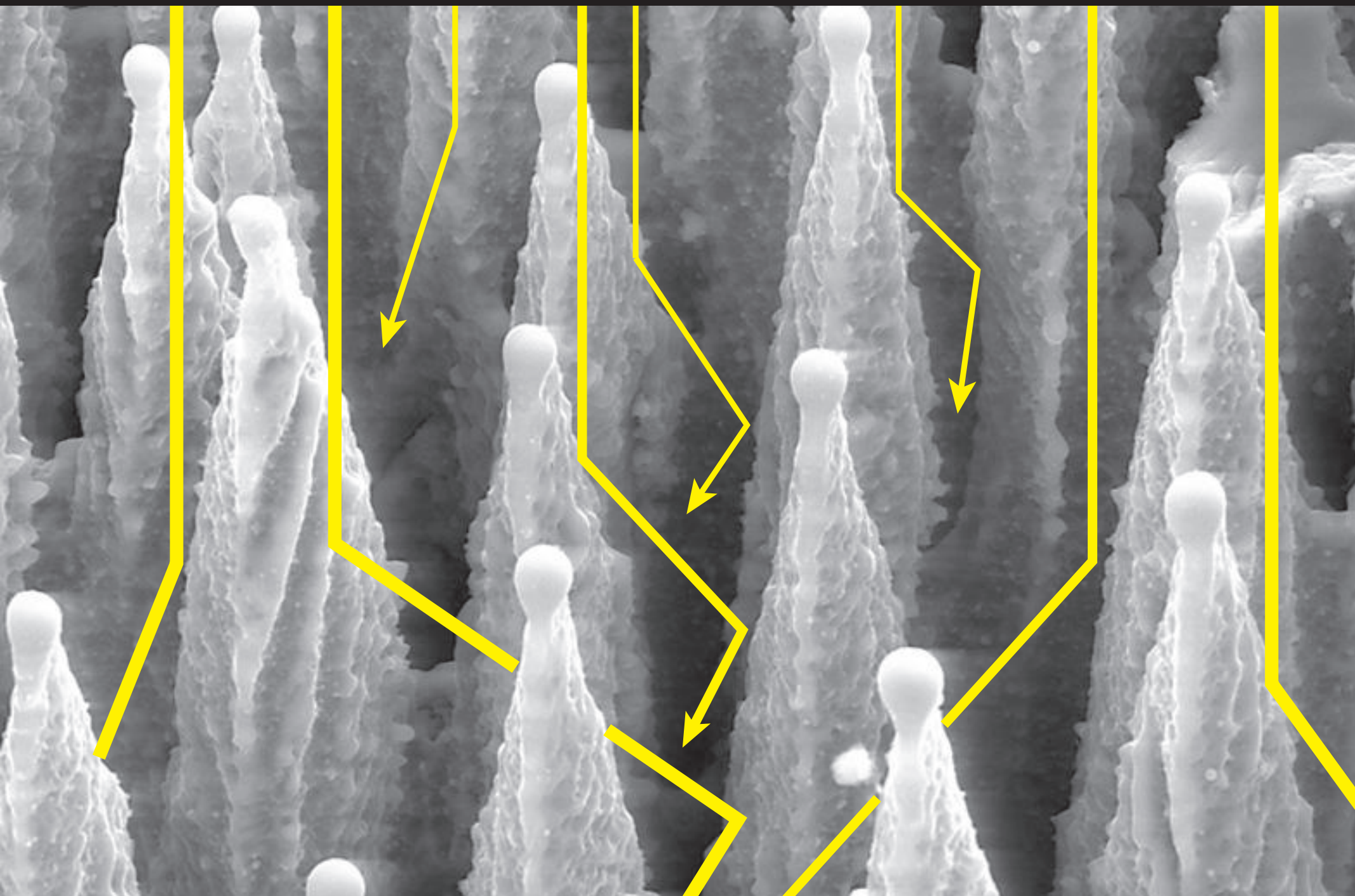


Creating intermediate band

absorptance $(1 - R_{int} - T_{int})$

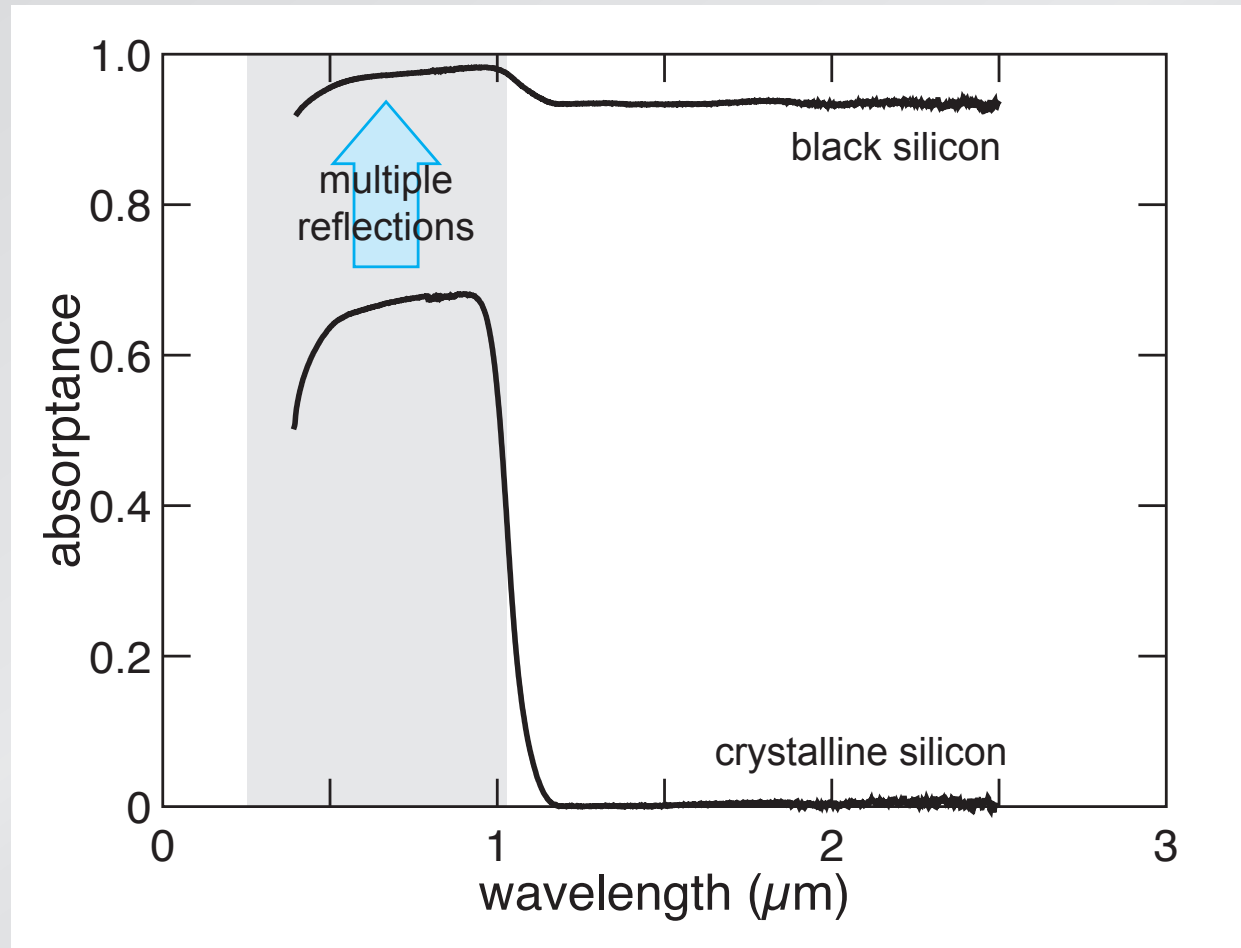


Creating intermediate band



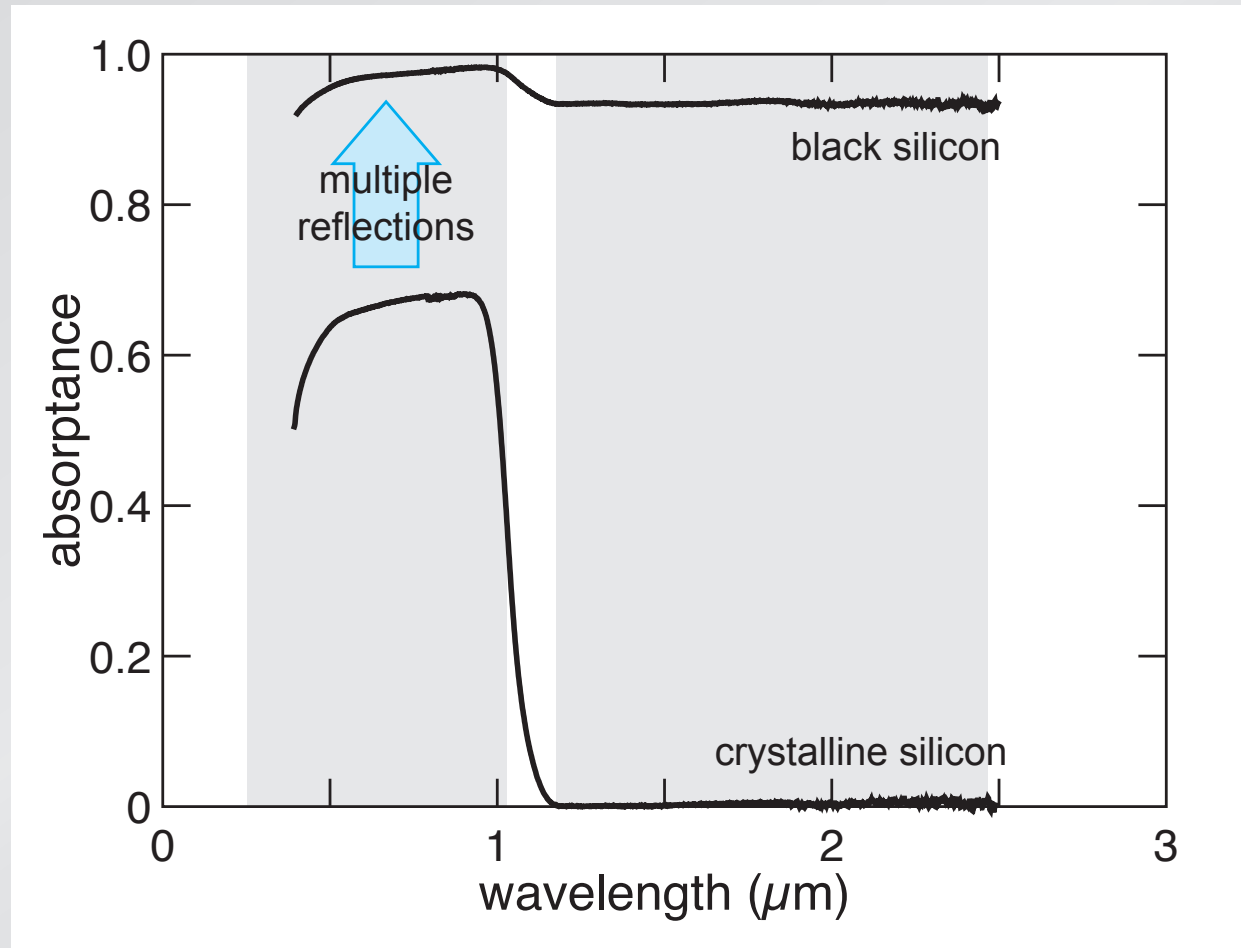
Creating intermediate band

absorptance $(1 - R_{int} - T_{int})$



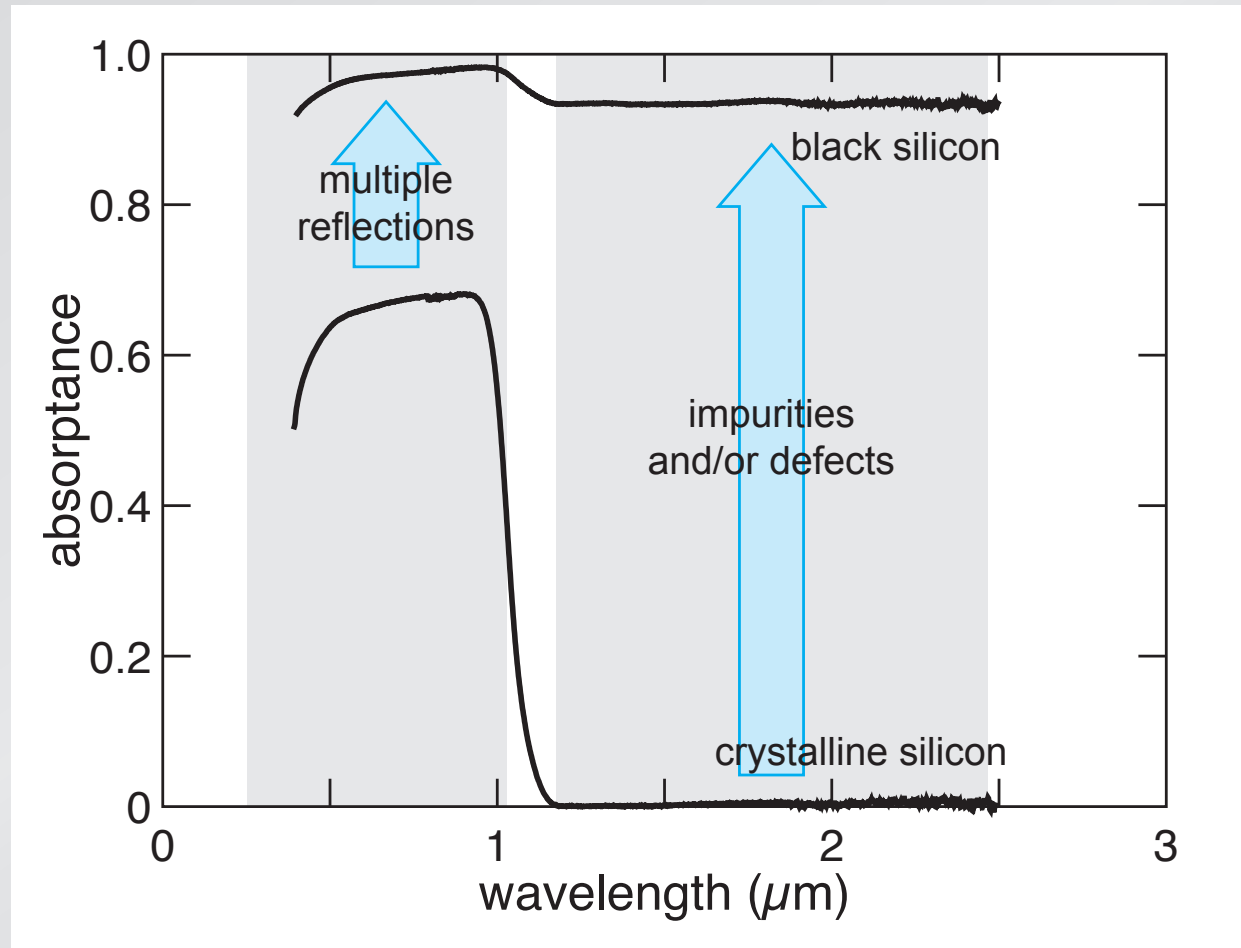
Creating intermediate band

absorptance ($1 - R_{int} - T_{int}$)



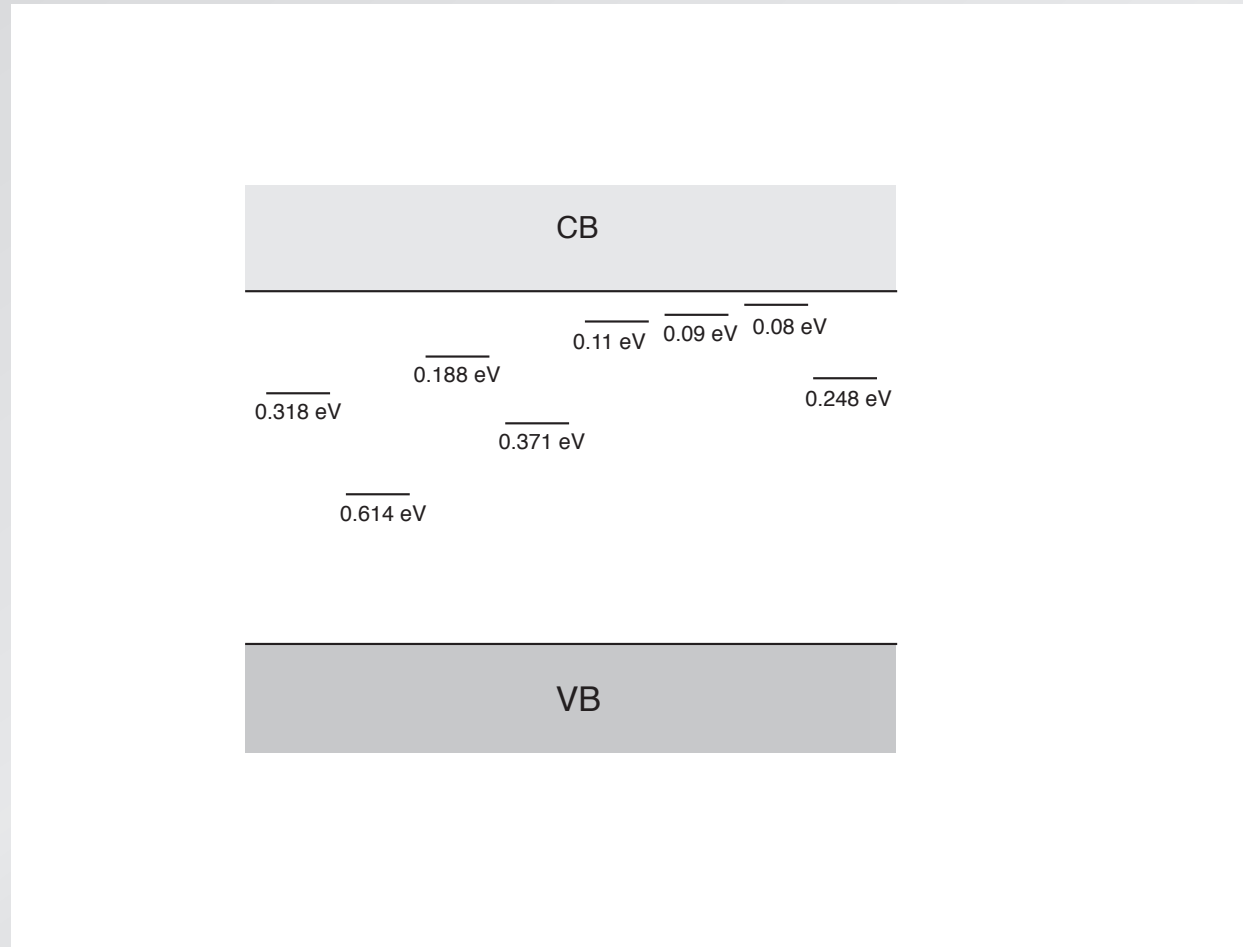
Creating intermediate band

absorptance $(1 - R_{int} - T_{int})$



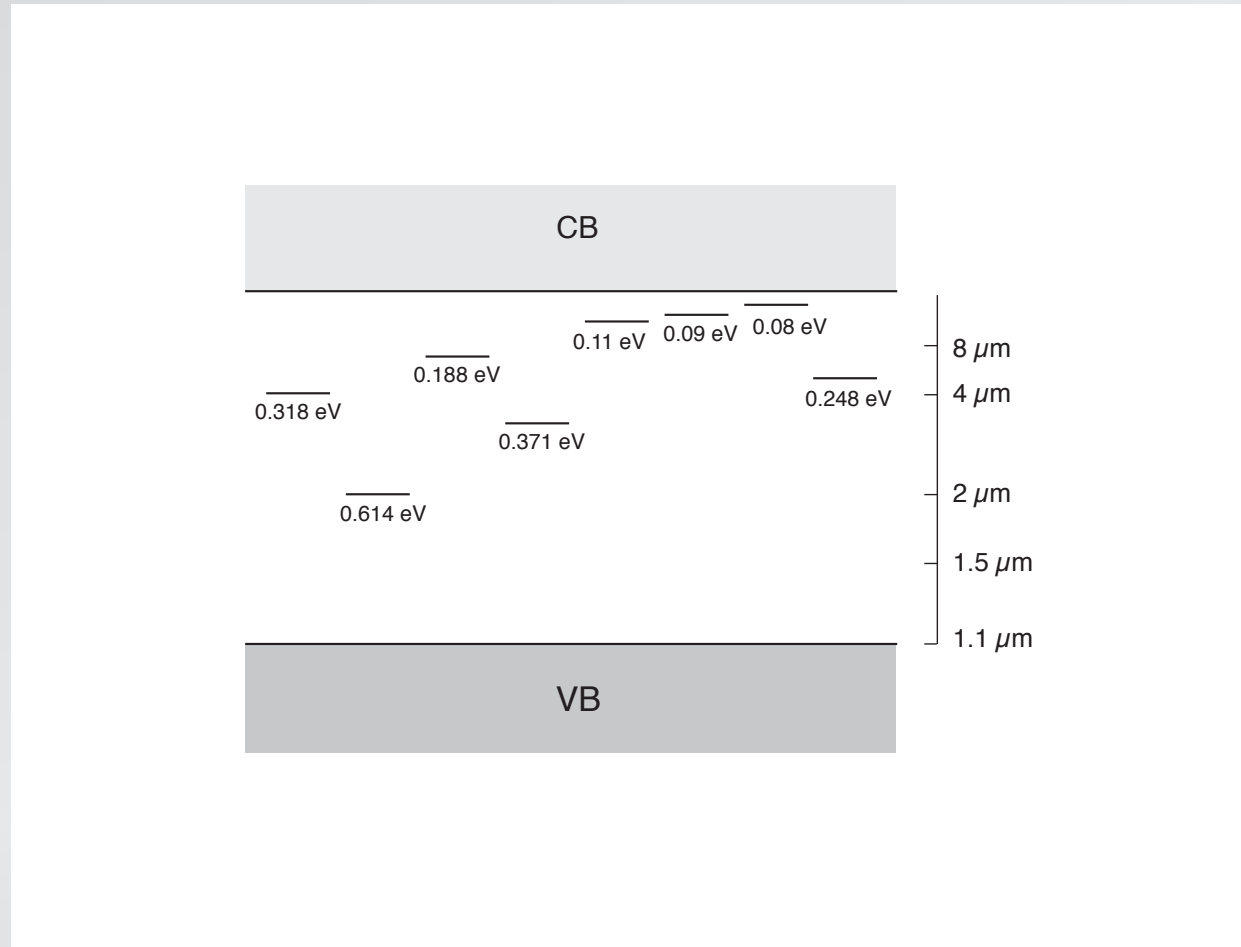
Creating intermediate band

1 part in 10^6 sulfur introduces donor states in gap



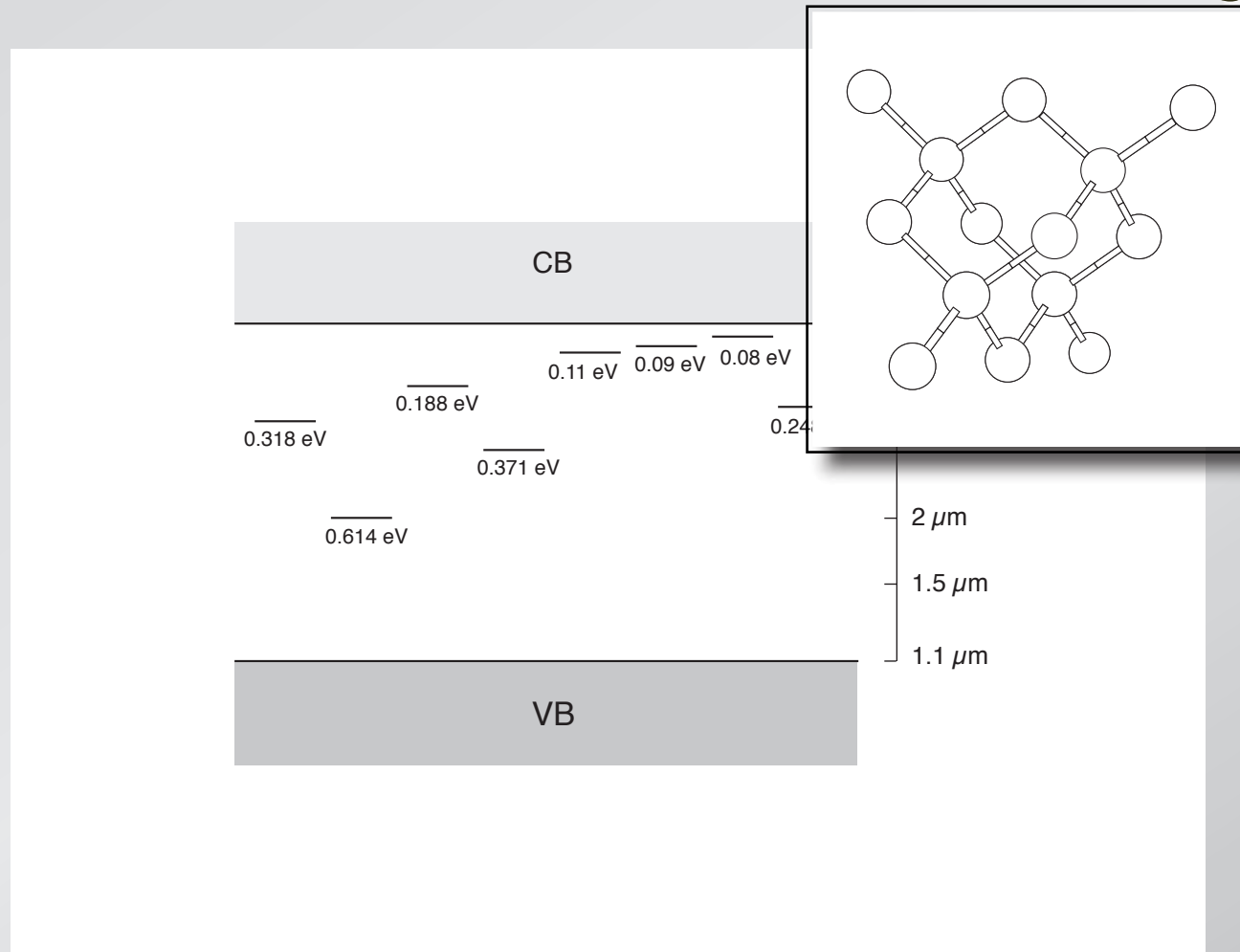
Creating intermediate band

1 part in 10^6 sulfur introduces donor states in gap



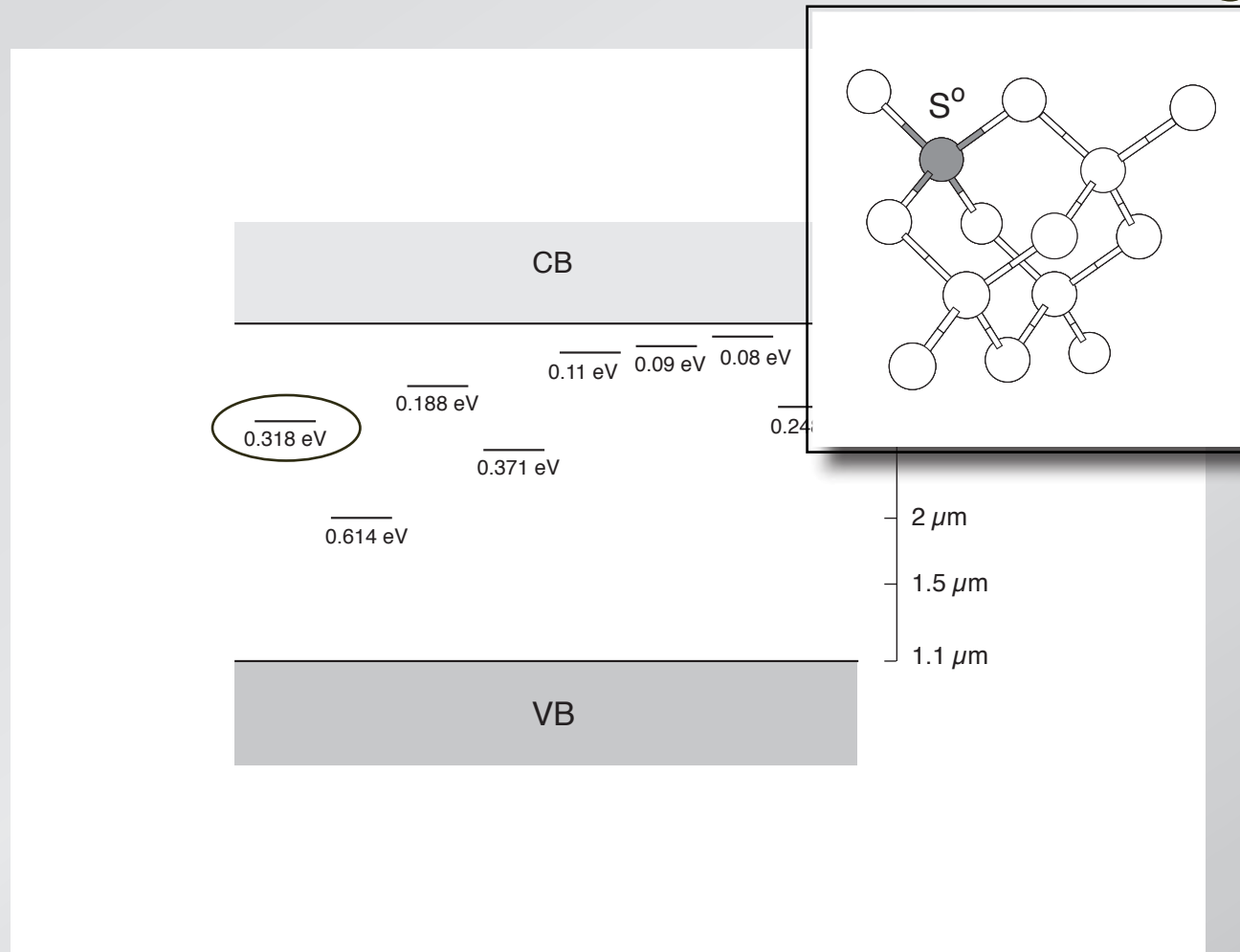
Creating intermediate band

1 part in 10^6 sulfur introduces donor states in gap



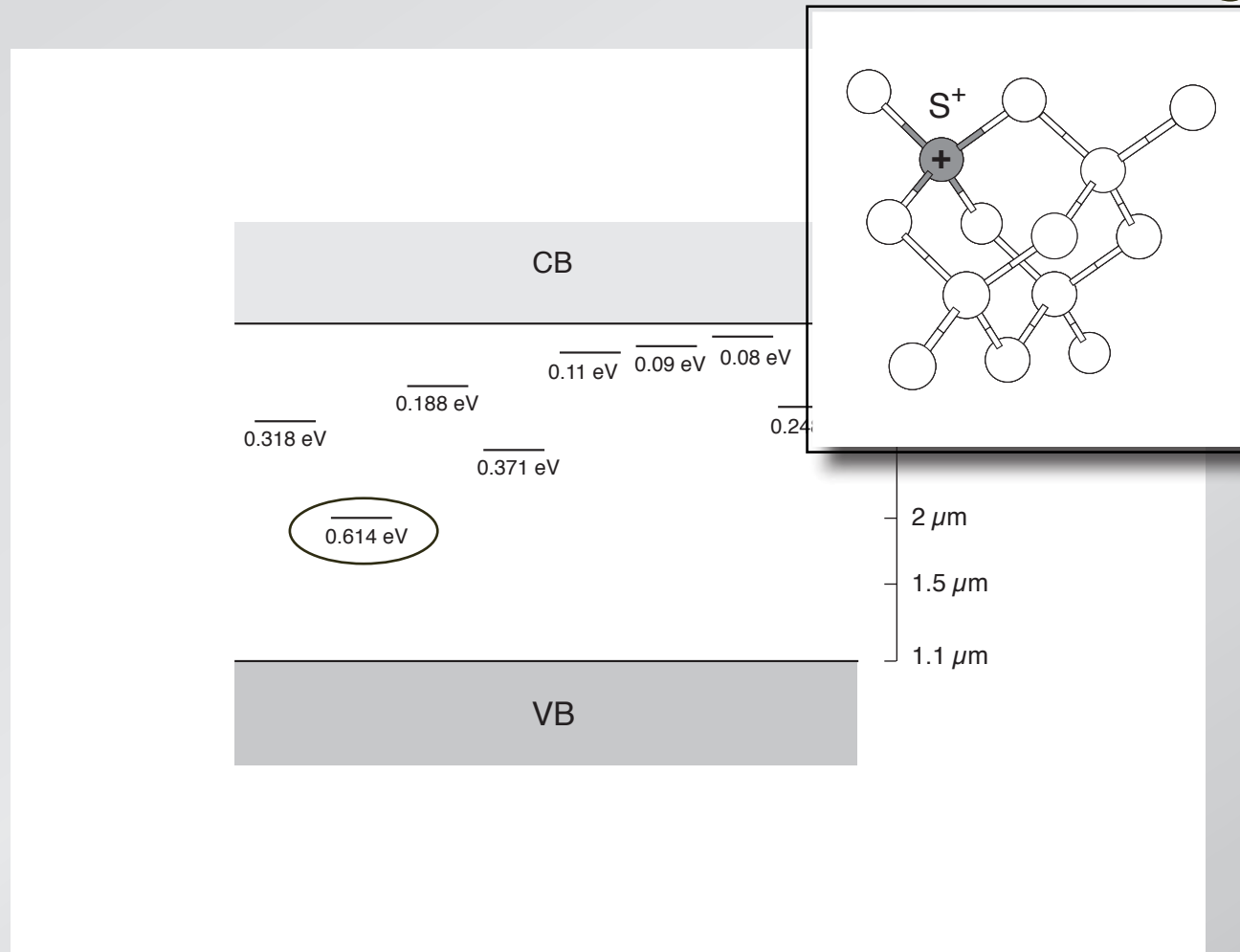
Creating intermediate band

1 part in 10^6 sulfur introduces donor states in gap



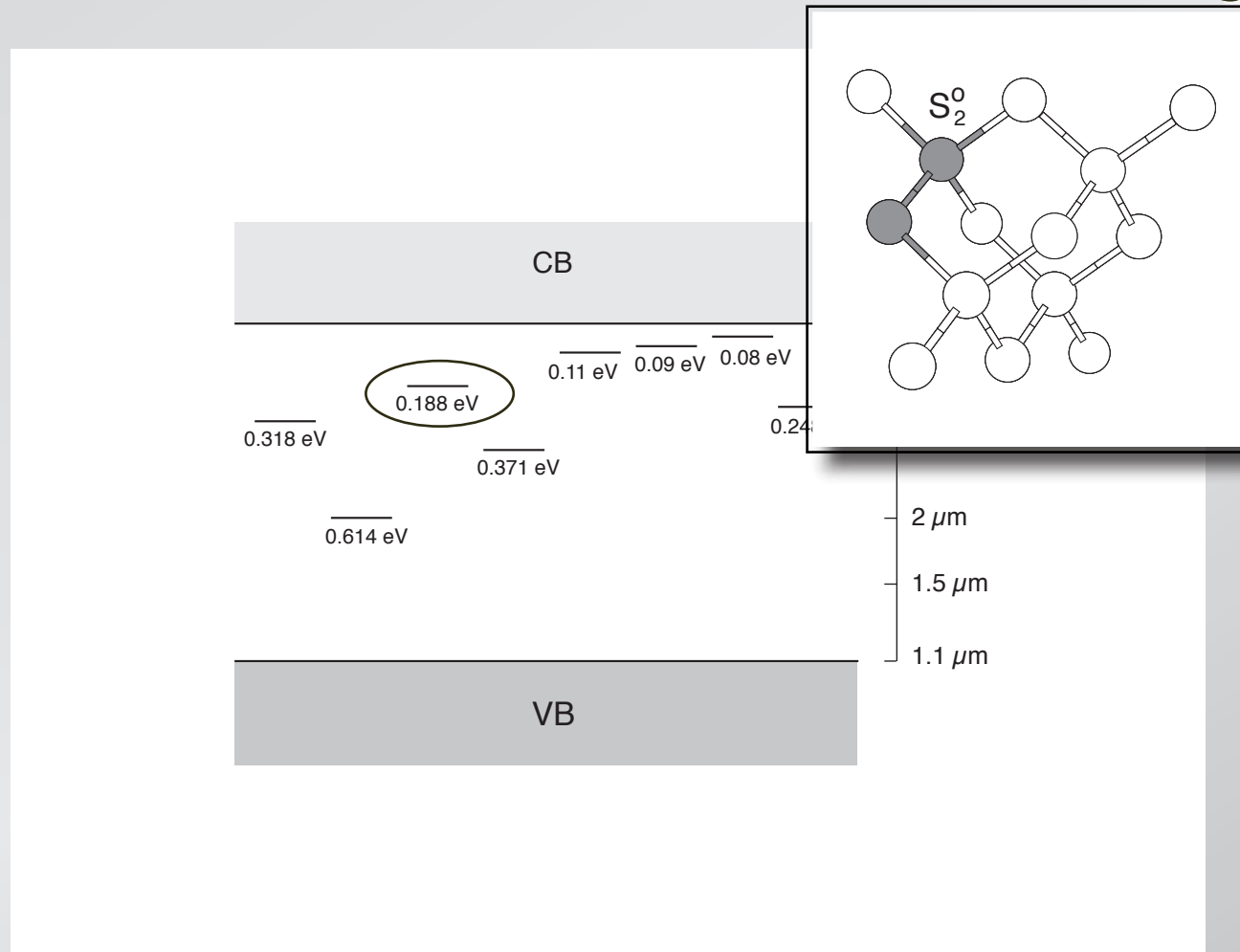
Creating intermediate band

1 part in 10^6 sulfur introduces donor states in gap



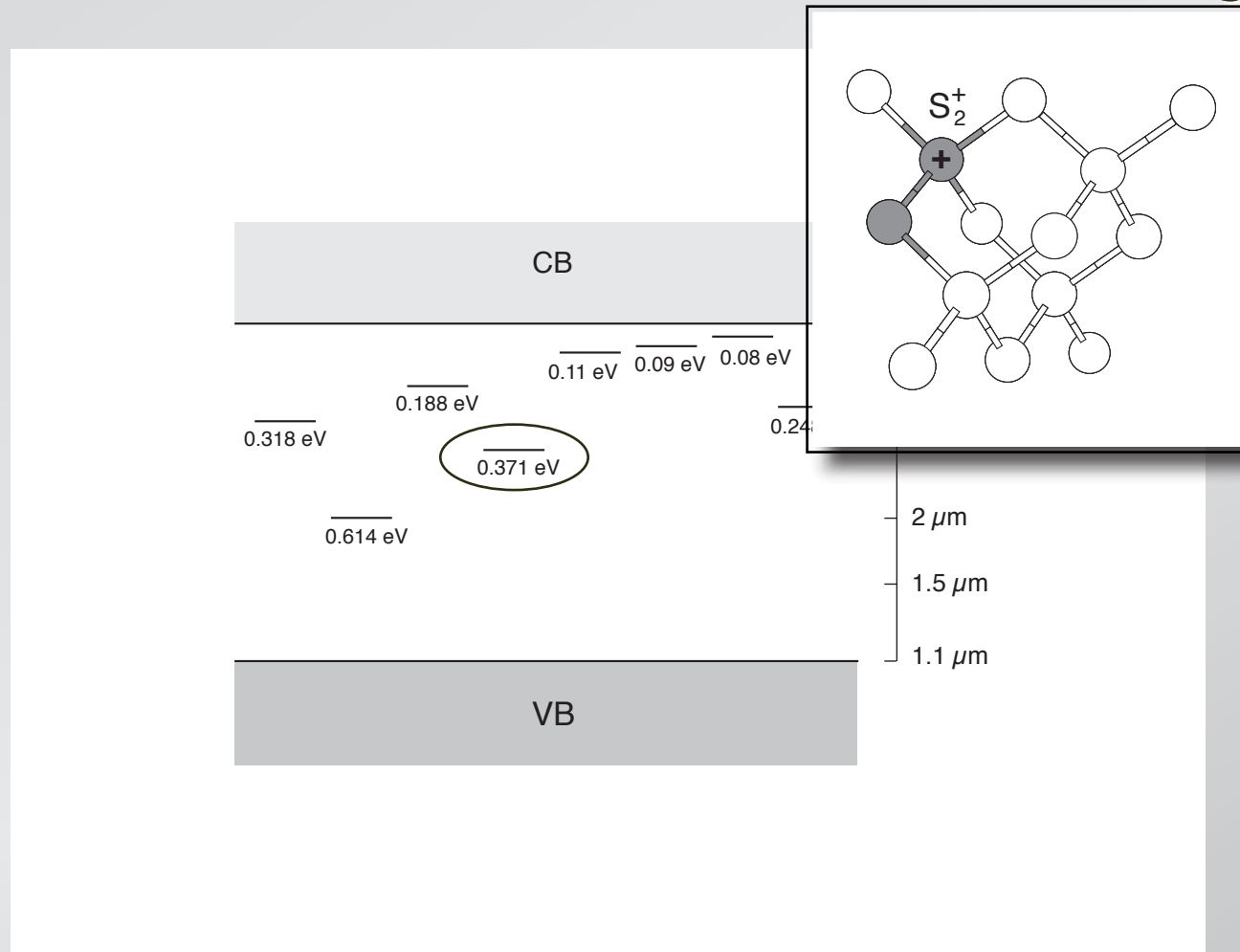
Creating intermediate band

1 part in 10^6 sulfur introduces donor states in gap



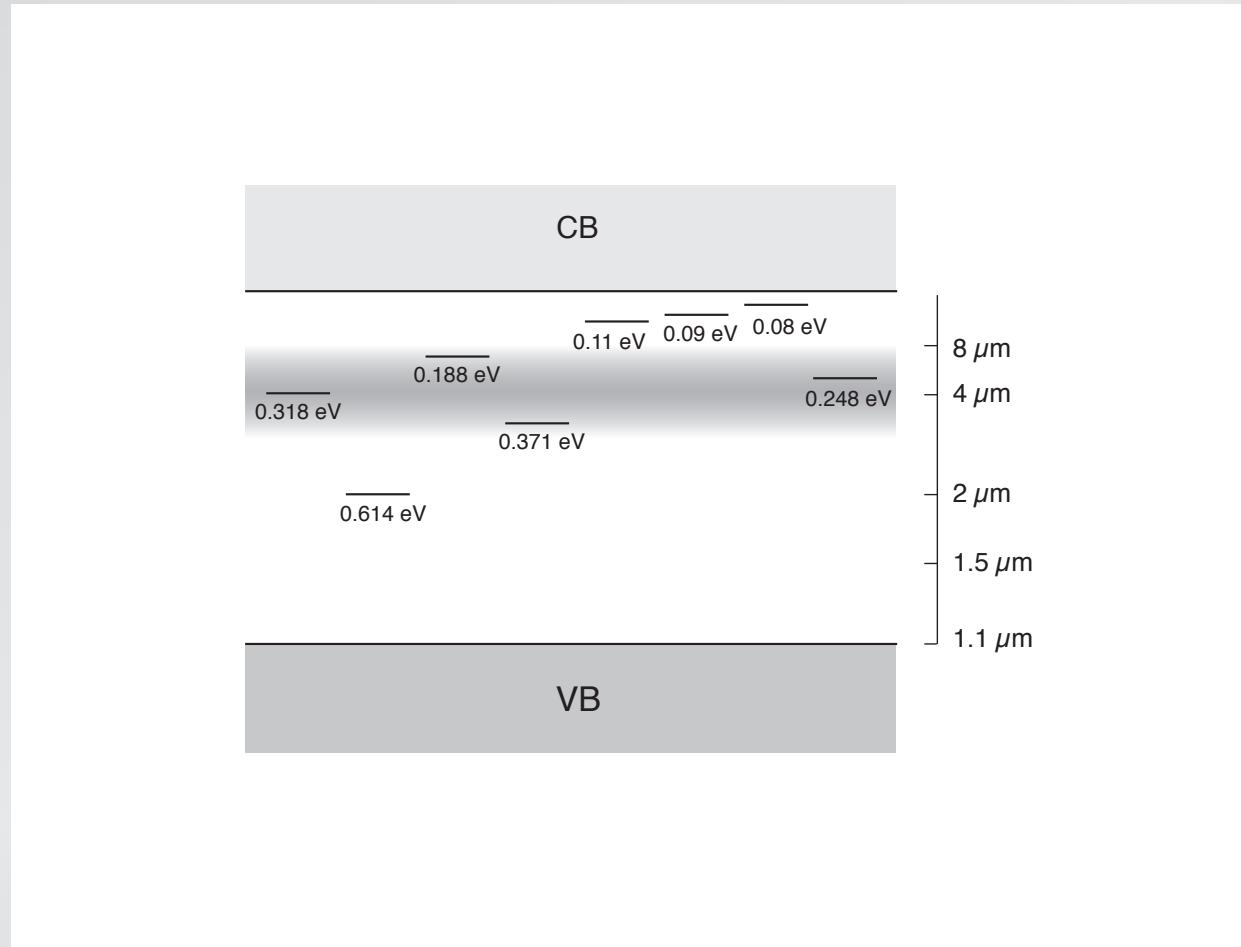
Creating intermediate band

1 part in 10^6 sulfur introduces donor states in gap



Creating intermediate band

at high concentration states broaden into band



Creating intermediate band

Outline

- **transient band structure changes**
- **creating an intermediate band**
- **semiconductor to metal transition**

Semiconductor to metal

PRL 108, 026401 (2012)

PHYSICAL REVIEW LETTERS

Insulator-to-Metal Transition in Selenium-Hyperdoped Silicon: Observation and Origin

Elif Ertekin,^{1,*} Mark T. Winkler,^{2,†} Daniel Recht,³ Aurore J. Said,³ Michael J. Aziz,³
Tonio Buonassisi,² and Jeffrey C. Grossman^{1,2,‡}

¹Department of Materials Science and Engineering, Massachusetts Institute of Technology, Cambridge Massachusetts 02139, USA
²Department of Mechanical Engineering, Massachusetts Institute of Technology, Cambridge Massachusetts 02139, USA
³Harvard School of Engineering and Applied Sciences, Cambridge Massachusetts 02138, USA

(Received 14 October 2011; published 11 January 2012)

Hyperdoping has emerged as a promising method for designing semiconductors with unique optical and electronic properties, although such properties currently lack a clear microscopic explanation. Combining computational and experimental evidence, we probe the origin of sub-band-gap optical absorption and metallicity in Se-hyperdoped Si. We show that sub-band-gap absorption arises from direct defect-to-conduction-band transitions rather than free carrier absorption. Density functional theory predicts the Se-induced insulator-to-metal transition arises from merging of defect and conduction bands, at a concentration in excellent agreement with experiment. Quantum Monte Carlo calculations confirm the critical concentration, demonstrate that correlation is important to describing the transition accurately, and suggest that it is a classic impurity-driven Mott transition.

DOI: 10.1103/PhysRevLett.108.026401

PACS numbers: 71.30.+h, 61.72.sd, 73.61.Cw, 78.20.Bh

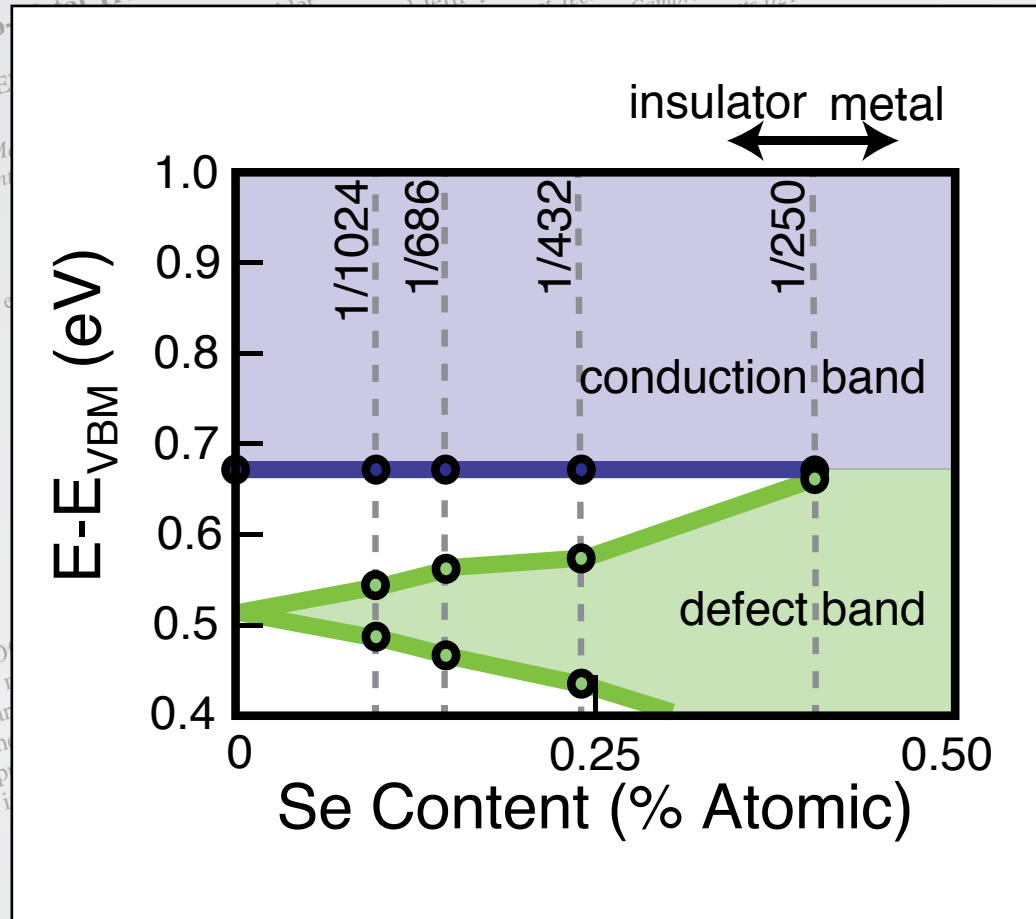
Of all the experimentally measurable physical properties of materials, electronic conductivity exhibits the largest variation, spanning a factor of 10^{31} from the best metals to the strongest insulators [1]. Over the last century, the puzzle of why some materials are conductors and others insulators, and the mechanisms underlying the transformation from one to the other, have been carefully scrutinized; yet even after such a vast body of research over such a long period, the subject remains the object of controversy. In 1956, Mott introduced a model for the insulator-to-metal transition (IMT) in doped semiconductors, in which long-ranged electron correlations are the driving force [2]. Hyperdoping (doping beyond the solubility limit) creates a new materials playground to explore defect-mediated IMTs in semiconductors. In this Letter, we identify a defect-induced IMT in silicon hyperdoped with selenium to concentrations exceeding 10^{20} cm^{-3} (compared to the equilibrium solubility limit [3] of about 10^{16} cm^{-3}) and we explore the detailed nature of the transition with both experiment and computation. We find that the IMT resembles a Mott transition. Additionally, we find that the transition at the IMT yields a metallic surface that is electrically efficient in

silicon appears to justify such interest. While isolated S and Se dopants are well-established deep double donors in silicon [3,14], the enhanced optical properties of hyperdoped silicon (in which these chalcogenic impurities are present at much higher concentrations) are not yet well understood. Further, unlike the prototypical system of phosphorus-doped silicon for which the IMT has been extensively studied and characterized [15,16], there are very few studies of an IMT resulting from deep defects such as chalcogens [17].

We prepared Se-doped silicon (Se:Si) samples using ion implantation followed by nanosecond pulsed-laser melting (PLM) and rapid resolidification. The PLM process enables chalcogen doping with concentrations exceeding 1% atomic; such samples exhibit unexplained optical properties including broad, featureless absorption of photons with energy lower than the band gap of silicon [9]. Silicon substrates (boron doped, $\rho \approx 25 \text{ } \Omega \text{ cm}$) were ion implanted with Se to nominal doses of 3×10^{15} and $1 \times 10^{16} \text{ cm}^{-2}$ using an ion beam energy of 176 keV. The implanted samples were exposed to four laser pulses (fluences of 1.7, 1.7, 1.7 and 1.8 J cm^{-2}). This fluence regimen results in a slightly shallower dopant profile, and higher peak Se concentration, than reported previously [18]. The Se-rich layer is crystalline, extends approximately 350 nm from the surface, and is electrically isolated from the substrate by the rectifying junction formed between the surface and the bulk. The depth profile was measured by secondary ion mass spectrometry [17,18]. Sample properties are described

Semiconductor to metal

DFT calculations



Ertekin et al., Phys. Rev. Lett. 108, 026401 (2012)

Semiconductor to metal

JOURNAL OF APPLIED PHYSICS 113, 213501 (2013)

Emergence of very broad infrared absorption band by hyperdoping of silicon with chalcogens

Ikuro Umezū,¹ Jeffrey M. Warrender,² Supakit Charnvanichborikarn,³ Atsushi Kohno,⁴ James S. Williams,³ Malek Tabbal,⁵ Dimitris G. Papazoglou,^{6,7} Xi-Cheng Zhang,^{8,a} and Michael J. Aziz⁹

¹Department of Physics, Konan University, Kobe 658-8501, Japan

²U.S. Army ARDEC–Benét Laboratories, Watervliet, New York 12189, USA

³Research School of Physics and Engineering, The Australian National University, Canberra, ACT 0200, Australia

⁴Department of Applied Physics, Fukuoka University, Fukuoka 814-0180, Japan

⁵Department of Physics, American University of Beirut, Beirut 1107 2020, Lebanon

⁶Institute of Electronic Structure and Laser, Foundation for Research and Technology Hellas, P.O. Box 1527, 71110 Heraklion, Greece

⁷Materials Science and Technology Department, University of Crete, P.O. Box 2208, 71003 Heraklion, Greece

⁸Department of Physics, Applied Physics and Astronomy, Rensselaer Polytechnic Institute, Troy, New York 12180, USA

⁹Harvard School of Engineering and Applied Sciences, Cambridge, Massachusetts 02138, USA

(Received 9 September 2012; accepted 29 April 2013; published online 3 June 2013)

We report the near through mid-infrared (MIR) optical absorption spectra, over the range 0.05–1.3 eV, of monocrystalline silicon layers hyperdoped with chalcogen atoms synthesized by ion implantation followed by pulsed laser melting. A broad mid-infrared optical absorption band emerges, peaking near 0.5 eV for sulfur and selenium and 0.3 eV for tellurium hyperdoped samples. Its strength and width increase with impurity concentration. The emergence of a broad MIR absorption band is consistent with subsequent thermal annealing. The formation of an impurity band from isolated deep donor levels as the concentration of chalcogen atoms in metastable local configurations increases. © 2013 AIP Publishing LLC.

I. INTRODUCTION

Silicon hyperdoped with chalcogens can be synthesized by pulsed laser irradiation in a sulfur-bearing atmosphere,^{1,2} ion implantation followed by pulsed laser melting,^{3,4} or pulsed laser mixing.⁵ This material has attracted interest because of its sub band gap absorption and has been studied as a candidate for infrared (IR) photodetectors^{6–8} and efficient solar cells.^{9–11} In addition, observations of carrier lifetime recovery for sufficiently high concentrations of titanium in silicon has aroused similar interest in this material.^{12,13} Chalcogen hyperdoping has been shown to cause an metal transition and has been proposed to form an impurity band in the silicon band gap.^{4,10,14–16} However, the mechanism causing the sub-bandgap absorption for this is that

II. EXPERIMENT

Double side polished p type (001) Si wafers, resistivity of 5–25 Ω cm, were ion implanted at room temperature with either 95 keV $^{32}\text{S}^-$, 176 keV $^{80}\text{Se}^+$, or 245 keV $^{130}\text{Te}^+$ to doses of 1×10^{16} ions/cm². The dose of $^{32}\text{S}^-$ was varied from 3×10^{14} to 1×10^{16} ions/cm² and pre-amorphized by 85 keV Si^- to doses of 3×10^{15} ions/cm² when the $^{32}\text{S}^-$ dose is not greater than 1×10^{15} ions/cm². Pulsed laser melting was performed using a XeCl excimer laser beam (308 nm, 25 ns FWHM, 50 ns total duration). Each sample received three laser shots at 1.7 J/cm² followed by a fourth laser shot at 1.8 J/cm². Time-resolved reflectivity of a 488 nm Ar^+ ion laser was used to measure the melt duration. The laser fluence was calibrated by comparing the melt duration with numerical solutions to the one-dimensional heat equation.¹⁸ The details of the sample preparation method and depth profiles of chalcogen atoms observed by secondary ion mass spectrometry (SIMS) are reported elsewhere.³ For the synthesis procedure is the same as for sulfur doped samples, but at higher fluences.

Semiconductor to metal

Emergence of very broad infrared absorption band by hyperdoping of silicon with chalcogens

Ikuro Umezu,¹ Jeff James S. Williams,³ and Michael J. Aziz

¹Department of Physics

²U.S. Army ARDEC

³Research School of

Australia

⁴Department of Applied

⁵Department of Physics

⁶Institute of Electronics

71110 Heraklion

⁷Materials Science

⁸Department of Physics

New York 12184

⁹Harvard School of

(Received 10/11/12)

We report

0.05–1.3 eV

ion implantation

emerges

Its strength

subsequently

the function

of carrier

lifetime

[http://dx.doi.org/10.1063/1.3661111]

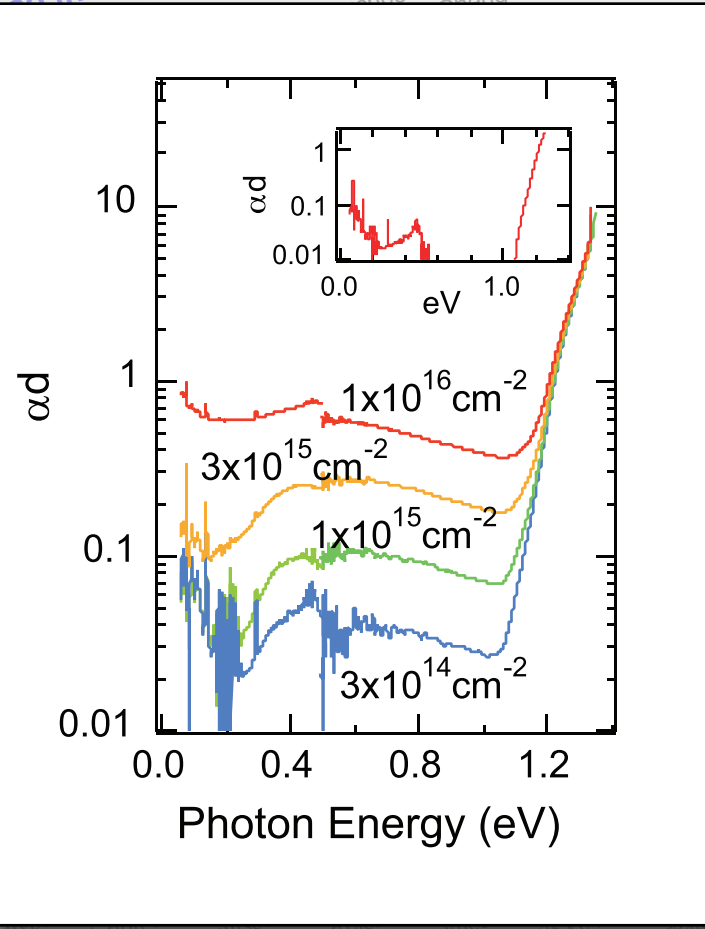
I. INTRODUCTION

Silicon hyperdoping has been achieved by pulsed laser irradiation followed by pulsed laser mixing.⁵ This material has been shown to be a promising candidate for infrared (IR) photodetectors^{6–8} and efficient solar cells^{9,10} because of its sub band gap absorption and has been shown to have a time recovery for sufficient interest.¹¹ In addition, observations of carrier lifetime in silicon has aroused similar interest.^{12,13} Chalcogen hyperdoping has been shown to cause a metal transition and has been proposed to form an intermediate phase between the sub-bandgap semiconductor and metal transition.^{4,10,14–16} However, the mechanism causing the sub-bandgap absorption in hyperdoped silicon is not clear for this is that

JOURNAL OF APPLIED PHYSICS 113, 213501 (2013)

Emergence of very broad infrared absorption band by hyperdoping of silicon with chalcogens

Ikuro Umezu,¹ Jeff James S. Williams,³ Atsushi Kohno,⁴ and Michael J. Aziz



27, Greece

the range synthesized by absorption band doped samples. markedly with consistent with concentration publishing LLC.

...ed p type (001) Si wafers, resistivity ion implanted at room temperature with 176 keV ⁸⁰Se⁺, or 245 keV ¹³⁰Te⁺ to ions/cm². The dose of ³²S⁻ was varied from 1 × 10¹⁶ ions/cm² and pre-amorphized by laser shots of 3 × 10¹⁵ ions/cm² when the ³²S⁻ dose was less than 1 × 10¹⁵ ions/cm². Pulsed laser melt-annealing was performed using a XeCl excimer laser beam (308 nm, 25 ns FWHM, 50 ns total duration). Each sample received three laser shots at 1.7 J/cm² followed by a fourth laser shot at 1.8 J/cm². Time-resolved reflectivity of a laser fluence was calibrated by comparing the melt duration with numerical solutions to the one-dimensional heat conduction equation.¹⁸ The details of the sample preparation method and depth profiles of chalcogen atoms observed by secondary ion mass spectrometry (SIMS) are reported elsewhere.³ For the synthesis procedure is the same as for sulfur doped samples, but at higher fluences.

Umezu et al., J. Appl. Phys. 113, 213501 (2013)

Semiconductor to metal

Understanding the Viability of Impurity-Band Photovoltaics: A Case Study of S-doped Si

by

Joseph Timothy Sullivan

Submitted to the Department of Mechanical Engineering
on May 18, 2013, in partial fulfillment of the
requirements for the degree of
Doctor of Philosophy

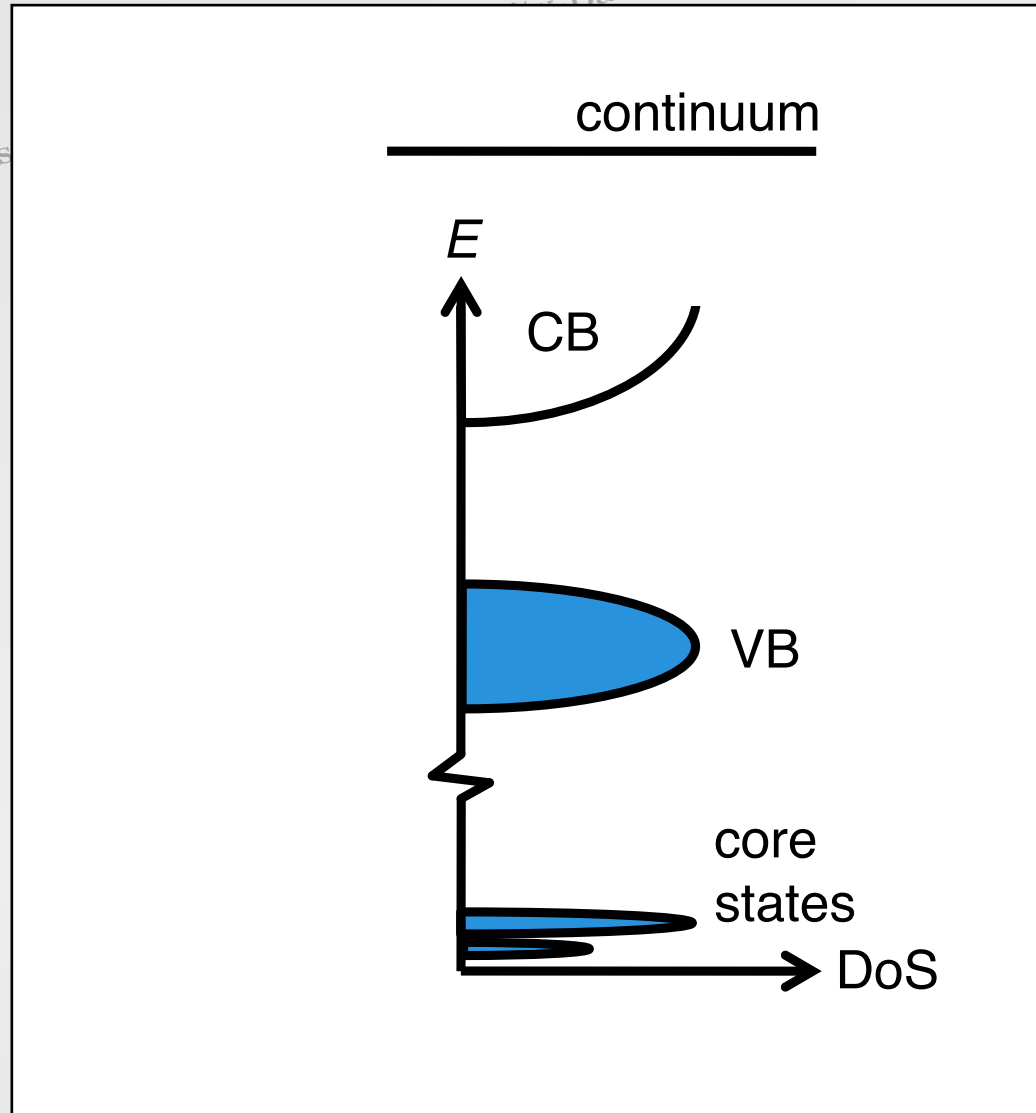
Abstract

This thesis explores the electronic structure, optical properties, and carrier lifetimes in silicon that is doped with sulfur beyond the equilibrium solid solubility limit, with a focus on applications as an absorber layer for an impurity-band photovoltaic device. The concept of an impurity-band material envisions the creation of a band of electronic states by incorporating high concentrations of deep-level dopants, which enable the generation of free carriers using photons with energy less than that of the band gap of the host semiconductor. The investigations reported in this thesis provide a framework for the appropriate selection of impurity-band candidate materials. The thesis is divided into three primary sections, one for each of three experimental techniques, respectively.

First, the electronic band structure is studied using synchrotron-based x-ray emission spectroscopy. These spectra provide the first insights into how the electronic structure changes as the sulfur concentration is increased across the metal-insulator transition, and how the electronic structure is linked to the anomalously high sub-band gap absorption. A discrete change in local electronic structure is seen that corresponds to the macroscopic change in electronic behavior. Additionally, a direct correlation is seen between sulfur-induced states and the sub-band gap absorption.

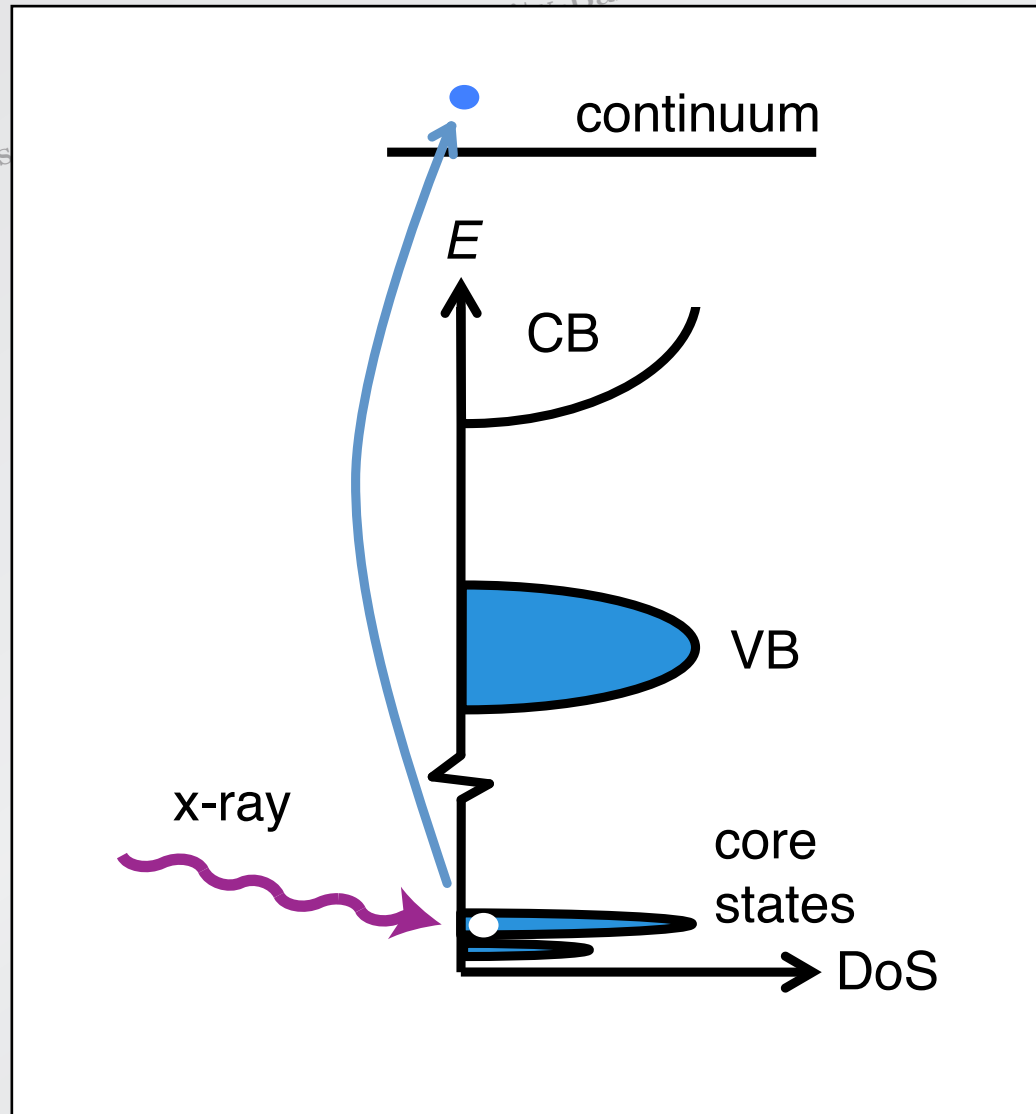
Next, the optical properties are studied using Fourier transform infrared spectroscopy. Extraction of the complex index of refraction is performed using numerical modeling. This determines the position of the sulfur-induced states within the conduction band, and the reflection measurements. Analysis of the transmission and reflection measurements for different sulfur concentrations and above the metal-insulator transition, with the conduction band structure unsuitable

Semiconductor to metal



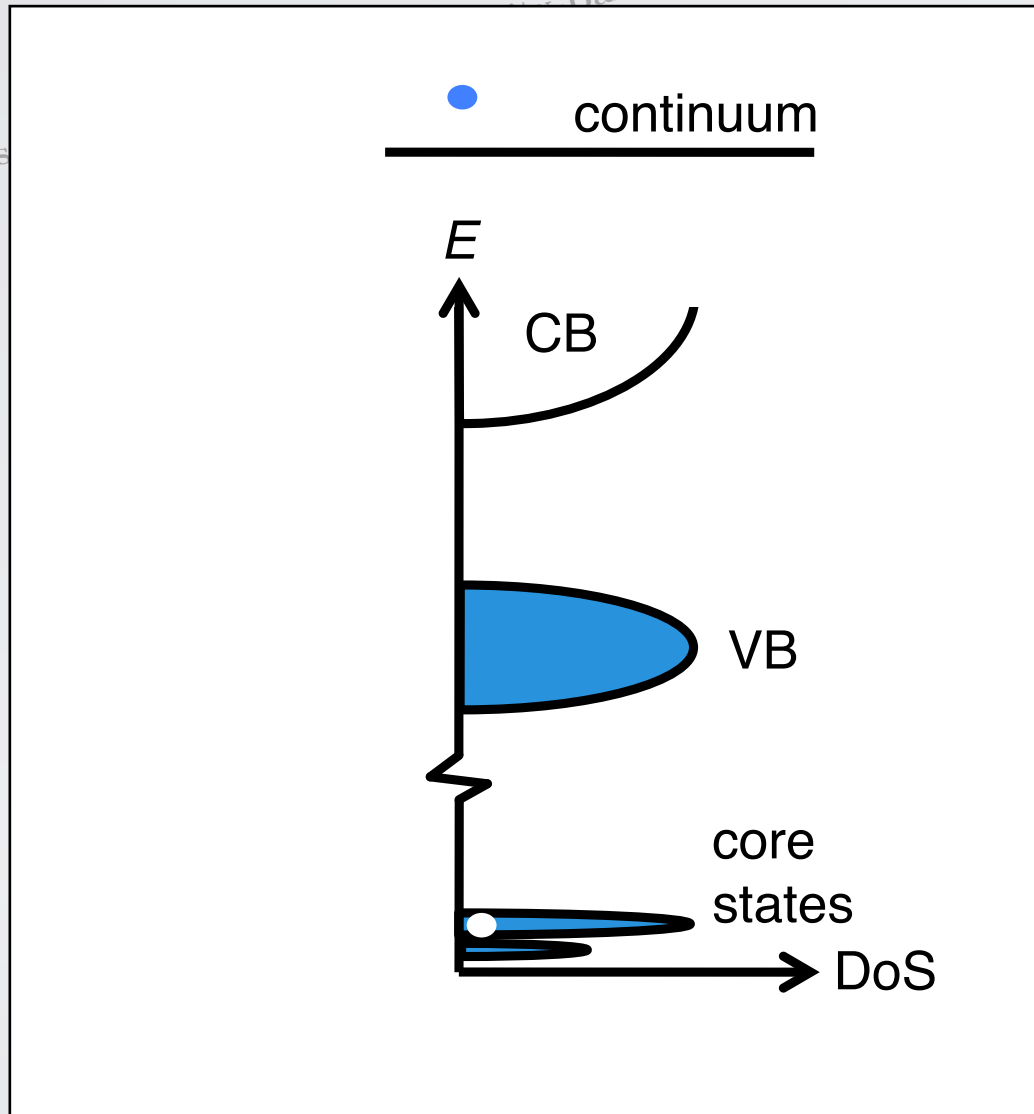
J. Sullivan, Ph.D. Thesis, MIT (2013)

Semiconductor to metal



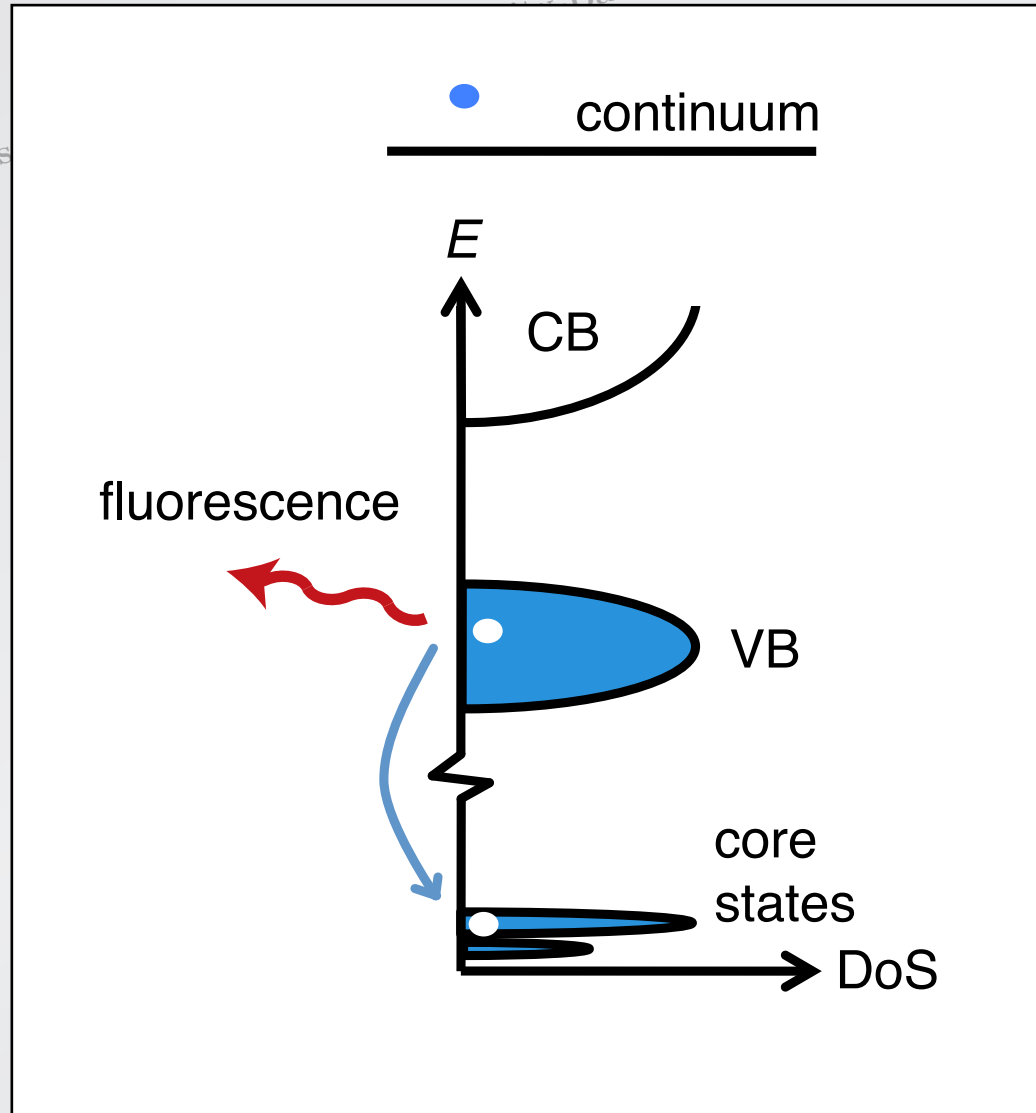
J. Sullivan, Ph.D. Thesis, MIT (2013)

Semiconductor to metal



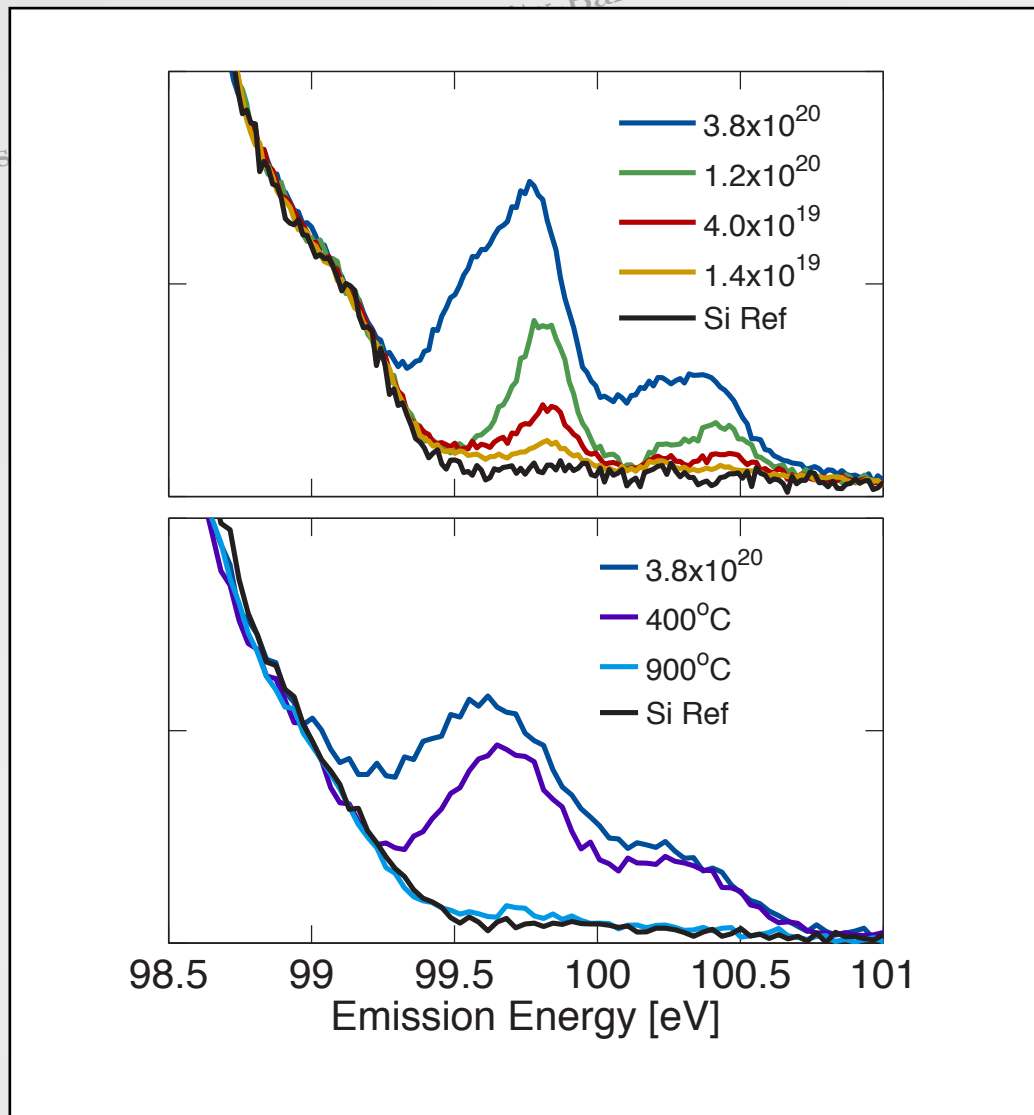
J. Sullivan, Ph.D. Thesis, MIT (2013)

Semiconductor to metal



J. Sullivan, Ph.D. Thesis, MIT (2013)

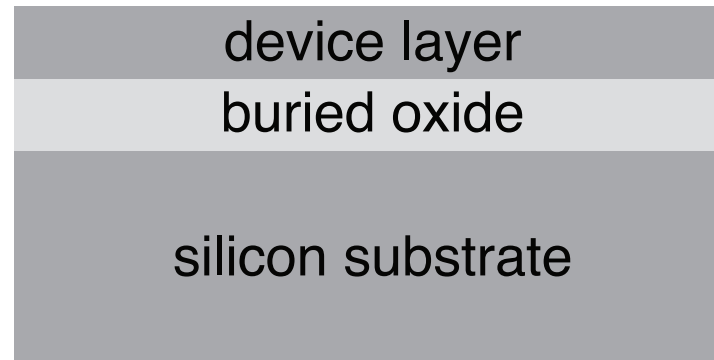
Semiconductor to metal



J. Sullivan, Ph.D. Thesis, MIT (2013)

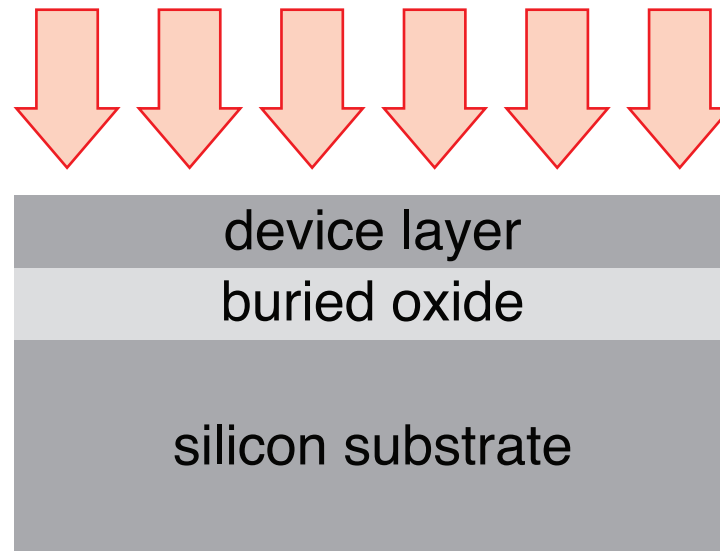
Semiconductor to metal

isolate surface layer for Hall measurements



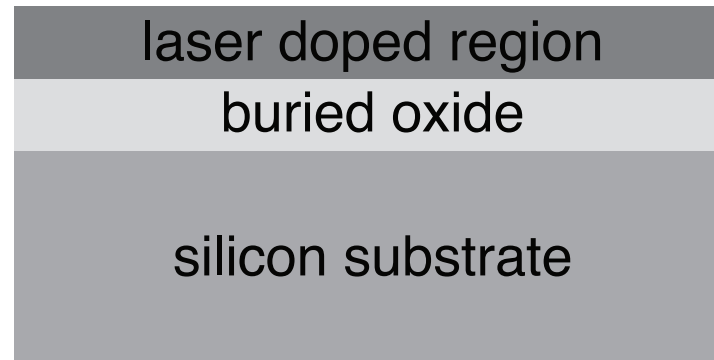
Semiconductor to metal

isolate surface layer for Hall measurements



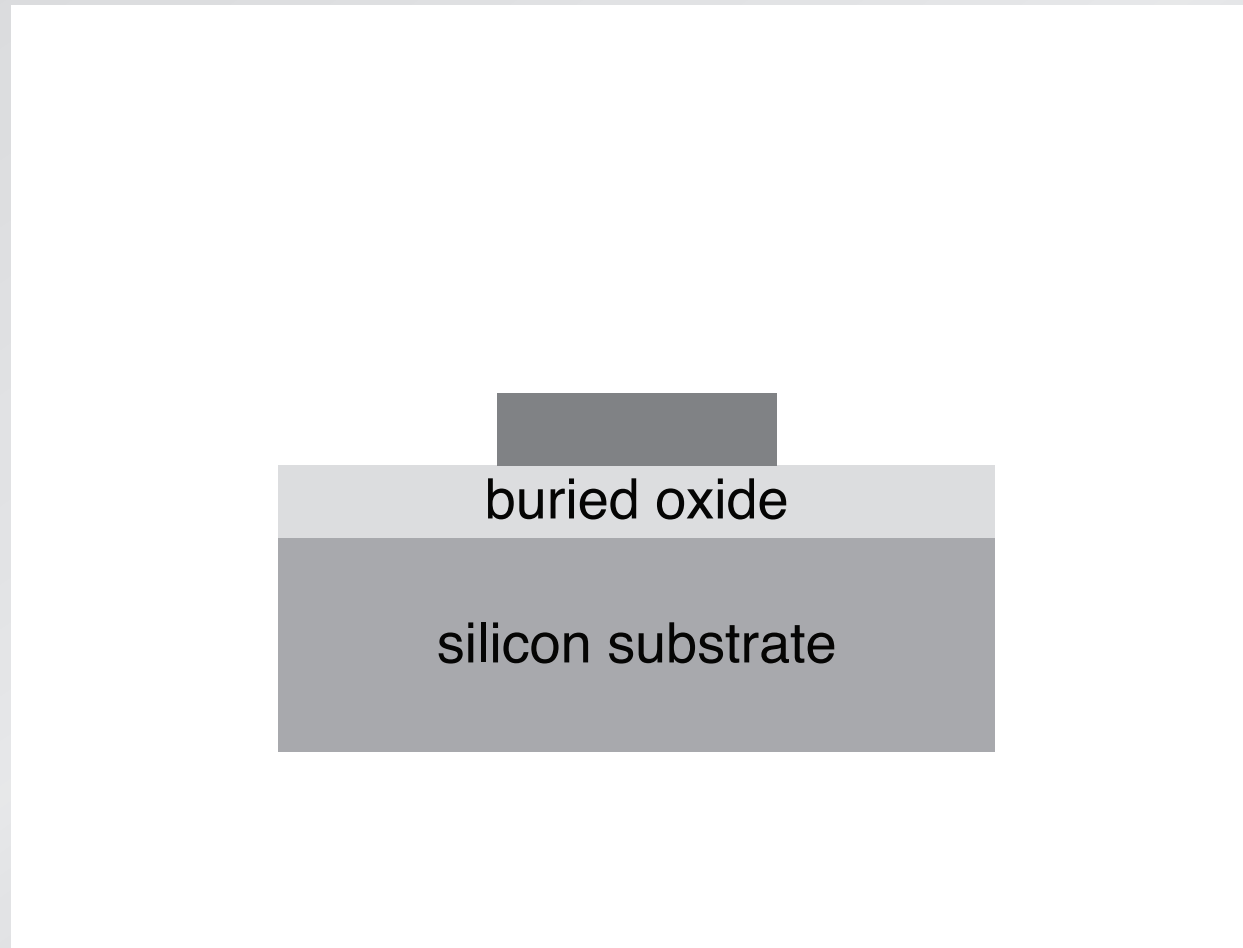
Semiconductor to metal

isolate surface layer for Hall measurements



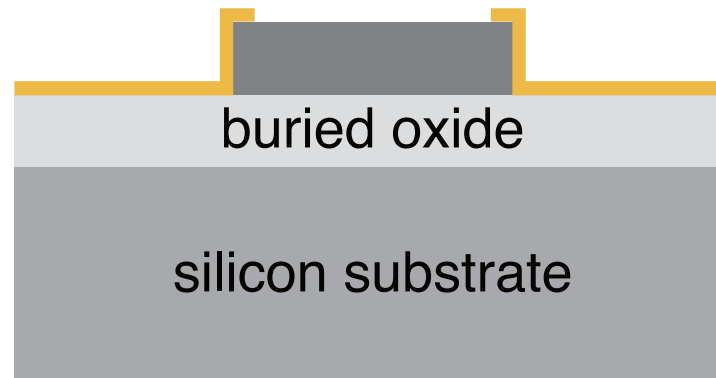
Semiconductor to metal

isolate surface layer for Hall measurements



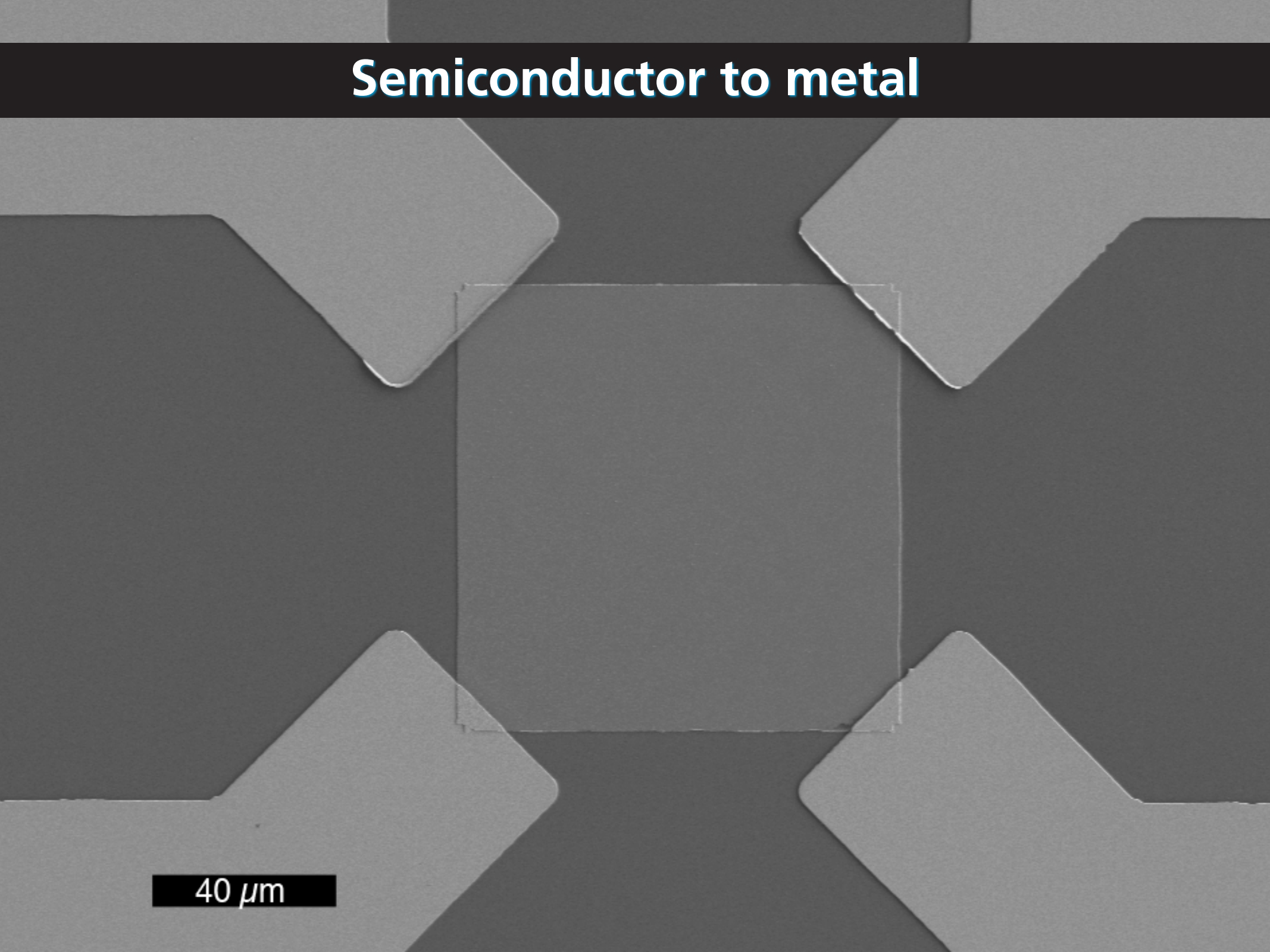
Semiconductor to metal

isolate surface layer for Hall measurements



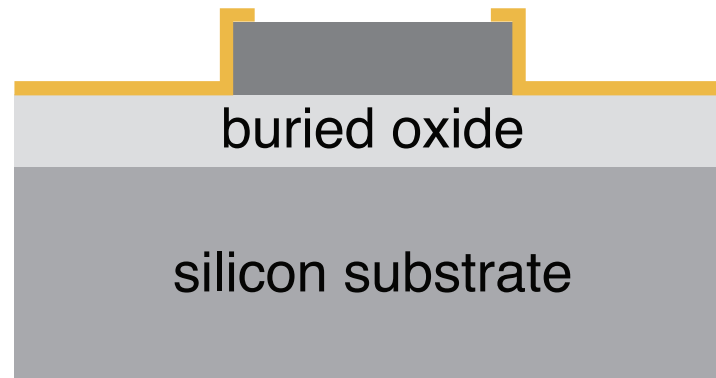
Semiconductor to metal

40 μm

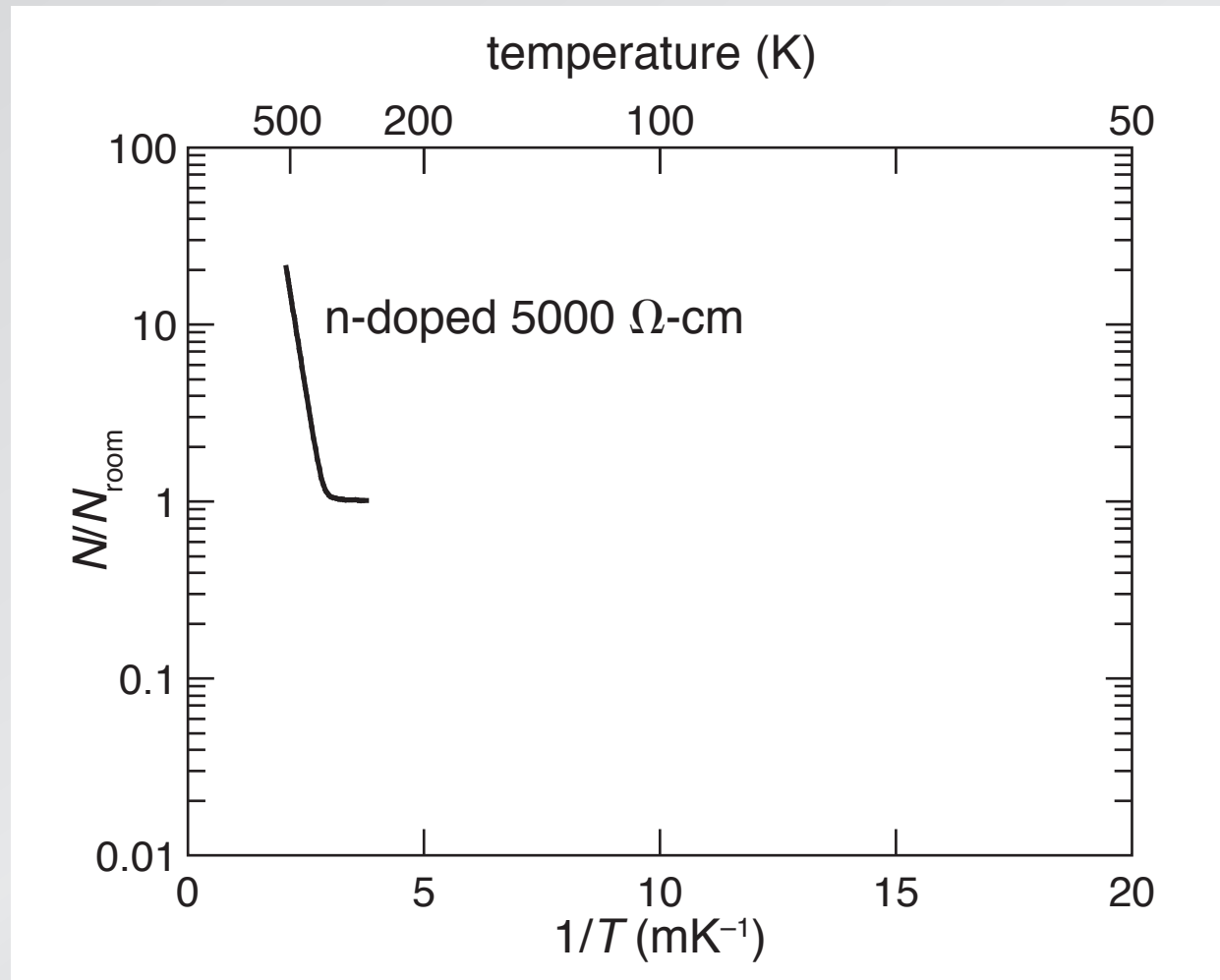
A grayscale micrograph showing a central square region surrounded by four trapezoidal regions. The central square is outlined with a thin white border. The trapezoidal regions are positioned at the top-left, top-right, bottom-left, and bottom-right corners relative to the central square. The background is a uniform dark gray. A scale bar in the bottom-left corner indicates a length of 40 micrometers.

Semiconductor to metal

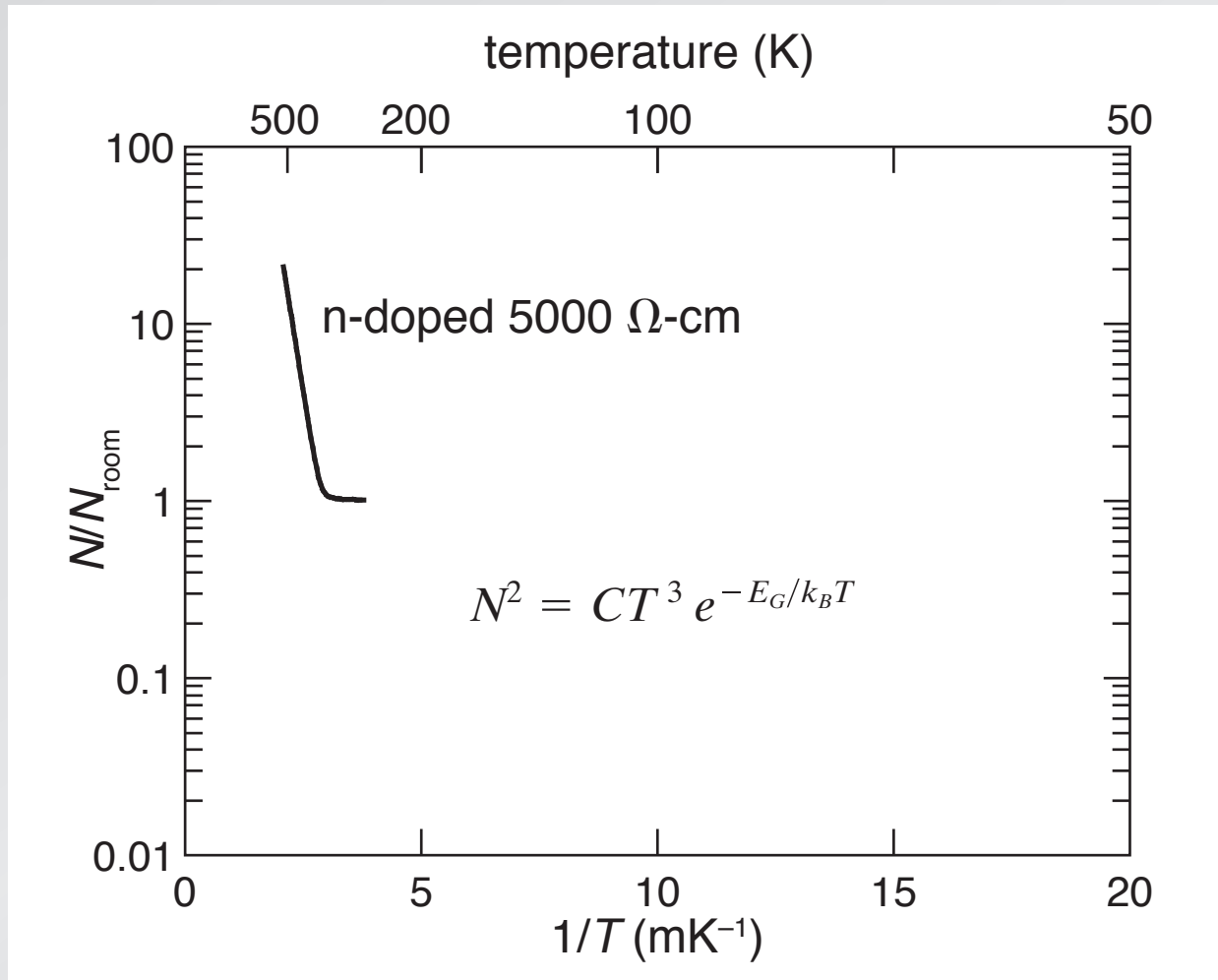
isolate surface layer for Hall measurements



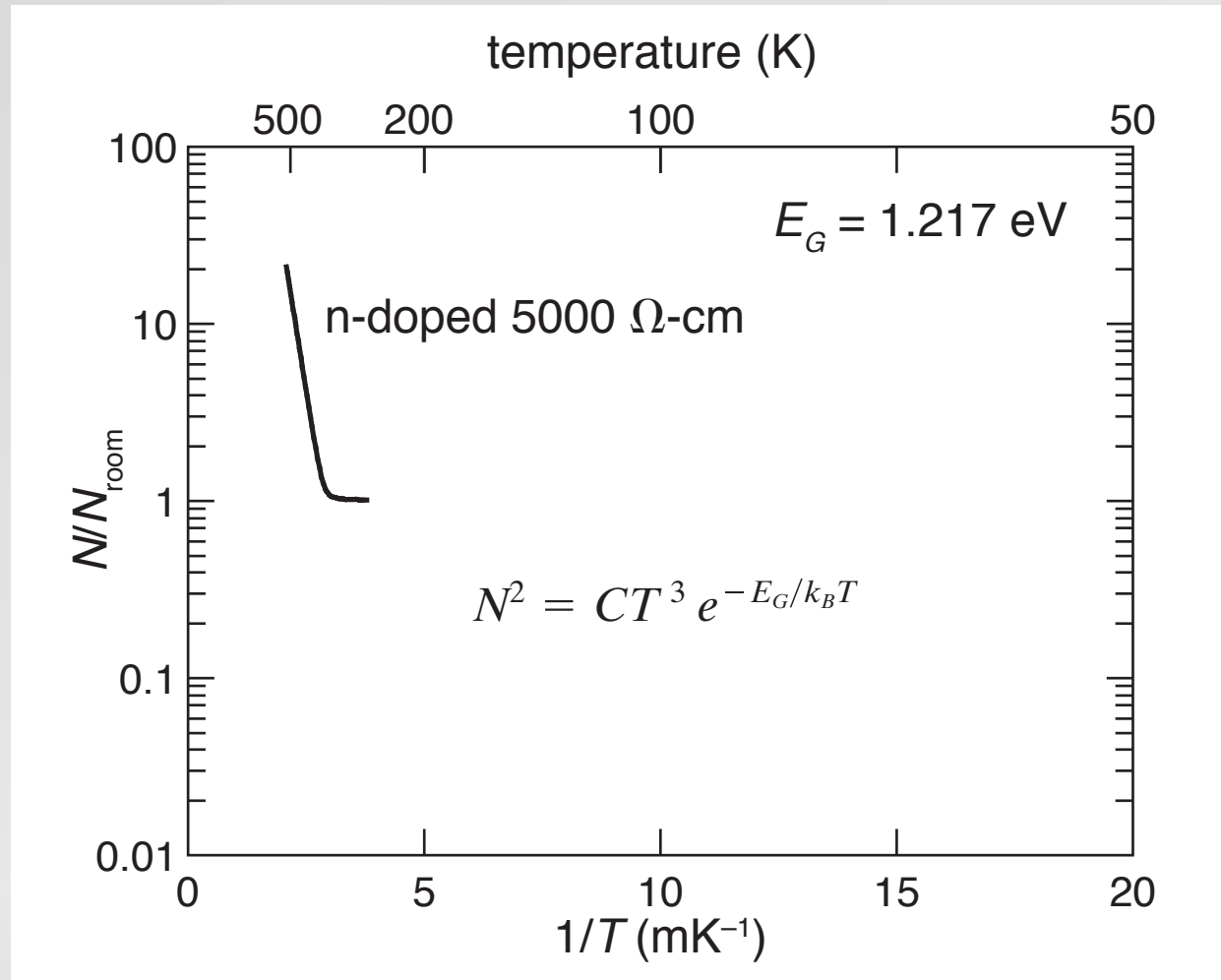
Semiconductor to metal



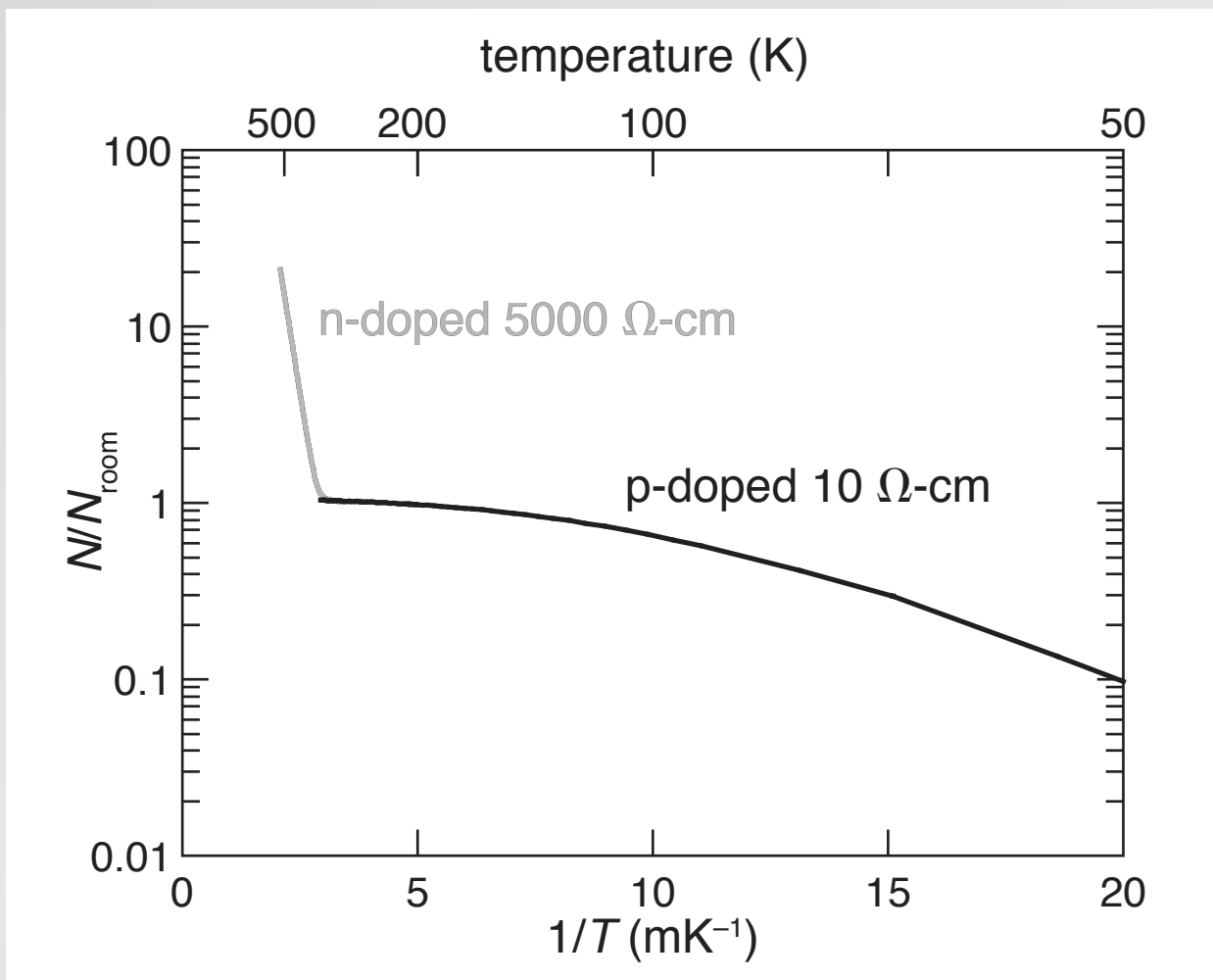
Semiconductor to metal



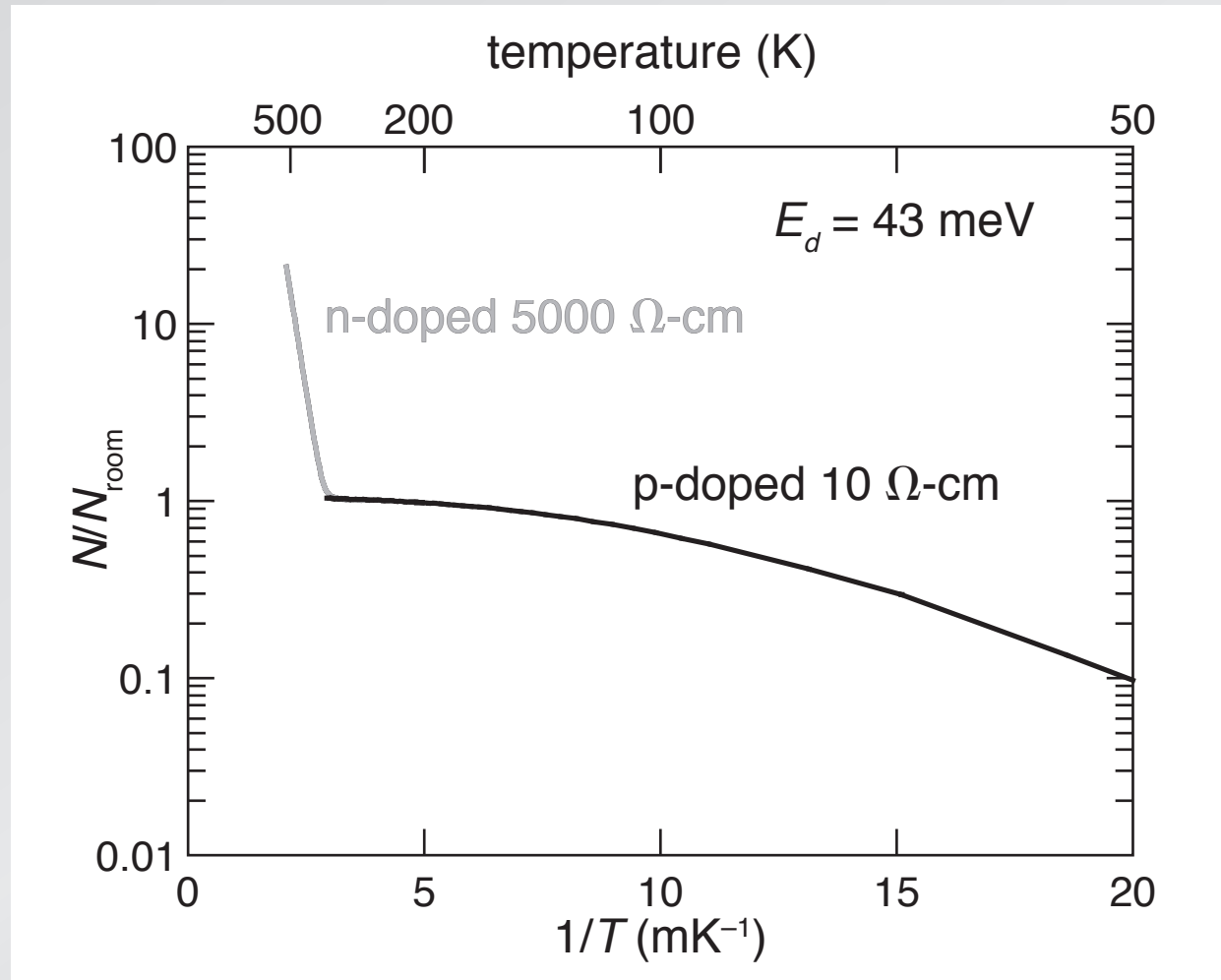
Semiconductor to metal



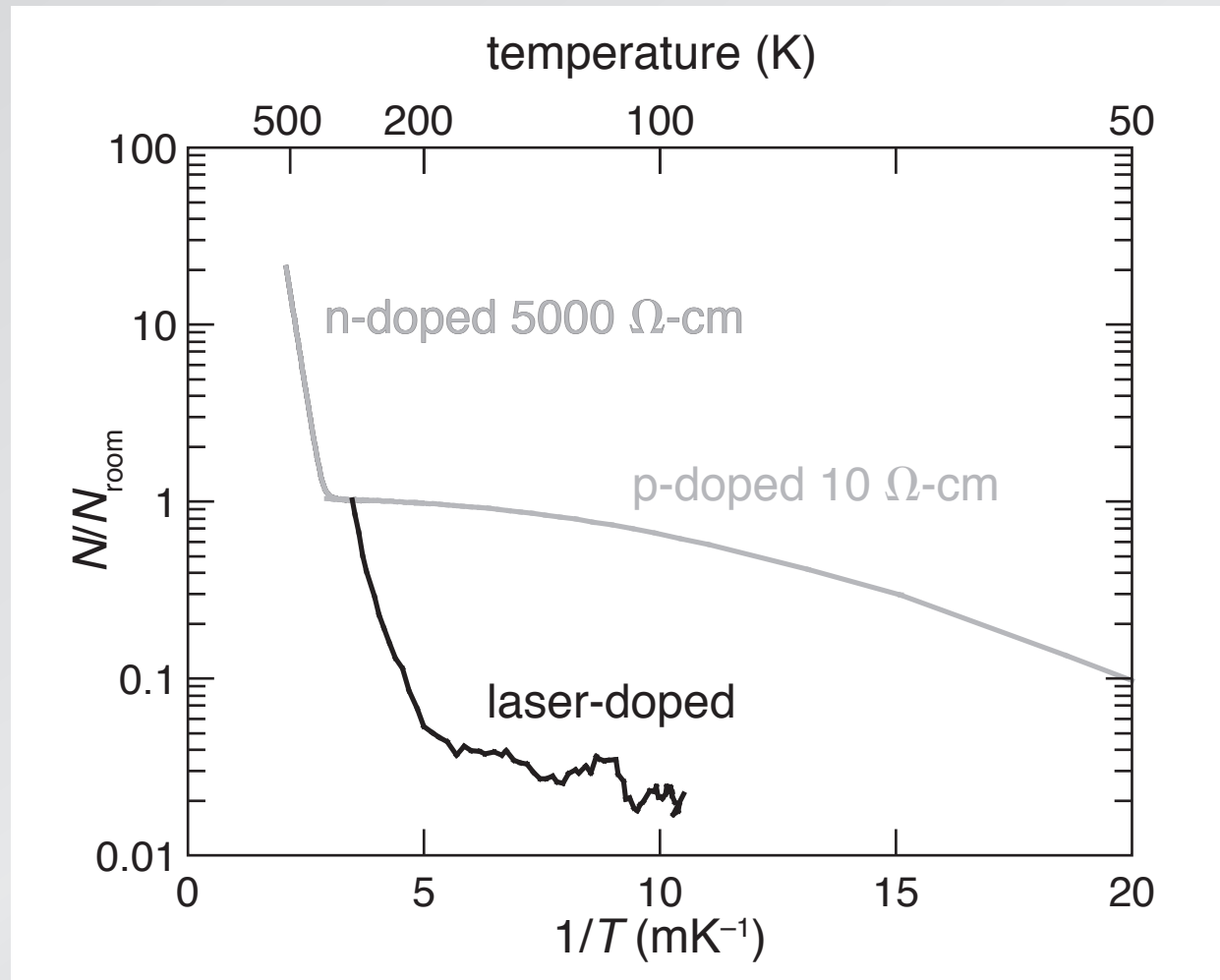
Semiconductor to metal



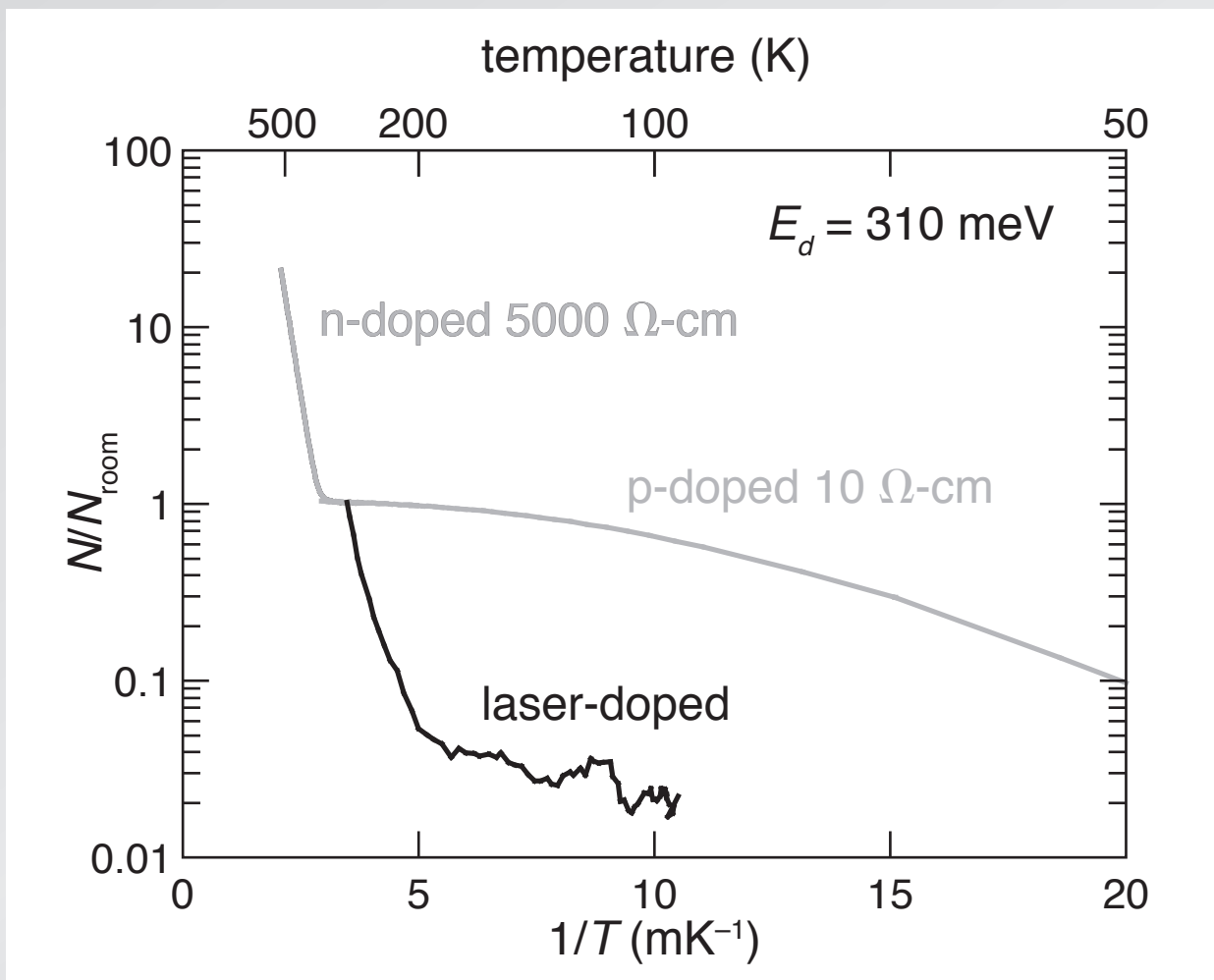
Semiconductor to metal



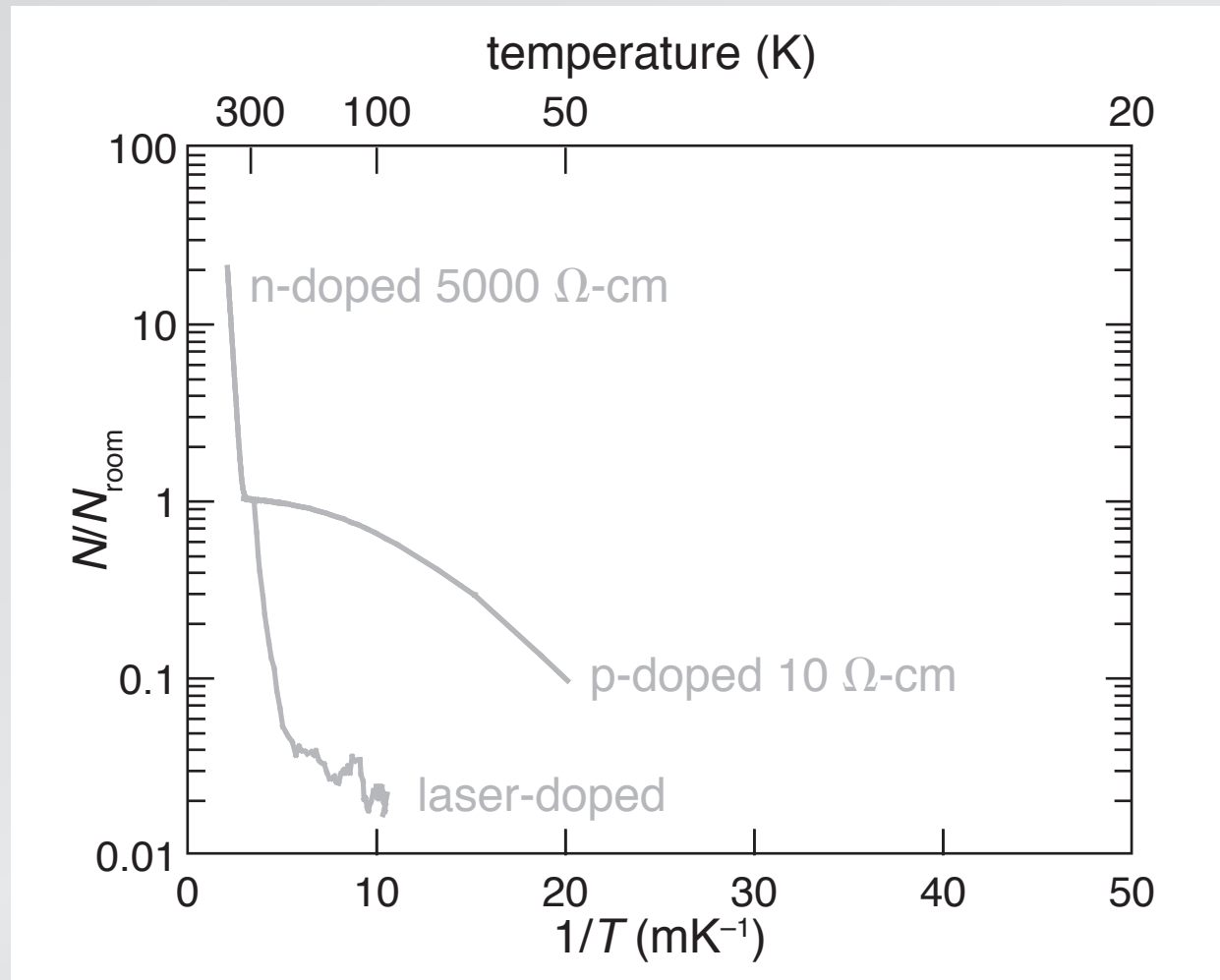
Semiconductor to metal



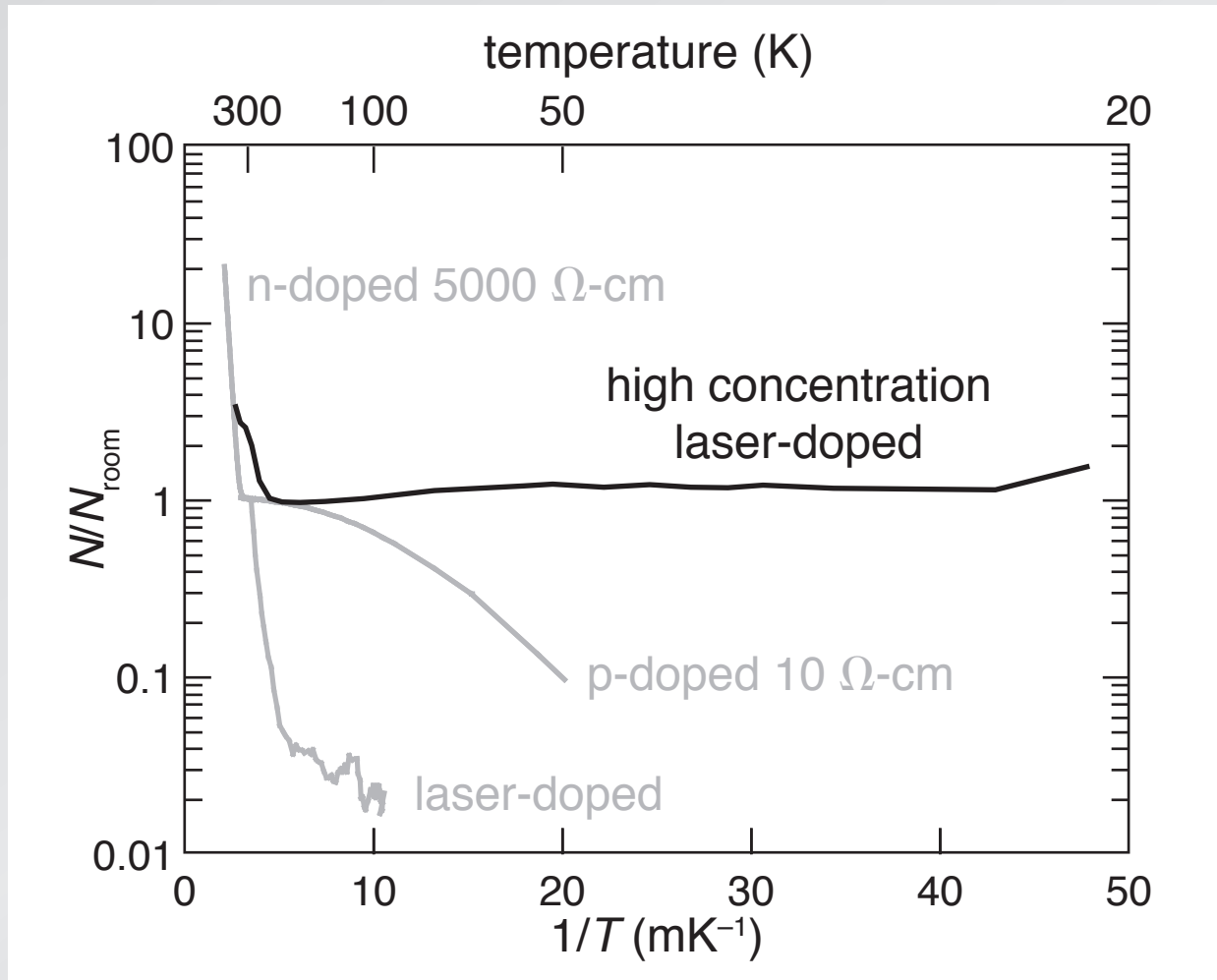
Semiconductor to metal



Semiconductor to metal



Semiconductor to metal



Conclusion

- **transient and metastable band structure changes**
- **both due to fs-induced nonequilibrium state**
- **a new way of manipulating band structure**



**Ben Franta
Hemi Gandhi
Alexander Raymond**

**Dr. Paul Callan
Dr. Jim Carey (SiOnyx)
Prof. Catherine Crouch (Swarthmore)
Dr. Shrenik Deliwala
Dr. Eric Diebold
Dr. Richard Finlay
Dr. Eli Glezer
Prof. Tsing-Hua Her (UNC Charlotte)
Dr. Li Huang
Dr. Albert Kim
Dr. Yu-Ting Lin
Dr. Michael Sheehy
Prof. Mengyan Shen (Lowell U)
Dr. Renee Sher
Dr. Yakir Siegal
Dr. Brian Tull
Dr. Marc Winkler
Dr. Claudia Wu
Dr. Rebecca Younkin
Dr. Haifei Albert Zhang
Prof. Li Zhao (Fudan U)**

**Prof. Augustinus Asenbaum (Vienna)
Prof. Alan Aspuru-Guzik (Harvard)
Prof. Michael Aziz (Harvard)
Prof. Michael Brenner (Harvard)
Prof. Tonio Buonassisi (MIT)
Prof. Steven Fahy (Cork)
Prof. Cynthia Friend (Harvard)
Prof. Silvija Gradecak (MIT)
Dr. Peter Grosse (Aachen)
Prof. Jeff Grossman (MIT)
Prof. Tim Kaxiras (Harvard)
Dr. Bonna Newman (MIT)
Matthew Smith (MIT)
Prof. Howard Stone (Princeton)
Joe Sullivan (MIT)
Dr. Paul Tangney (Princeton)

Dr. Richard Farrell (RMD)
Dr. François Génin (LLNL)
Dr. Arie Karger (RMD)
Dr. Pat Maloney (NVSED)
Dr. Richard Meyers (RMD)
Dr. Martin Pralle (SiOnyx)
Dr. Mark Wall (LLNL)
Dr. Jeffrey Warrander (ARDEC)**

Funding:

Army Research Office

DARPA

Department of Energy

NDSEG

National Science Foundation

for more information and a copy of this presentation:

ericmazur.com

Follow me!



@eric_mazur